HIG-78-8

GL03297

SEISMIC STUDIES ON KILAUEA VOLCANO, HAWAII ISLAND

By

W. Suyenaga, M. Broyles, A. S. Furumoto,
R. Norris, and M. D. Mattice

Hawaii Institute of Geophysics
Honolulu, Hawaii

Geothermal Resources Exploration in Hawaii:
Number 5

November 1978

NATIONAL SCIENCE FOUNDATION, Grant GI-38319
and
ENERGY RESEARCH AND DEVELOPMENT AGENCY, Grant E(04-3)-1093

Charles E. Helsley
Director,
Hawaii Institute of Geophysics

ABSTRACT

This volume contains reports on seismological studies done in conjunction with other geophysical and geochemical studies of the Hawaii Geothermal Project. The studies were conducted on the easternmost portion of the East Rift Zone of Kilauea Volcano, near the eventual site of the initial well, HGP-A, drilled by the Hawaii Geothermal Project. The micro-earthquake survey by Suyenaga and Furumoto found, among other patterns of seismicity, a small cluster of events at 1-to 3-km depth in the immediate vicinity of HGP-A. Another micro-earthquake survey conducted by Mattice and Furumoto over a high electrical conductivity anomaly located west of HGP-A found it to be probably more seismically active than the area around the well site. Norris and Furumoto contoured noise levels but found no local amplification at any frequency associated with the geothermal reservoir. However, noise may be associated with magmatic activity. The crustal structure of the area was studied with two sets of seismic refraction profiles reported by Suyenaga and by Broyles. The surface layer has a low but highly variable velocity (0.8 to 1.6 km/sec) and consists of interlayered aa and pahoehoe flows with large voids. A jump in velocity to 2.5 to 3.0 km/sec occurs near sea level and is attributed to saturation of water. A layer of velocity about 5.0 km/sec lies between the 3.0-km/sec and a 7.0-km/sec layer. The latter is interpreted as the dike complex and locally is found as shallow as 2 to 2.5 km. Furumoto combines microearthquake, source mechanism, gravity and thermal data into an interpretation of the process of geothermal reservoir formation in the East Rift Zone.

Table of Contents

Figures

Page

Tables

MICROEARTHQUAKE STUDY OF THE EAST RIFT ZONE OF KILAUEA, PUNA, HAWAII

W. Suyenaga and A.S. Furumoto

Hawaii Institute of Geophysics
University of Hawaii
Honolulu, Hawaii 96822

ABSTRACT

A seven-seismometer array centered on the east rift of Kilauea Volcano in Puna, Hawaii was deployed during a three-week period in summer, 1974 as part of the Hawaii Geothermal Project. Comparison with earthquake counts in the area by a station of the Hawaiian Volcano Observatory's network showed that the recording period was one of slightly greater than normal activity but did not contain the large swarms that occasionally occur. The array recorded events down to magnitude -0.8. Two categories of events are analyzed. Earthquakes from the portion of the east rift near the Kilauea summit indicate that high velocity material extends through the rift zone to the Puna area. Earthquakes in the vicinity of the array were evenly distributed to a depth of 7 km in a 3 km-wide band vertically beneath the surface expression of the rift zone. Below 7 km, hypocenters are scattered vertically beneath the rift zone and slightly to the south. With another crustal model based on recent seismic refraction, however, a band of earthquakes dipping about 60° to the south is superimposed on a cluster of shallow events (1- to 3-km depth). These latter earthquakes may be an indication of geothermal activity since many of them are 1 to 2 km beneath the site of Hawaii Geothermal Project Well A. A distinct absence of activity on the rift zone to the northeast of the network, in both the Hawaiian Volcano Observatory records and the data collected here, indicates very poor chances of finding a geothermal reservoir in that region.

INTRODUCTION

Geothermal reservoirs are characterized by high seismicity, and in some cases hypocenters of microearthquakes are useful in delineating a fault or fault zone in which hot water travels to the surface (Ward, 1972). Consequently, in support of the Hawaii Geothermal Project, a microearthquake survey was conducted during three weeks in August and September, 1974, in an area of the east rift zone of Kilauea that other studies had considered promising (e.g. Abbott, 1975; Klein and Kauahikaua, 1975.

This paper presents the survey results and compares them with a summary of data compiled over the years by the Hawaiian Volcano Observatory (HVO).

LOWER EAST RIFT EARTHQUAKES RECORDED BY THE HAWAIIAN VOLCANO OBSERVATORY

The east rift zone of Kilauea extends southward from the summit caldera for about 8 km, then bends eastward and proceeds through the Puna district of Hawaii and out to sea (Macdonald and Abbott, 313-318, 1970). The Hawaiian Volcano Observatory has for years maintained at least one seismic station near the east rift in Puna (lower east rift). The station was located in Pahoa (PAH) until 1970 when it was phased out in favor of a location at Puu Honualula (PHO)(Fig. 1). The stations are intended for long-term seismic observations and to maintain continuity over the years, so a suitable threshold is set for instrument gain to overcome some of the noise caused by adverse weather conditions and cultural activity. The lower east rift microearthquake count from the PHA and PHO records serves as a preliminary index of seismicity for that part of Kilauea's volcanic system. A monthly count of local events recorded at these stations was accumulated from HVO Summaries (Fig. 2 and Appendix). The monthly totals show scattered periods of extremely high activity (e.g. Aug-Sept 1964; Nov-Dec 1964; July 1966-Feb 1967; and July-Aug 1968) interspersed on a background of low activity. Closer examination reveals that these periods can be considered as swarms, sequences of earthquakes that have no principal event (Ward and Bjornsson, 1971). The number of recorded events during swarms (Feb-May 1970 and Aug-Sept 1975) and during background activity increased by a order of magnitude when the recording moved to Puu Honuaula. This is probably because Puu Honuaula is a quieter recording site and is closer to the seismically active region (Fig. 3) rather

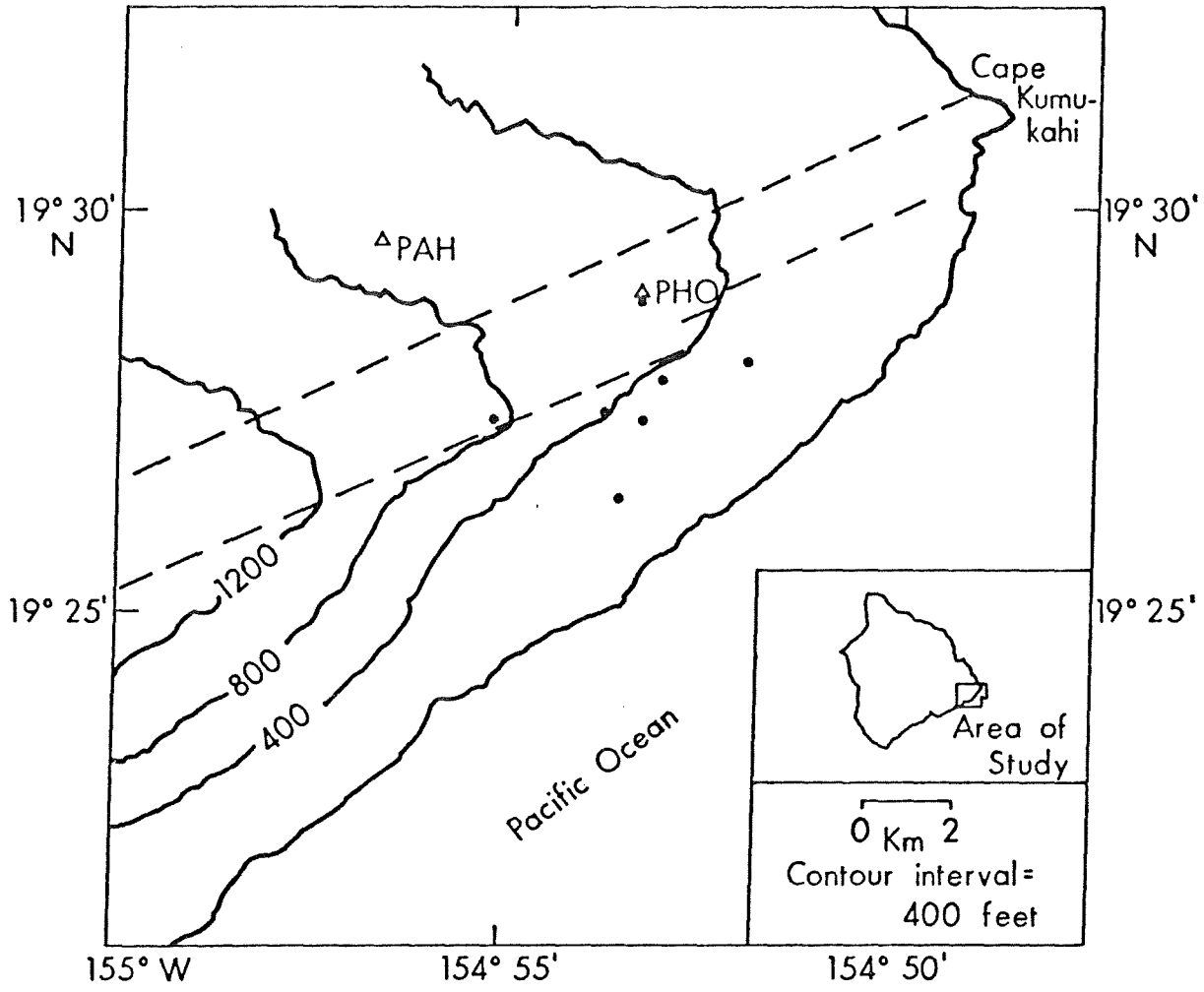

Figure 1. Map of Puna, Hawaii. Dashed lines show approximate boundaries of the surface expression of the east rift zone of Kilauea Triangles, and dots show seismometer locations of the Hawaiian Volcano observatory network and of the Malama-Ki array, respectively.

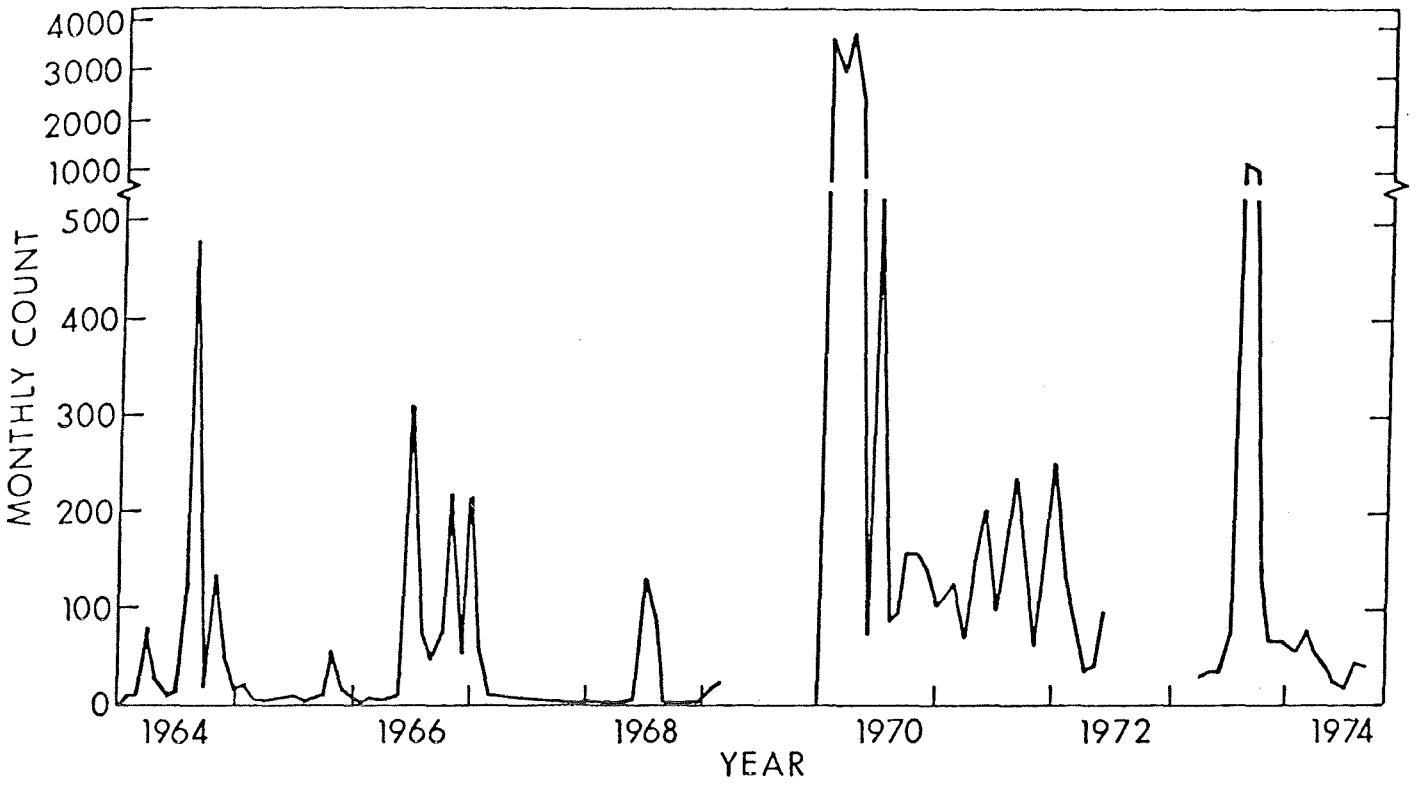

Figure 2. Monthly count of local events for the lower east rift from Hawaiian Volcano Observatory Summaries. Counts were taken from the eastern east rift category for 1964 to the first quarter of 1969 and from the lower east rift category from 1970 to 1973. Monthly count for 1974 was provided by the staff of the HVO.

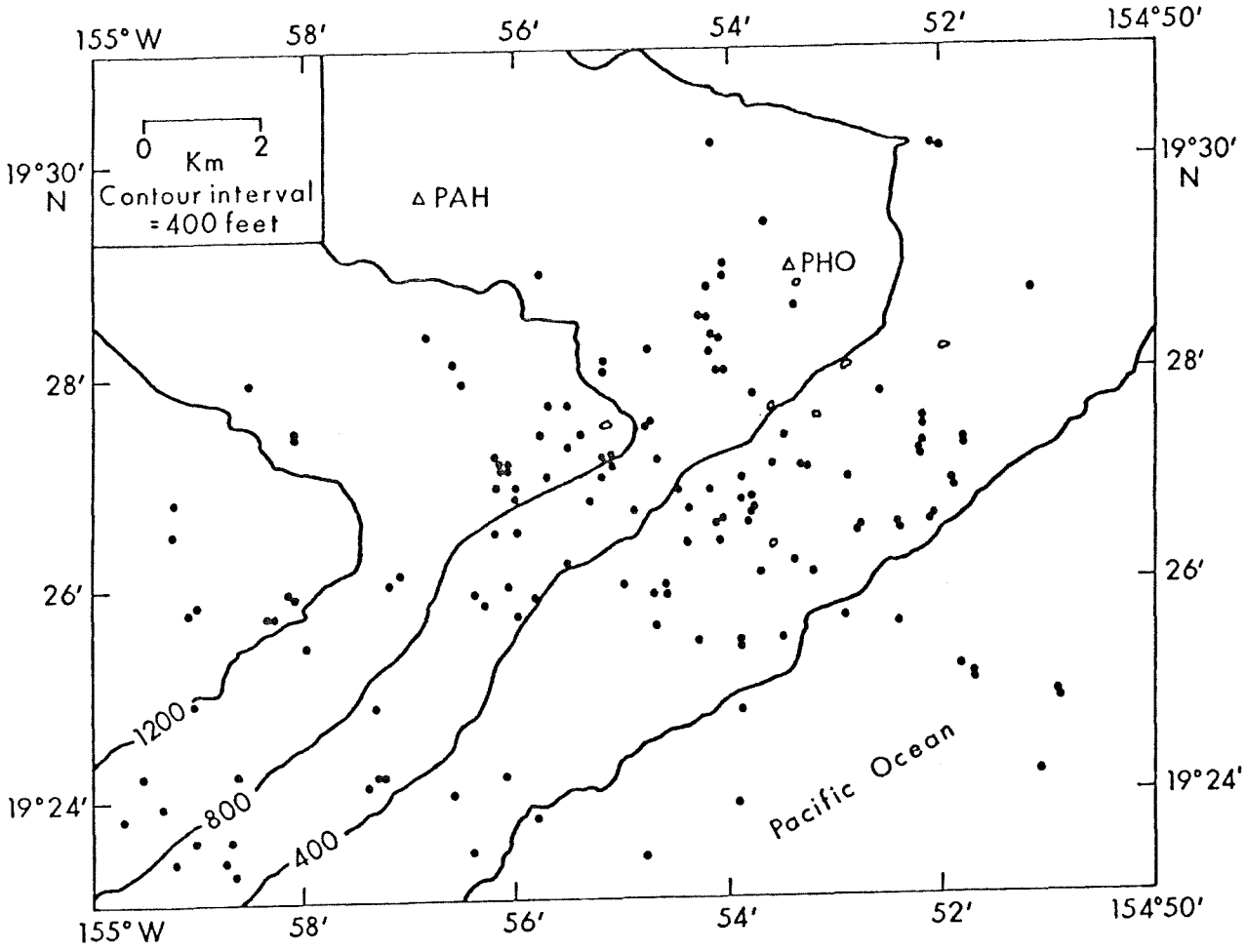

Figure 3. Epicenters of Puna district earthquakes located by the Hawaiian Volcano Observatory network, 1964-1973. Included are events with magnitude greater than 2.5 and well-determined smaller ones. The events are listed in the Appendix. Triangles show HVO stations and dots denote the epicenters. Open circles show locations of Malama-Ki array.

Table 1. Malama-Ki seismic array

Station	Latitude(N)	Longitude(W)	Elevation (m)	Station delay* (sec)
LL2	19°27.61'	154°53.61'	110	0.0
LL3	28.02'	52.91'	122	0.0
LL4	27.54'	53.21'	90	0.0
West	27.47'	55.18'	265	+0.02
South	26.35'	53.60'	66	-0.01
North	28.79'	53.40'	194	-0.01
East	28.16'	52.00'	82	+0.03

*Based on the assumption that the difference in elevation originates in the 5.1-km/sec layer.

than because of a real increase in activity.

The lower east rift (LER) count for the period January to September 1974 is shown in Fig. 2. PHO was located several hundred yards away from our North station. Our array recorded all the LER events plus a few events not included in the LER count. This is probably due to wider dispersal and higher gain settings of our instruments. The average for the entire period was 1.59 events per day. Average LER count for the 22-day period the array operated was 1.89 events/day. The maximum 22-day average was 2.95 events/day during 8-29 March. Thus our counts were taken during a period of slightly greater than normal earthquake activity for 1974, but certainly not during a period of peak activity.

In addition to LER event counts, all earthquakes with eipcenters located in our area of study were gathered from the HVO Summaries (Appendix) and plotted in Fig. 3. Comparison with our results will be discussed later.

FIELD METHODS

The base station was located just outside the University of Hawaii Agricultural Experiment Station at Malama-Ki. Henceforth, our array will be referred to by the latter name. The Malama-Ki array consisted of seven stations (Fig. 1 and Table 1). Near the base were three stations (LL2, LL3 and LL4), each of which was a Mark Product L4C 1-Hz geophone and a Sprengnether AS-110A seismic amplifier modified to produce an FM output. The signals from the three near stations were transmitted by wire to the base station and there multiplexed and recorded. Configuration at four distant stations (North, East, South, and West) was the same except that between the amplifier and multiplexing was a ST Communication VHF/FM transmitter-receiver. The three land-line and four telemetered multiplexed signals were each recorded on one channel of a Hewlett-Packard 3960 Instrumentation Recorder. The two remaining tape channels recorded second ticks and WWVH broadcast with audio comments. The response of the recording system at the gain and filter settings used (78-db gain, to 5-30-Hz filter band) is shown in Fig. 4.

At station LL2, a portable seismometer (Sprengnether MEQ-800) produced a paper recording for each day, which was used to identify events and their approximate arrival times.

The survey was conducted during 16 August to 9 September, 1974. No unusual problems were encountered in setting up the

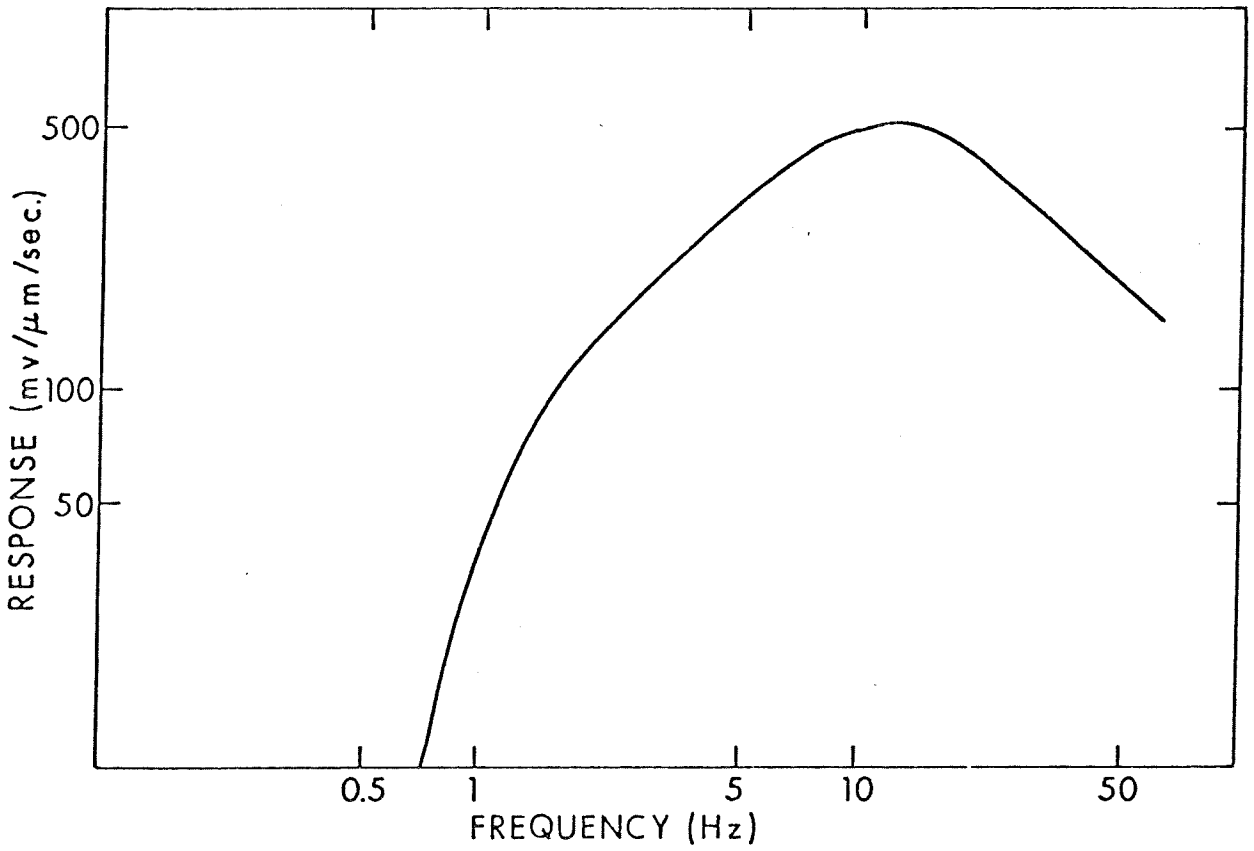

Figure 4. Malama-Ki system response at 78-db gain and 5- to 30-Hz passband filter.

system. The tape recorder generated so much heat that an air conditioning system was required, so a generator was on almost continuously. This precluded the use of a fourth land line seismometer near the base station.

From 20 August, recording was continuous except for a three-day period (25 to 27 August) when the tape recorder needed repair, periods of not more than three hours for maintenance at the base, and periods of poor transmission from the telemetered stations caused by low battery levels. A rotating system of battery replacement alleviated the latter problem. About 357 hours of recording was collected.

DATA ANALYSIS

Calculation of hypocenters

Recordings of most of the earthquakes were played back directly through a Visicorder Model 406B with galvanometer M400-120. Some of the smaller events were first amplified so the P arrivals would be as clear as possible.

Hypocenters were calculated with HYP071, a computer program provided by the U.S. Geological Survey,(Lee and Lahr, 1971). various test parameters within the program were developed for California earthquakes and seismic arrays, some were changed according to suggestions in Lee and Lahr (1974). On the recommendation of Ward and Gregerson (1973), the critical F-parameter for the multiple regression test was set to 0.5.

Two crustal models were used in the hypocenter calculation. The first was the revised general model by Ward and Gregerson (1973) (Table 2). Earlier, Hill (1969) developed crustal models based on seismic refraction along the coastline of Hawaii. One of Hill's (1969) recording units was located near Cape Kumukahi just north of the rift zone with shots fired along the southeastern coast (Fig. 1). As pointed out later in this paper, the rift zone probably has a high velocity core with lower velocity flanks. The paths used by Hill (1969) traversed both regions; this may be the reason why a simple two-dimensional model could not be resolved. Hypocenters recalculated using a model similar to Hill's (Table 2) yielded almost indentical epicenters with depths within the 2-km error of those calculated using the Ward and Gregerson (1973) model. The crustal model on refraction work done by the Hawaii Geothermal Project and reported by Broyles et al. (1978) is characterized by a shallow 7.0-km/sec layer when compared with the other models (Table 2).

One of the problems encountered in hypocenter determination was due to the sensitivity of HYP071 to the choice of

Table 2. Crustal models

Ward and Gregerson (1973) Model A		Hill (1969) Cape Kumukahi*		Broyles et al. (1978)	
Velocity (km/sec)	Depth to top of layer (km)	Velocity (km/sec)	Depth to top of layer (km)	Velocity (km/sec)	Depth to top of layer (km)
1.8	0.0	1.8	0.0	1.0	0.0
				2.5	0.15
3.1	0.2	3.1	0.2	2.9	0.3
5.1	1.7			5.7	1.6
6.7	5.4	6.8	4.0	7.0	2.3
				7.4	9.2
8.3	13.2	8.3	13.2	8.3	13.2

*Top two layers are from Model A. Lower layers were approximated from the range of alternatives given by Hill for the Cape Kumukahi line along the Kau-Puna coast.

initial hypocenter in its iteration process. The initial trial hypocenter is 5 km under the station with the earliest arrival. For distant earthquakes, the HYP071 solution may be a local RMS minimum of station residuals that is nearer the array than the real location. To separate near and distant events, a list of possible distant events was made on the basis of the assumption that at all stations they produce records of approximately equal duration and frequency. The pattern of arrivals across the array indicated that almost all of the events originated to the west of the array. HYP071 was used to caluclate hypocenters with an initial hypocenter (19 21.5'N, 155 15'W, 5-km depth) in the vicinity of the Kilauea summit (Table 3 and Fig. 5). Station residuals for these hypocenters were usually less than or equal to those for the hypocenters near the array; however, the accuracy, particularly in distance, of the newly calculated hypocenters is probably poor since the array is situated far to one side.

Hypocenters of earthquakes near the Malama-Ki array were located by HYP071, and only a station delay (Table 1) was used for differences in elevation. The hypocenters are shown in Figs. 7-10 and are listed in Tables 4 and 5 . The concentration of hypocenters at 5-km depth is probably an artifact of the choice of that depth as the starting point of the iteration. For most events the horizontal and vertical errors are on the order of one km or less. Events with larger errors were discarded, except for six listed in Table 4 that were kept because they were well recorded.

Magnitude

The general formula for local magnitude is $M_L = \log D - \log D_0$ where D is displacement and D_0 is displacement for a $M_L = 0$ earthquake. O'Neill and Healy (1973) showed that for P waves of Parkfield, California earthquakes, $D_0 = 0.28r^{-1.7}$ where D_0 is in microns and r, the hypocentral distance, is in kilometers. Using this value,

$$M_L = \log D - \log 0.28 + 1.7 \log r. \qquad (1)$$

From (1), M_L for some earthquakes near Malama-Ki were calculated (Table 6). Determination of magnitude was hampered by the low dynamic range of the FM equipment which, coupled with the high amplification levels, caused the recordings of many of the larger earthquakes to be off scale. The recording system clipped at magnitude greater than about 0.5 and was able to record events down to about -1. The range in M_L was -0.8 to 0.3. The magnitudes of many of the very small earthquakes were not used in the following analysis.

Another way of calculating earthquake magnitude is to measure its duration time--that is, the time from initial P

Table 3. Distant earthquakes

		HVO location				Malama-Ki location			P residuals						
Date	Time	Lat(N)	Long(W)	Z	Mag	Lat(N)	Long(W)	Z	LL2	LL3	LL4	N	E	S	W
740822	2223	19 19.0	155 15.4	6	1.6	19 21.5	155 15.0	9	+.08		.00			+.15	+.10
740830	1830	20.3	12.1	7	2.5	27.7	12.7	5			+.01	.00		+.15	-.35
740831	2042	20.2	17.8	26	3.1	29.9	22.8	5	+.24	.00	+.01	+.01	+.08	+.15	+.03
740902	0529	21.5	14.9	25	2.2	30.1	18.6	5	.00	-.07	+.07	.00		+.15	
740906	1324	22.4	24.3	8	2.4	16.3	18.1	5							

Hypocenter data calculated with crustal model
from Ward and Gregerson (1973)

Table 4.

Date	Time	Epicenter Lat N	Epicenter Long W	Depth km	No. Sta.	RMS	ERH	ERZ	QM
740823	1557	19-28.89	154-54.46	1.74	4	0.03			C1
740824	0923	19-29.38	154-55.75	2.29	5	0.06	10.1	11.7	D1
740828	2123	19-26.51	154-53.99	14.32	5	0.01	0.5	1.7	C1
740828	2243	19-28.84	154-54.09	2.66	5	0.01	0.4	0.8	C1
740829	0035	19-26.99	154-54.00	12.56	6	0.01	0.6	1.9	C1
740829	1532	19-28.70	154-54.11	1.79	5	0.01	0.2	0.5	C1
740829	1539	19-28.89	154-54.66	7.44	4	0.01			C1
740829	1747	19-28.36	154-53.55	1.63	6	0.03	0.4	0.1	C1
740829	2257	19-28.12	154-53.36	1.77	4	0.02			C1
740830	2030	19-28.89	154-53.70	2.40	6	0.04	0.9	0.9	C1
740830	2242	19-28.89	154-54.01	2.30	5	0.06	2.4	1.9	C1
740831	0736	19-29.56	154-54.07	5.00	5	0.02	1.6	2.0	C1
740831	0859	19-28.76	154-53.37	9.48	7	0.01	0.3	0.8	B1
740831	0900	19-27.92	154-57.21	8.13	4	0.01			C1
740831	1449	19-28.44	154-53.75	1.45	4	0.00			C1
740831	2007	19-28.19	154-55.28	5.00	5	0.04	0.5	1.4	C1
740831	2242	19-28.10	154-55.28	9.38	7	0.03	2.1	4.5	C1
740901	0156	19-27.93	154-53.68	9.80	7	0.01	0.4	1.7	B1
740901	0619	19-29.79	154-56.51	0.06	4	0.01			C1
740901	1535	19-28.49	154-53.02	2.36	4	0.00			C1
740901	1717	19-30.06	154-53.50	1.44	4	0.06			C1
740902	0025	19-28.89	154-52.52	3.80	5	0.03	2.1	1.9	C1
740902	0144	19-31.65	154-54.04	0.61	5	0.01	21.1	21.5	D1
740902	1232	19-29.20	154-54.90	4.03	4	0.02			C1
740902	1545	19-27.91	154-53.57	13.15	6	0.02	1.5	7.7	D1
740902	1600	19-28.56	154-54.71	5.00	5	0.06	1.1	1.8	C1
740902	1857	19-28.89	154-53.86	2.13	4	0.01			C1
740902	2109	19-30.02	154-53.50	5.00	5	0.06	0.4	0.4	C1
740902	2117	19-27.42	154-55.87	5.00	5	0.01	1.0	1.3	C1
740902	2240	19-29.61	154-54.36	4.31	4	0.01			C1
740902	2309	19-29.46	154-53.96	2.70	6	0.04	3.3	1.8	D1
740902	2311	19-29.20	154-54.79	4.19	4	0.01			C1
740903	0502	19-28.11	154-53.77	2.44	5	0.00	0.1	0.1	C1

740903	0502	19-28.11	154-54.79 154-53.77	4.19 2.44	4 5	0.01 0.00	0.1	0.1	C1 C1
740903	1142	19-27.71	154-56.21	5.00	5	0.03	2.3	2.8	C1
740903	2044	19-28.08	154-54.18	2.14	6	0.01	0.1	0.2	D1
740904	1422	19-27.22	154-53.45	7.52	6	0.02	0.7	2.1	C1
740905	0051	19-29.71	154-54.14	5.00	5	0.04	7.5	10.0	D1
740906	2319	19-29.67	154-53.50	5.00	5	0.08	4.8	5.7	D1
740909	0211	19-28.54	154-55.97	5.00	6	0.09	8.9	11.3	D1

Hypocenter data calculated with crustal model
from Broyles et al. (1978)

Table 5.

Date	Time	Epicenter Lat N	Epicenter Long W	Depth km	No. Sta.	RMS	ERH	ERZ	QM
740823	1557	19-28.41	154-53.64	1.48	4	0.00			C1
740824	0923	19-29.97	154-56.28	1.58	5	0.08	20.1	23.6	D1
740828	2123	19-26.22	154.53.82	13.43	5	0.01	0.3	0.8	C1
740828	2243	19-30.07	154-53.96	5.00	5	0.02	3.2	3.5	D1
740829	0035	19-26.93	154-54.01	11.83	6	0.01	0.6	2.0	C1
740829	1531	19-30.31	154-54.00	5.00	5	0.03	3.4	3.3	D1
740829	1539	19-28.89	154-54.68	6.66	4	0.01			C1
740829	1747	19-29.69	154-53.71	5.00	6	0.13	2.1	2.6	C1
740829	2257	19-31.46	154-56.45	0.41	4	0.10			C1
740830	2030	19-29.21	154-53.68	2.14	6	0.03	0.8	0.2	C1
740830	2242	19-30.49	154-55.25	2.11	5	0.10	15.8	82.6	D1
740831	0736	19-29.61	154-54.14	3.46	5	0.02	2.0	1.4	C1
740831	0859	19-28.79	154-53.33	8.46	7	0.01	0.3	0.9	C1
740831	0900	19-27.95	154-57.38	5.00	4	0.01			C1
740831	1449	19-28.38	154-53.74	1.21	4	0.00			C1
740831	2007	19-27.98	154-55.28	5.00	5	0.04	0.8	1.8	C1
740831	2242	19-28.00	154-55.44	9.25	7	0.03	2.7	6.2	D1
740901	0156	19-27.95	154-53.63	10.01	7	0.01	0.5	2.5	B1
740901	0619	19-53.23	155-24.91	1.12	4	0.04			C1
740901	1535	19-28.48	154-53.04	2.20	4	0.00			C1
740901	1717	19-30.57	154-56.00	0.63	4	0.08			C1
740902	0025	19-29.67	154-51.43	2.29	5	0.02	9.5	48.5	D1
740902	0144	19-30.40	154-52.21	0.52	5	0.05	1.0	0.4	C1
740902	1232	19-29.48	154-55.26	2.78	4	0.02			C1
740902	1545	19-27.94	154-53.63	12.47	6	0.02	1.5	8.0	D1
740902	1600	19-28.79	154-54.89	5.00	5	0.07	1.7	2.3	C1
740902	1857	19-28.89	154-53.99	1.76	4	0.01			C1
740902	2109	19-32.89	154-53.50	5.00	5	0.08	121.6	42.0	D1
740902	2117	19-27.43	154-55.91	2.49	5	0.01	1.3	7.8	D1
740902	2240	19-30.00	154-54.66	3.26	4	0.00			C1
740902	2309	19-28.76	154-53.50	1.64	6	0.05	2.2	1.9	C1
740902	2311	19-29.48	154-55.12	3.13	4	0.01			C1
740903	0502	19-28.12	154-53.75	2.14	5	0.01	0.1	0.1	C1

	0502	19-28.12	154-53.75	2.14	5	0.01	0.1	0.1	C1
740903	1142	19-27.71	154-58.14	5.00	5	0.02	6.7	7.0	D1
740903	2044	19-28.58	154-54.32	5.00	6	0.05	0.4	1.0	C1
740904	1422	19-27.20	154-53.48	6.81	6	0.02	0.7	2.3	C1
740905	0051	19-30.35	154-54.10	3.30	5	0.05	14.5	8.1	D1
740906	2319	19-30.28	154-53.50	5.00	5	0.10	11.1	9.3	D1
740909	0211	19-28.79	154-56.56	2.59	6	0.09	15.9	17.5	D1

Table 6

Comparison of Magnitudes and Duration Time

for Malama-Ki Earthquakes

Date yr.mo.day	Time hr.min.	M_L	Duration (sec)
740823	1557	-0.5	6.5
24	0923	-0.1	6.5
29	1747	-0.7	8.5
29	2257	-0.8	8.5
30	2030	-	8.0
30	2242	-	7.5
31	2007	-0.2	4.5
31	2242	-	9.5
740901	0156	+0.3	7.0
01	0619	-	5.0
01	1535	-0.8	4.5
02	0025	-	21.0
740902	0144	-	7.0
02	1545	-	16.0
02	1600	-0.5	2.5
02	1857	-1.1	-
02	2109	-0.1	4.0
02	2117	0.0	4.8
02	2309	-0.4	5.5
02	2311	-	2.5
04	1422	0.0	10.0
05	0051	-0.5	3.2
06	2319	-0.7	2.4
09	0211	-0.2	-

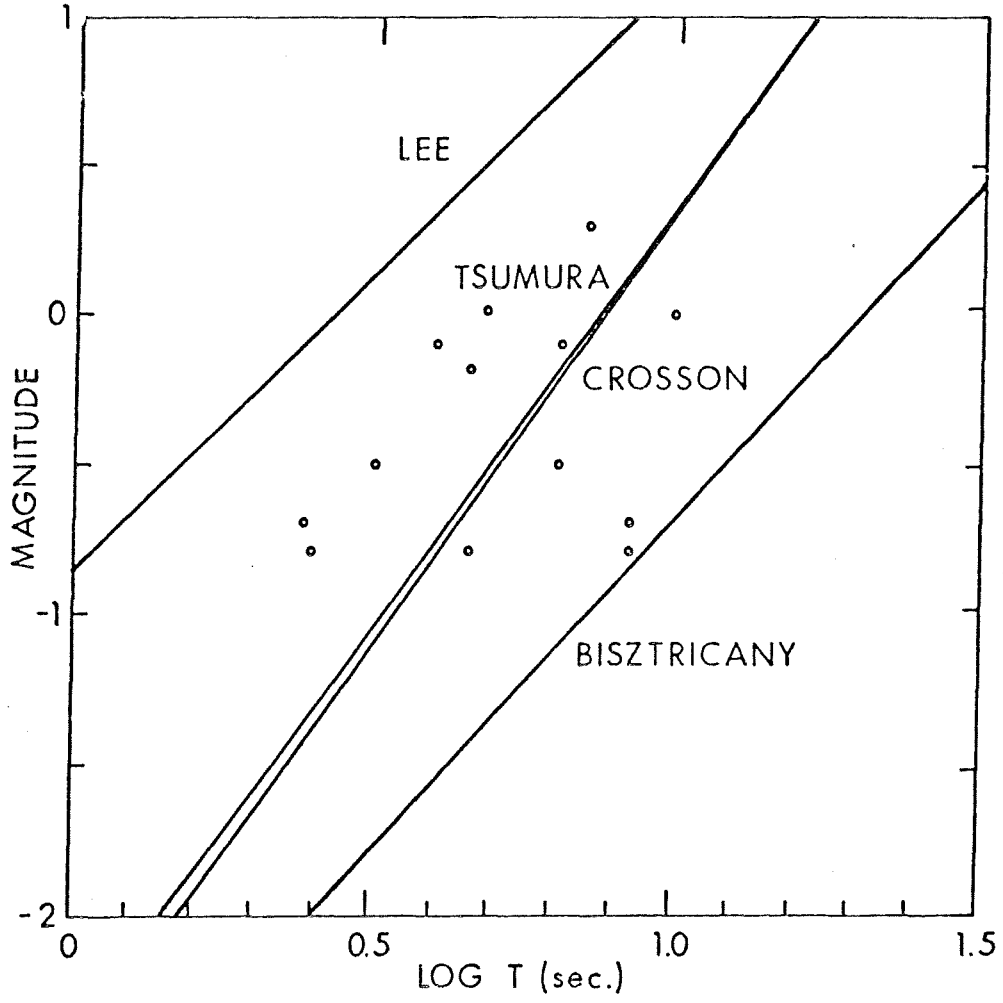

Figure 6. Magnitude versus duration for some microearthquakes near the Malama-Ki array. Dots indicate magnitude and duration for events listed in the Appendix. Lines are extrapolations of magnitude-duration relationships derived at greater magnitudes (Table 5).

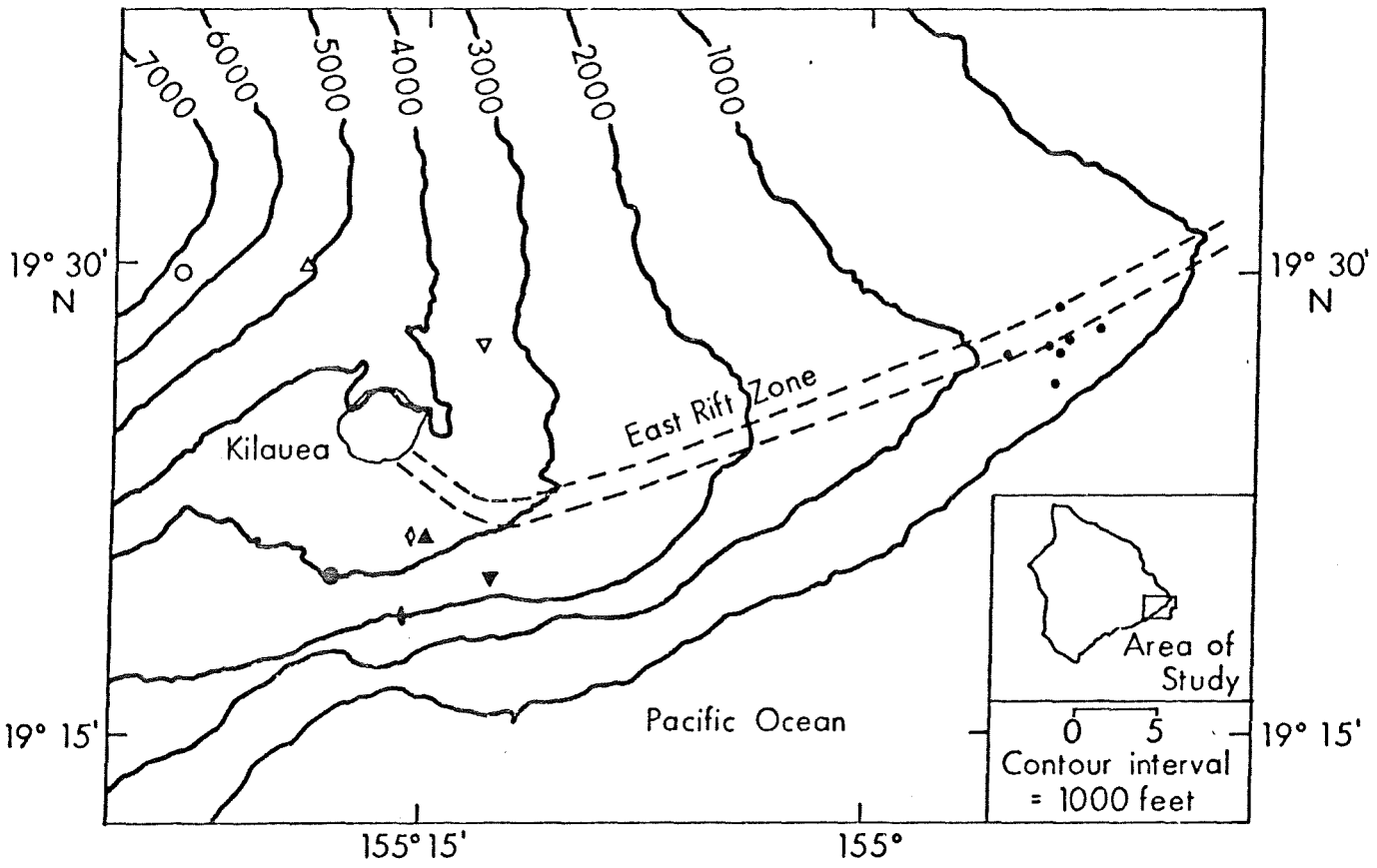

Figure 5. Earthquakes near the Kilauea summit. Solid and open symbols denote epicenters by Hawaiian Volcano Observatory and Malama-Ki array, respectively. Symbols denote following earthquakes (Table 3): ◊ - 222223, ▽ - 301830, 0 - 312042, Δ - 020529. Dashed lines show approximate boundaries of the surface expression of the east rift zone. Dots indicate stations of the Malama-Ki array.

arrival to the point where the earthquake signal reaches noise level. The relation between magnitude (m) and duration time (T) is of the form

$$m = a + b \log T + c\Delta$$

where a, b, and c are constants, T is in seconds, and Δ is the hypocentral distance (Real and Teng, 1973). If Δ is in kilometers, c is on the order of 0.001 and thus is negligible in our case. Table 4 lists values of a and b calculated in different studies along with the magnitude range of the earthquakes measured.

The duration times for the earthquakes near the Malama Ki array were measured and averaged (Table 6). These times were plotted against the magnitudes calculated earlier along with extrapolations of the four magnitude-duration relationships listed in Table 7 and plotted in Figure 6. The correlation of duration time with magnitude is similar to that of the other studies. All values but one fall within the bounds of the extensions of the other studies, which suggests that such linear extrapolations can be made, although more data would be needed to make such a statement convincing.

9° 30' N

RESULTS AND DISCUSSION

Earthquakes from the Upper East Rift

° 15'

A number of recorded events that occurred on the upper portion of the east rift zone (near the Kilauea summit) were also located by the Hawaiian Volcano Observatory (R. Koyanagi, written communication) (Table 7). Four such earthquakes were located northward by the Malama-Ki array (Fig. 6). (A fifth earthquake, on 06 September at 1320h, occurred on the west side of the Kilauea summit. Its path to Malama-Ki included the heterogeneous area under Halemaumau and thus was not subjected to the following simple analysis.)

With HYP071, the HVO hypocenter was assumed to be fixed and travel times were calculated to the stations in the array. Results showed a delay at South station relative to the rest of the array of about 0.1 to 0.2 (Table 7). With the exception of an extremely early arrival at West and a late one at LL2, this pattern of residuals indicates a consistently late arrival at South. Examination of the arrival times showed that North, LL2, LL3, LL4, and South arrivals were nearly equal, West was advanced, and East was delayed, indicating a source to the west of the array, whereas the real source was to the southwest. Ward and Gregerson (1973) and Ellsworth and Aki (1975) showed that the east rift near the summit consists of higher velocity material. We propose that the high velocity material continues through the entire rift zone, coinciding with a gravity maximum over it (Kinoshita, 1965;

Table 7. Magnitude-duration relationships

Reference	a	b	Magnitude range	Area
Crosson (1972)	-2.46	2.82	1.7 - 4	Puget Sound
Lee et al. (1972)	-0.87	2.00		Central California
Tsumura (1967)	-2.53	2.85	1 - 5	Honshu
Bisztricsany (1958)	-2.92	2.25		East Europe

Furumoto et al., 1976). Seismic energy of earthquakes near the summit travels mostly through the faster zone to the Malama-Ki array. Since South station is the only one significantly off the rift (Fig. 5), energy travels to it through lower velocity material after being refracted off the rift zone, thus explaining the delay.

Earthquakes near the Malama-Ki array

Calculated hypocenters of earthquakes near the summit indicated a delay at South station. To see whether there was a similar delay at South for the events near the array, these events were divided into those with South arrivals and those in which South arrivals were not recorded or were not used in hypocenter determination (Fig. 7). There is no separation between the hypocenters of two groups, implying that any delay had little effect on epicenter calculation (Figs. 7 and 8).

As a further test, the hypocenters of earthquakes with usable south arrivals were relocated after having been corrected for a 0.2-sec delay at South station. Earthquakes with depths less than 5 km were relocated deeper and slightly southward. In either case, most of the earthquakes occur within the 3-km band vertically beneath the surface rift zone.

For earthquakes deeper than about 6 km, the effect of compensation for a delay at South caused hypocenters to migrate toward it or shallower and southward, but even these locations were scattered over a wide area. Thus the pattern of hypocenters of these few earthquakes does not delineate an unambiguous zone tending either vertically or toward the south.

On the other hand, with the crustal model of Broyles et al. (1978) (Table 2), a definite southward-dipping pattern of about 60° is noted (Fig. 10). This is superimposed on a cluster of events between 1- and 3- km depth. Although there have been suggestions that the rift zone dips southward (e.g. Moore and Krivoy, 1964), Macdonald (1965) and Fiske and Jackson (1972) present considerable evidence for a vertical rift zone. Combined with seismicity (Koyanagi et al., 1972) and geodetic (Swanson et al., 1971) studies that indicate that the south flank is mobile, the present situation is either that magma is injected into a vertical rift zone that in turn pushes the south flank seaward or that magma intrudes into a vertical zone of weakness caused by gravitational stresses within the flanks. Our study, however, presents conflicting results (Figs. 8 and 10) concerning the orientation of the rift zone.

Earthquakes occur within the entire southern flank of Kilauea and might not be due to the mechanism of intrusion but to the resultant movement of the whole flank (Koyanagi et al., 1972). Deeper earthquakes might be part of this

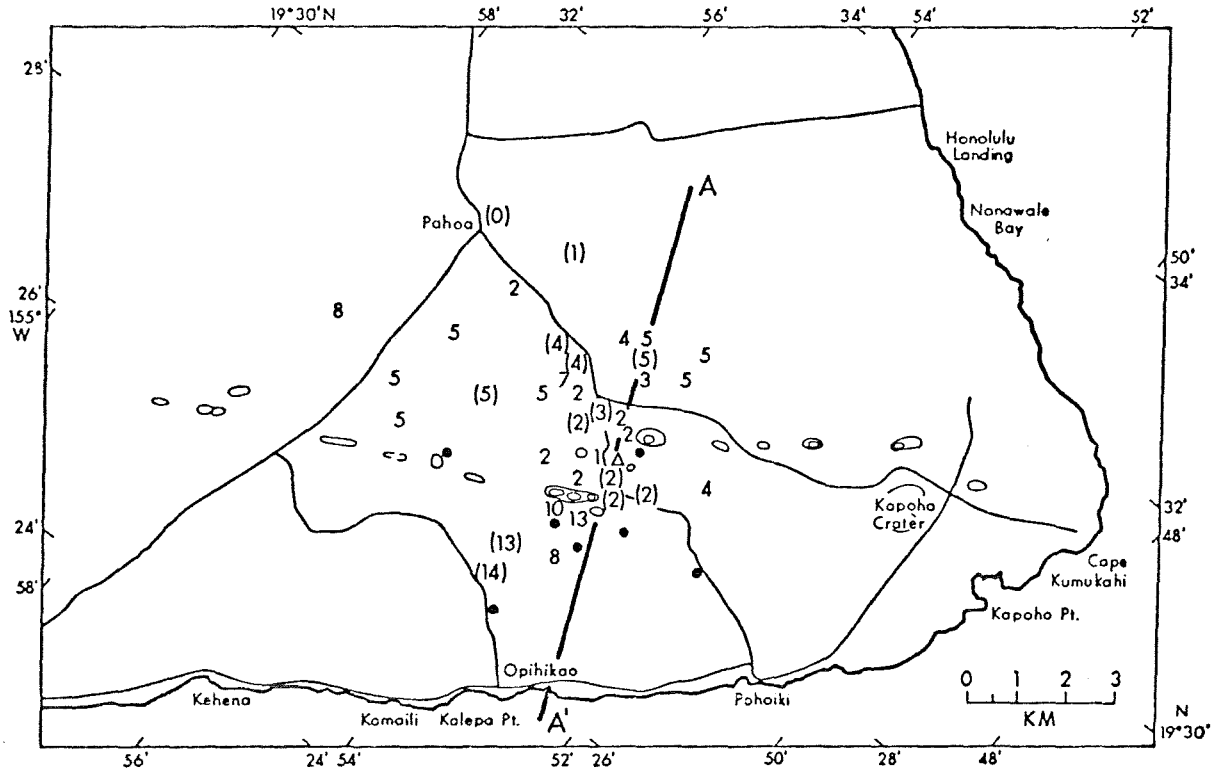

Figure 7. Epicenters of earthquakes near the Malama-Ki array with crustal model A of Ward and Gregerson (1973). Solid dots are seismometer locations; triangle is site of HGP Well A. Numbers on the epicenters indicate depth in kilometers. Numbers in parentheses indicate epicenters calculated without South station data.

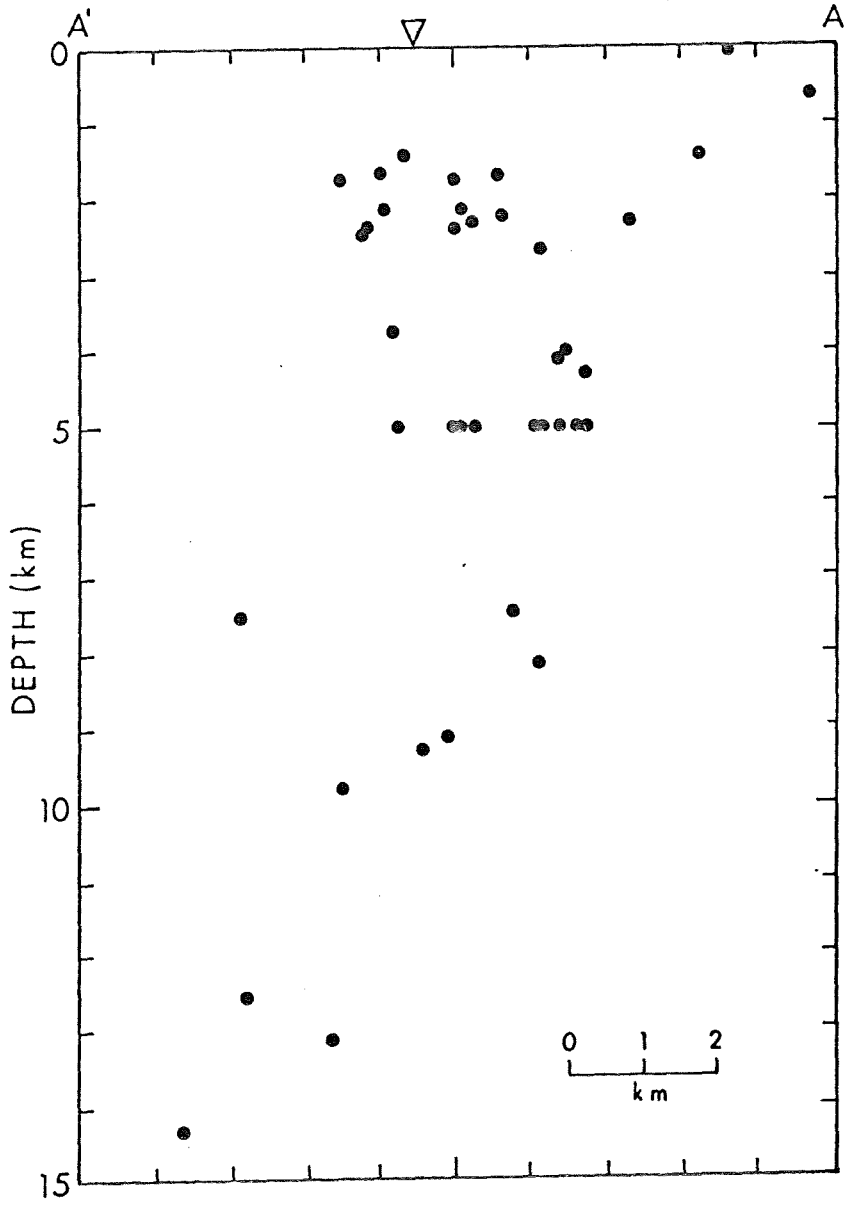

Figure 8. Projection of hypocenters along plane with surface trace AA' in Figure 7. Triangle is location of HGP Well A.

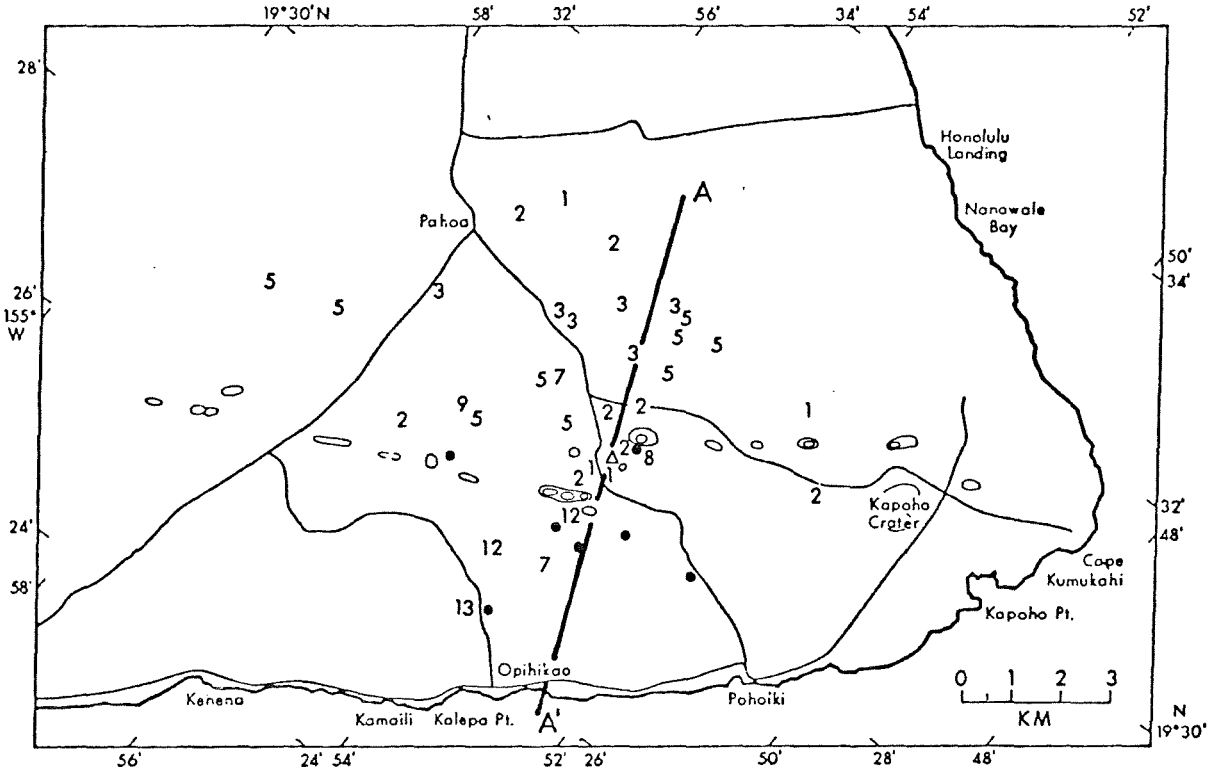

Figure 9. Epicenters of earthquakes near the Malama-Ki array with crustal model of Broyles et al. (1978). Solid dots, triangle, and numbers have same meaning as in Figure 7.

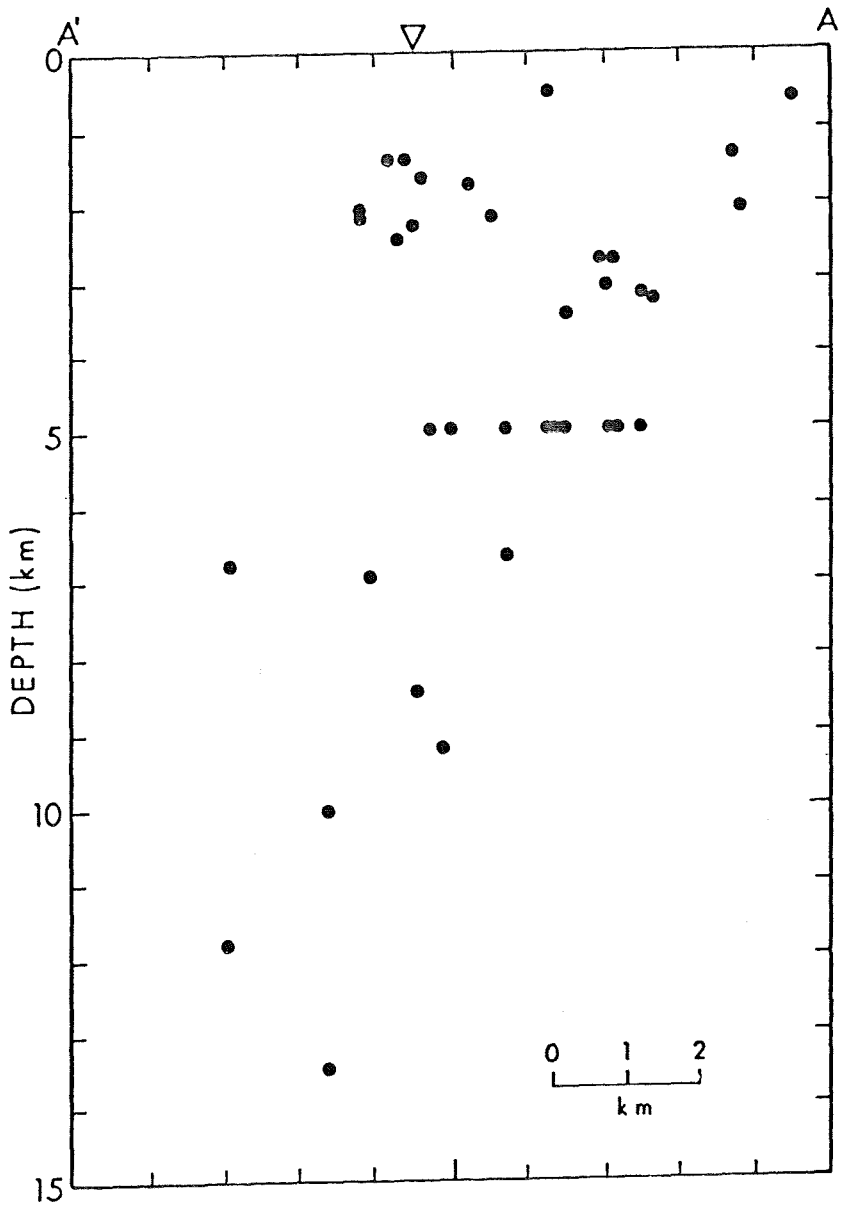

Figure 10. Projection of hypocenters along plane with surface trace AA' in Figure 9. Triangle is location of HGP Well A.

process, whereas shallower events can be directly attributed to the after-effects of dike intrusion. Fault mechanism solutions would help clarify the situation but were not done in this study.

Epicenters shown in (Fig. 3) were calculated by the HVO network in which most of the stations are near the Kilauea summit with at least one station in the Puna area. As a result of this control these epicenters are more reliable than the Malama-Ki epicenters near the summit. The HVO earthquakes were scattered throughout the rift zone and on its south flank. Those that occurred during swarms were concentrated near our West station and slightly to the south, fairly close to the activity during our survey.

A noticeable lack of activity in the rift zone to the northeast of Puu Honuaula also was apparent on our survey (Fig. 7). This area is not entirely lacking in seismicity--considerable activity was associated with the Kapoho eruptions of 1955 and 1960 (Macdonald and Abbott, 1970 --pp. 84-97,) but evidently there is no non-volcanic seismicity. Other evidence for a discontinuity in the rift zone at Puu Honuaula includes recent eruptive vents, and the pattern of self potential (C. Zablocki, pers. comm., 1975) and gravity (R. Norris, pers. comm., 1975) anomalies. On the other hand, Richter et al. (1964), on the basis of the orientation of cracks and vents, imply that the rift zone is continuous through this feature. If the discontinuity is real then perhaps its cause is that the buttress against Mauna Loa dies out in this area. A test for this would be to see whether deformation measurements show movement northward and southward.

Geothermal Prospects

Ward (1972) reviewed the use of microearthquakes in geothermal prospecting. Hamilton and Muffler (1972) located a fault zone 4 km long and 1 km wide in the Geysers area of California. Ward and Jacob (1971) located microearthquakes in the Ahuachapan area of El Salvador that fell on a plane interpreted as a fault along which hot water rose toward the surface. Ward and Bjornsson (1971) showed that microearthquakes in Iceland occurred in a number of zones, most of which coincided with geothermal areas. Their data support the hypothesis that earthquake swarms occur in regions where the crust is weakened so that it supports only small stresses.

For several reasons, it is difficult to compare these studies with the present one in Puna. For one, the surveys reported in Ward (1972) were done in "major zones of high temperature". For instance, the boundary of the thermal area at Krisuvik, Iceland encompasses about 70 km^2 with microearthquake activity concentrated in a smaller portion within that area (Ward and Bjornsson, 1971). The geothermal reservoir in

Puna, if it exists, may be smaller than a few square kilometers and probably is not as powerful as the Geysers. Therefore it will produce less seismic activity, and locating it will be more sensitive to hypocenter accuracy than locating a larger field. Second, in the Puna area, seismicity in the east rift zone is not confined spatially but extends over the crest of the entire rift zone and on its south flank (Koyanagi et al., 1972). If the activity were entirely geothermal then the summit and upper east rift would be considered better geothermal sources. However, much of the activity is probably from sources other than a geothermal reservoir, such as the settling of the volcanic mass especially after a magmatic event (Koyanagi et al., 1972).

With all these difficulties plus the fact that hypocenter patterns shown in Figures 8 and 10 clearly do not fall along a single plane but rather in 2- to 3- km-wide bands, it was first thought that these results could not be used to determine a specific drilling location. However, after the successful drilling of Hawaii Geothermal Project Well A (see Figs. 7 and 9 for location), it was noted that a cluster of shallow earthquakes in the vicinity of the well could possibly be related to geothermal activity (Fig. 8). The hypocenter pattern based on crustal model by Broyles et al. (1978), which became available after drilling had commenced, further emphasized the isolation of the events near the well site from the other events.

The seismicity of Puna can be applied to geothermal prospecting in a negative sense. The lack of activity in the Kapoho region indicates that Kapoho is not likely to be a geothermal reservoir despite the recent activity there.

ACKNOWLEDGMENTS

The authors extend special thanks to Zig Ching, who assisted in all phases of the study and was particularly valuable in the field work. Bob Koyanagi kindly provided advice and allowed the use of records at the Hawaiian Volcano Observatory. Carrol Dodd designed and built the seismic recording system and assisted in the field work. Roger Norris and Seth Thompson also assisted in the field work. Mr. Higashi of the University of Hawaii Agricultural Station at Pahoa and Y. Okamura were very cooperative while we were recording. Mike Broyles helped in the data analysis. Carol Yasui coordinated the entire effort.

REFERENCES

Abbott, A. T., 1975. Photogeologic survey: Imagery from infrared scanning of the rift zones of Kilauea and Mauna Loa. In Hawaii Geothermal Project Summary Report for Phase 1, p. 29-32, Univ. of Hawaii.

Bisztricsany, E., 1958. A new method for the determination of the magnitude of earthquakes. Geofiz. Kozlemen., v. 7, p. 69-96.

Broyles, M.L., W. Suyenaga and A.S. Furumoto, 1978. Structure of the East Rift of Kilauea Volcano, Hawaii, from seismic and gravity data. Submitted to J. Volcanol. and Geothermal Res.

Crosson, R. S., 1972. Small earthquakes, structure and tectonics of the Puget Sound region. Bull. Seismol. Soc. Am., v. 62, p. 1133-1171.

Ellsworth, W. L. and K. Aki, 1975. High-resolution lateral crust and upper mantle structure of Kilauea volcano, Hawaii, (abstract). Eos Trans. AGU, v. 56, p. 394.

Fiske, R. S. and E. D. Jackson, 1972. Orientation and growth of Hawaiian volcanic rifts: The effect of regional structure and gravitational stresses. Proc. Roy. Soc. Lond. A, v. 329, p. 299-326.

Furumoto, A. S., R. Norris, M. Kam and C. Fenander, 1976. Gravity profile and the intrusive zone. Hawaii Geothermal Project Initial Phase II Progress Report, p. 26-31, Univ. of Hawaii.

Hamilton, R. M. and L. J. P. Muffler, 1972. Microearthquakes at the Geysers, California, geothermal area, J. Geophys. Res., v. 77, p. 2081-2086.

Hill, D. P., 1969. Crustal structure of the island of Hawaii from seismic-refraction measurements. Bull. Seismol. Soc. Am., v. 59, 101-130.

Kinoshita, W. T., 1965. A gravity survey of the island of Hawaii. Pacific Sci., v. 19, p. 339-340.

Klein, D. P. and J. P. Kauahikaua, 1975. Geoelectric-geothermal exploration on Hawaii Island: Preliminary results. Hawaii Inst. Geophys. Report HIG-75-6, 23 pp.

Koyanagi, R. Y., D. A. Swanson and E. T. Endo, 1972. Distribution of earthquakes related to mobility of the south flank of Kilauea volcano, Hawaii. U. S. Geol. Surv. Prof. Pap. 800-D, p. D89-D97.

Lee, W.H.K. and J. C. Lahr, 1971. HYP071: A computer program for determining hypocenter, magnitude and first motion pattern of local earthquakes, U. S. Geol. Surv. Open File Rept., 100 pp.

Lee, W.H.K. and J. C. Lahr, 1974. Revisions of HYP071, 4 pp.

Lee, W.H.K., R. E. Bennett and K. L. Meagher, 1972. A method of estimating magnitude of local earthquakes form signal duration. U. S. Geol. Surv. Open File Report.

Macdonald, G. A., 1965. Hawaiian calderas. Pacific Sci., v. 19, p. 320-334.

Macdonald, G. A. and A. T. Abbott, 1970. Volcanoes in the Sea: The Geology of Hawaii, Univ. Hawaii Press, 441 pp.

Moore, J. G. and H. L. Krivoy, 1964. The 1962 flank eruption of Kilauea volcano and structure of the east rift zone. J. Geophys. Res., v. 69, p. 2033-2045.

O'Neill, M. E. and J. H. Healy, 1973. Determination of source parameters of small earthquakes from P-wave rise time. Bull. Seismol. Soc. Am., v. 63, p. 599-614.

Real, C. R. and T. Teng, 1973. Local Richter magnitude and total signal duration in Southern California, Bull. Seismol. Soc. Am., v. 63, p. 1809-1827.

Richter, D. H., W. U. Ault, J. P. Eaton, and J. G. Moore, 1964. The 1961 eruption of Kilauea volcano, Hawaii. U. S. Geol. Surv. Prof. Paper 474-D, 34 pp.

Swanson, D. A., W. A. Duffield and R. T. Okamura, 1971. Seaward displacement of the south flank of Kilauea volcano, Trans. Am. Geophys. Union, v. 52, p. 372.

Tsumura, K., 1967. Determination of earthquake magnitude from total duration of oscillation, Bull. Eq. Res. Inst., Tokyo U., v. 45, p. 7-18.

Ward, P. L., 1972. Microearthquakes: Prospective tool and possible hazard in the development of geothermal resources. Geothermics, v. 1, p. 3-12.

Ward, P. L. and S. Bjornsson, 1971. Microearthquakes, swarms and the geothermal areas of Iceland. J. Geophys. Res., v. 76, p. 3953-3982.

Ward, P. L. and K. H. Jacob, 1971. Microearthquakes in the Ahuachapan geothermal field, El Salvador, Central America. Science, v. 173, p. 328-330.

Ward, P. L. and S. Gregersen, 1973. Comparison of earthquake locations determined with data from a network of stations and small tripartite arrays on Kilauea volcano, Hawaii. Bull. Seismol. Soc. Am., v. 63, p. 679-711.

APPENDIX

Two data sets were accumulated from Hawaiian Volcano Observatory Summaries between 1964 and 1974: monthly totals of event counts (Table A1) and earthquake epicenters, depths, and magnitudes (Tables A2 and A3). Data were not available for the last three quarters of 1969, the last two quarters of 1972, and the first quarter of 1973.

The monthly event counts were taken from the summaries column heading eastern east rift from 1964 to the first quarter of 1969, and from lower east rift from 1970 to 1973.

Earthquake epicenters are given for all events with magnitude greater than 2.5 and for well-determined smaller ones. In 1970, the location of the station in the Puna area was changed from Pahoa (PAH) to Puu Honuaula (PHO). Also in that year, the method of determining hypocenters was computerized. These two changes did not noticeably alter the pattern of epicenters. Table A2 lists all the earthquakes with epicenters plotted in Figure 3 of the text. Table A3 lists events with epicenters east of 155°W and in the vicinity of the Island of Hawaii but which lie outside the boundaries of Figure 3.

Table A1. Monthly count of local events for Puna area from Hawaiian Volcano Observatory Summaries

	1964	1965	1966	1967	1968	1969	1970	1971	1972	1973	1974
Jan.	4	12	2	215	8	5	6	98	255		68
Feb.	6	20	0	55	5	23	3722	117	137		58
Mar.	5	7	3	6	5	20	3042	127	87		80
Apr.	79	2	0	1	1		3904?	62	32	29	55
May	23	0	0	0	6		2449?	155	40	36	42
June	5	3	4	0	5		74?	206	99	33	23
July	12	8	310	4	132		552?	99		75	19
Aug.	119	0	72	3	82		86?	178		1227	46
Sept.	478	2	46	2	2		94	240		1173	42
Oct.	15	5	73	4	2		158	148		140	
Nov.	130	53	217	3	3		156	58		66	
Dec.	6	0	47	14	46		141	176		67	

? Data not available on some days

Table A2. Lower east rift earthquakes

DATE	TIME	EPICENTER LAT N	EPICENTER LONG W	DEPTH KM	MAG
640530	2057	19-32.0	154-52.9	5.	2.2
640731	1133	19-27.3	154-55.5	3.	2.4
640827	1422	19-26.5	154-52.8	5.	2.8
640830	1220	19-25.8	154-59.0	8.	2.8
640830	1222	19-25.8	154-59.0	8.	2.1
640831	0757	19-27.1	154-56.1	5.	3.2
640901	0639	19-27.1	154-56.1	5.	3.7
640901	2157	19-27.1	154-56.1	5.	2.0
640902	0211	19-27.1	154-56.1	5.	2.0
640902	0258	19-26.9	154-56.0	3.	2.4
640902	0403	19-26.8	154-56.0	3.	2.6
640903	0546	19-28.2	154-54.8	5.	2.7
640906	0309	19-27.2	154-54.7	5.	2.5
640906	0833	19-27.0	154-52.9	3.	2.4
640907	0610	19-26.7	154-53.8	3.	2.8
640907	0613	19-26.7	154-53.8	3.	3.0
640910	1109	19-27.7	154-55.5	5.	2.4
640912	2127	19-27.7	154-55.7	2.	2.7
640913	0339	19-26.8	154-55.9	2.	2.7
640914	0602	19-26.5	154-56.2	3.	3.8
640914	0621	19-27.5	154-54.8	3.	2.5
640914	1921	19-27.5	154-54.8	3.	2.5
640916	1834	19-25.9	154-55.8	3.	2.4
640919	1206	19-27.2	154-56.2	5.	2.1
641030	1918	19-23.6	154-59.0	8.	2.0
641112	0300	19-23.5	154-56.4	8.	3.1
641112	2208	19-26.0	154-54.6	3.	2.5
650402	0243	19-25.9	154-51.2	6.5	2.4
651019	0615	19-26.0	154-56.1	8.	2.2
651108	0048	19-24.5	154-50.0	37.	3.4
651110	1349	19-23.9	154-53.9	10.	2.3
651111	1619	19-25.8	154-56.3	3.	2.4
651119	1128	19-25.7	154-52.9	3.	3.1
660705	2310	19-26.1	154-57.1	9.	2.7
660708	0635	19-26.8	154-55.3	0.	2.3
660713	0203	19-25.5	154-53.5	3.	3.0
660717	2216	19-28.4	154-52.5	5.	2.4
660729	0528	19-26.2	154-55.5	3.	2.2
660731	2001	19-28.5	154-54.3	0.	2.3
660801	0225	19-27.0	154-55.2	0.	2.5
660801	1902	19-27.1	154-55.1	0.	2.7
660806	2057	19-28.8	154-54.2	3.	3.7
660811	1830	19-28.6	154-54.7	3.	2.3
660811	1830	19-25.5	154-54.7	3.	2.3
660814	0015	19-27.2	154-55.1	3.	3.5
660923	1033	19-27.9	154-56.5	3.	2.8
661106	0637	19-27.2	154-55.2	0.	2.7
661113	0132	19-26.2	154-53.4	3.	2.5
661114	0256	19-29.0	154-54.1	0.	2.6
661116	1919	19-25.9	154-54.6	0.	3.0
661117	0517	19-26.5	154-56.0	0.	3.5
670124	1223	19-25.7	154-56.0	5.	1.8
670125	0324	19-26.7	154-54.4	5.	2.3
670126	0430	19-27.8	154-53.8	0.	2.7
670126	0432	19-26.9	154-54.2	5.	3.4
670128	1242	19-24.2	154-56.1	1.	2.4
670128	1243	19-28.9	154-54.1	8.	3.0
670128	2143	19-26.0	154-55.0	3.	2.3
670216	2149	19-26.8	154-59.2	0.	3.3
670216	2152	19-25.8	154-55.8	5.	1.8
670928	0322	19-24.2	154-51.1	7.	2.6
671019	1116	19-23.0	154-56.6	40.	3.3
671102	1446	19-28.6	154-53.4	9.	3.0
680101	0102	19-23.8	154-55.8	6.	2.5
680708	0435	19-23.4	154-58.7	10.	2.3
680712	0553	19-24.9	154-59.0	5.	2.0
680720	1552	19-28.0	154-55.2	6.	2.1
680721	1646	19-26.8	154-53.8	6.	2.3
680723	0815	19-27.0	154-55.7	5.	2.5

Table A2. (cont.)

680730	1540	19-28.2	154-54.2	7.	2.0
680730	2357	19-26.6	154-53.8	5.	2.2
680731	0422	19-27.4	154-55.8	5.	2.3
680731	1441	19-26.9	154-54.5	5.	2.5
680801	0721	19-28.1	154-55.2	9.	2.2
680801	1219	19-26.0	154-57.2	2.0	2.6
680805	0838	19-26.4	154-54.1	5.	2.6
680812	0637	19-27.4	154-55.4	5.	2.7
680816	0152	19-23.4	154-59.4	5.	2.2
690123	2104	19-26.5	154-59.2	55.	2.7
690124	0148	19-26.1	154-53.2	8.	2.4
700219	1846	19-30.7	154-59.5	8.5	
700222	0148	19-29.4	154-53.7	6.8	2.7
700223	0451	19-27.3	154-50.5	5.0	2.3
700302	0740	19-24.1	154-57.4	8.0	
700303	1341	19-24.9	154-50.9	7.3	
700303	1838	19-27.2	154-52.2	5.0	2.0
700303	1930	19-25.1	154-51.7	2.4	2.1
700303	2000	19-27.8	154-52.6	4.8	2.8
700304	1021	19-26.5	154-52.4	5.5	2.0
700304	2100	19-27.4	154-53.5	4.5	2.3
700305	0332	19-24.0	154-58.5	0.3	
700305	0417	19-30.1	154-52.1	8.0	
700306	0643	19-27.3	154-51.8	4.8	2.6
700307	0307	19-25.4	154-53.9	0.9	3.1
700307	0828	19-26.5	154-52.8	8.0	2.0
700307	1201	19-27.5	154-52.2	6.0	2.3
700308	0808	19-23.3	154-58.6	6.3	
700310	1809	19-27.4	154-58.1	8.0	
700428	0314	19-25.2	154-51.8	3.5	2.5
700428	1523	19-26.7	154-54.9	1.5	3.5
700430	0846	19-25.2	154-55.5	2.4	2.1
700503	0730	19-26.2	154-51.7	8.0	2.5
700505	1448	19-26.6	154-52.1	8.0	2.2
700525	1627	19-26.1	154-57.1	8.2	-
700605	1736	19-24.8	154-53.9	13.6	2.1
700609	0246	19-23.2	154-56.3	7.5	2.1
700623	1654	19-23.4	154-59.2	8.0	2.0
700626	1623	19-27.0	154-53.9	7.9	2.0
700701	0317	19-24.2	154-58.6	4.7	1.9
700704	2313	19-26.3	154-52.0	6.2	2.4
700719	1958	19-25.6	154-52.4	8.5	2.2
700724	0432	19-23.9	154-59.3	5.7	2.4
701030	0204	19-26.9	154-56.2	53.3	-
701207	2240	19-23.8	154-59.7	10.0	1.8
710110	2158	19-28.1	154-56.6	2.9	2.1
710201	0519	19-25.4	154-58.0	0.1	1.6
710316	2017	19-26.4	154-54.4	4.4	-
710326	0537	19-22.2	154-59.7	8.3	2.2
710410	2359	19-26.0	154-56.1	4.7	-
710604	1834	19-25.9	154-56.4	5.2	-
710703	1744	19-24.0	154-56.6	40.1	2.6
710922	1756	19-23.6	154-58.7	4.4	-
711027	0401	19-26.9	154-51.9	8.5	-
711027	0449	19-27.3	154-52.2	8.8	-
711108	2235	19-22.4	154-57.9	24.5	-
711206	1554	19-26.8	154-53.9	14.1	2.3
711207	1008	19-22.7	154-56.6	5.5	2.9
711207	1838	19-23.0	154-53.5	6.0	-
711213	2102	19-24.2	154-59.5	7.1	2.0
711225	1416	19-27.1	154-53.6	5.6	-
720228	1902	19-26.6	154-54.1	4.7	2.0
730408	0509	19-27.9	154-58.5	7.6	1.7
730508	1349	19-23.4	154-54.8	3.1	2.9
730527	1446	19-27.1	154-53.3	8.0	1.2
730909	0553	19-28.6	154-54.3	2.6	2.3
730916	1528	19-28.0	154-54.1	2.5	2.5
730916	2148	19-28.3	154-54.2	1.1	-
730917	1952	19-25.9	154-58.1	2.7	-
730918	0437	19-25.7	154-58.3	2.5	-
730918	0717	19-24.2	154-57.3	4.0	-

Table A3. Lower east rift earthquakes

DATE	TIME	EPICENTER LAT N	EPICENTER LONG W	DEPTH KM	MAG
640224	0524	19-17.2	154-50.9	8.	2.3
640327	0210	19-21.8	154-54.8	3.	2.4
640815	1815	19-20.0	154-48.0	8.	2.4
640918	0656	19-18.0	154-56.5	8.	2.3
641023	0658	19-19.9	154-59.5	8.	2.6
650209	0343	19-21.3	154-59.0	5.	3.0
650210	2005	19-38.4	154-59.6	20.	2.3
650216	0231	19-17.5	154-44.0	20.	3.2
650322	1422	19-16.1	154-59.7	5.	2.2
650327	0625	19-24.0	154-36.0	40.	2.3
650411	2039	19-15.0	154-43.0	50.	2.6
650425	1928	19-32.0	154-45.0	3.	2.5
650531	0027	19-51.8	154-54.9	8.	2.0
650908	1854	19-15.8	154-55.5	35.	2.7
651105	1931	18-58.1	154-57.9	40.	2.7
651202	0237	19-46.5	154-50.4	45.	3.8
651205	1905	19-35.2	154-57.8	30.	3.8
660109	2046	19-12.3	154-43.3	8.	2.2
660804	0517	20-54.0	154-55.0	13.	3.0
660808	0934	19-17.5	154-57.1	0.	2.9
660902	0840	19-19.7	154-51.7	40.	2.6
660928	2336	19-17.9	154-59.9	8.	2.3
661118	2329	19-20.6	154-59.3	0.	2.3
670521	1655	19-23.0	154-49.3	45.	3.4
670531	0315	19-17.8	154-43.0	40.	2.8
670607	0934	19-22.0	154-52.9	6.	2.2
670616	1340	18-58.3	154-59.5	8.	3.3
670812	0918	19-17.3	154-50.2	40.	2.5
671006	0616	19-14.2	154-55.0	5.	2.3
671007	1319	19-36.7	154-47.7	8.	2.4
671007	2032	19-10.1	154-58.7	8.	2.3
671113	0745	19-41.9	154-49.1	40.	3.0
671126	0038	19-24.7	154-46.0	13.	2.7

MICROEARTHQUAKE STUDY OF THE OPIHIKAO ANOMALY, PUNA, HAWAII

M. O. Mattice
A. S. Furumoto

Hawaii Institute of Geophysics
University of Hawaii
Honolulu, Hawaii 96822

ABSTRACT

A reconnaissance microearthquake survey over an electrical anomaly on the lower east rift zone of Kilauea volcano, Hawaii, recorded 8.5 earthquakesper day. We have concluded that the seismic level detected is normal for this area. Coincidence of the electrical anomaly and the seismic activity is striking. This geophysical evidence coupled with geologic evidence suggest geothermal sources. We recommend that a well be drilled within this anomaly to a depth of at least two kilometers.

INTRODUCTION

The Opihikao anomaly is an area of low electrical resistivity on the lower east rift zone of Kilauea volcano, Hawaii (Fig. 1), Klein et al., (1975). It is also an area of anomalous self-potential (Zablocki, 1977). The Opihikao anomaly is located between 19°28' and 19°24'N latitude, 154°59' and 154°56'W longitude, near the junction of Highway 13 and Kamaili Road. Steam seeps are present in the area.

To determine whether geothermal activity is the cause for the anomaly, as has been suggested, rapid reconnaisance microearthquake surveys were carried out. The first one, done by W. Suyenaga and A. S. Furumoto in the summer of 1973, recorded only one event in 40 hours. As the recording was done only during daylight hours, the poor result can be attributed to background noise. The second one was done with only two seismographs during the months of April and May in 1978, but because continuous day and night observations were carried out, results were significant. This report will deal with the second survey.

Field work was carried out for 20 days from March 23 to April 20, 1978. Three hundred sixty hours of recorded data provide the basis for this study.

METHODS

Two Sprengnether MEQ-800 portable high-gain seismographs with paper recordings were utilized. Instrument locations were as indicated in Figures 3, 5, and 7. Station separation was 2.17 km. Paper was changed every 20 to 30 hours, and batteries were rotated every two days. The time-marking device on one instrument malfunctioned, eliminating the possibility of comparing P-arrival times, so data analysis was limited to S-P times.

The crustal profile used in epicenter calculations was developed by Broyles et al. (1978), using seismic refraction data shot along Hawaii's coastline (Fig. 2).

Epicenters were calculated first with a depth assumption of 2 km. If the result was not reasonable, shallower depths were assumed; a depth assumption too shallow has the effect of dispersing the epicenters rather than concentrating them. Distance of epicenters from instrument stations were calculated with:

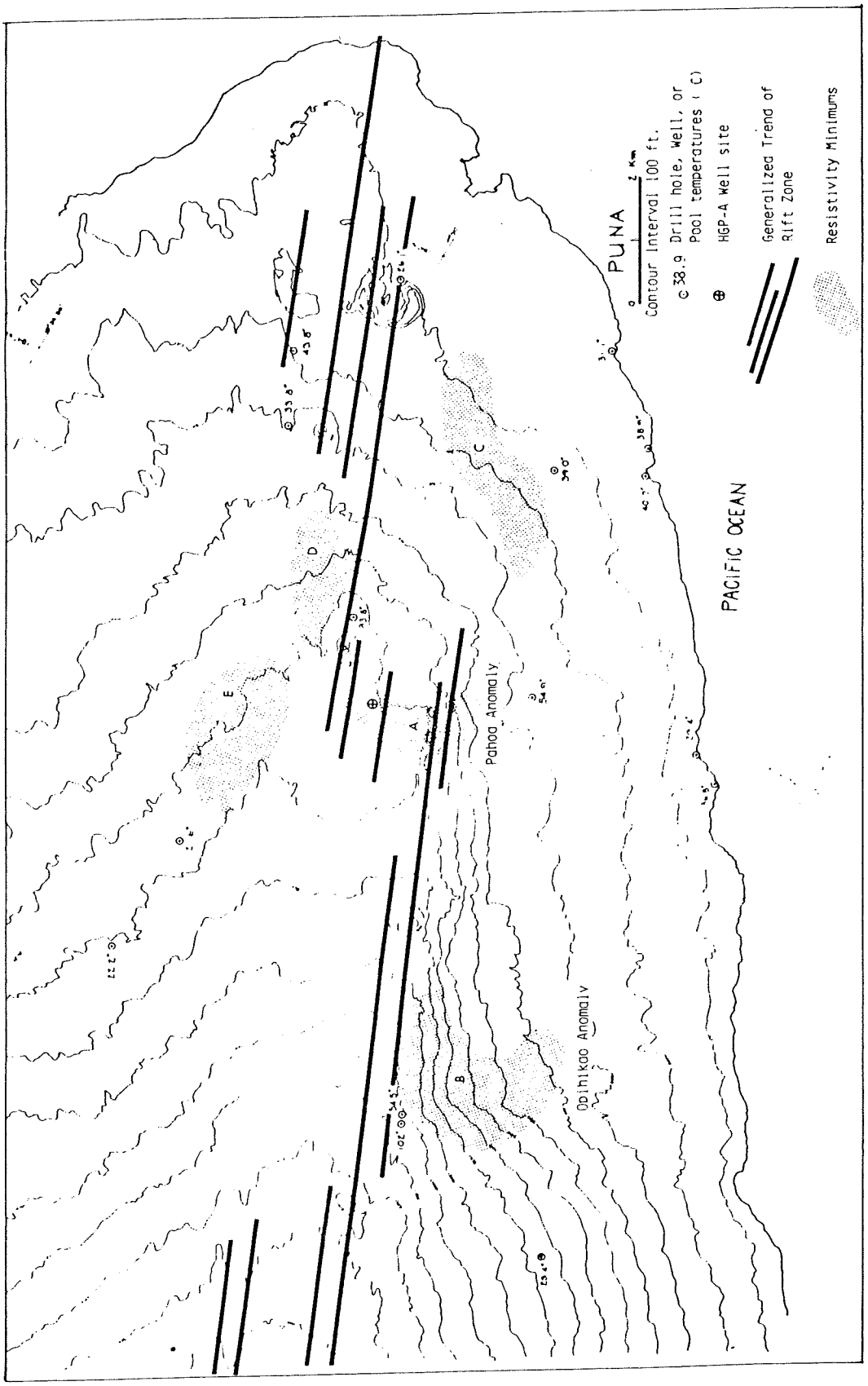

Figure 1. Contour map of the Puna area showing locations of Opihikao and Pahoa anomalies. The resistivity minimums (stippled areas) were compiled from five different types of geoelectric surveys performed from 1973 to 1975 (Klein et al., 1975).

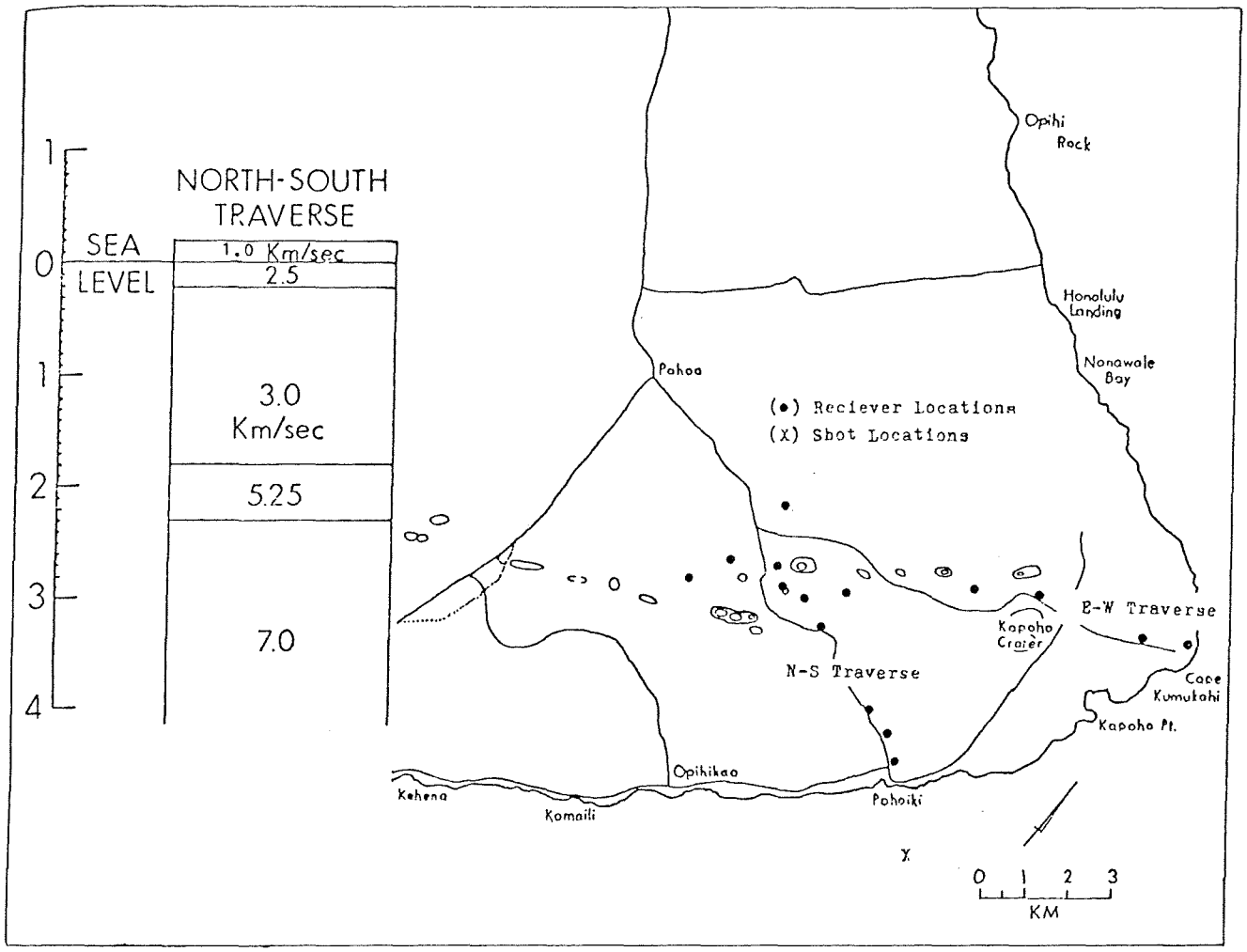

Figure 2. Refraction profile used to compute microearthquake epicenters (Broyles, this volume).

From 1973 to 1975 ... surveys performed (Klein et al., 1975).

$$X = \frac{(t_s - t_p)(V_s V_p)}{V_p - V_s}$$

where:

t_s = S-wave arrival time (sec)

t_p = P-wave arrival time (sec)

V_p = P-wave velocity

V_s = S-wave velocity = $\frac{V_p}{\sqrt{3.5}}$ for basalt

X = distance (km)

At 2-km depth, V_p = 5.25 km/sec; thus,

$$X = \frac{t_s - t_p - 0.71}{.166} \text{ km}$$

where 0.71 sec represents the amount of time to account for earthquakes 2 km directly below the seismograph station.

The 2-km hypocenter depth assumption was based on a microearthquake survey by Suyenaga and Furumoto (1978). They calculated that "most of the earthquakes occur within the 3-km band vertically beneath the surface rift zone." This band lies between 1 and 4 km deep. Their survey was undertaken approximately 7 km east of the Opihikao anomaly.

RESULTS

With data from only two instruments, a pair of epicenter solutions are possible for each earthquake. We define such solutions as apparent epicenters. The apparent epicenters are represented on Figure 3 by two dots, one open and one closed. Depth of focus is ambiguous.

Over a 15-day period, 145 earthquakes were recorded; of these, 128 had S-P times less than 2 sec or epicenter locations within 7.8 km of the station array. The average within this 7.8-km radius is 8.5 microearthquakes per day. The average with S-P time less than 1 sec or within a 1.75-km radius is 4.5 earthquakes per day.

Earthquake density distributions determined from epicenter locations are represented by contours in Figure 3, 5 and 7. Contours indicate equal number of earthquakes per

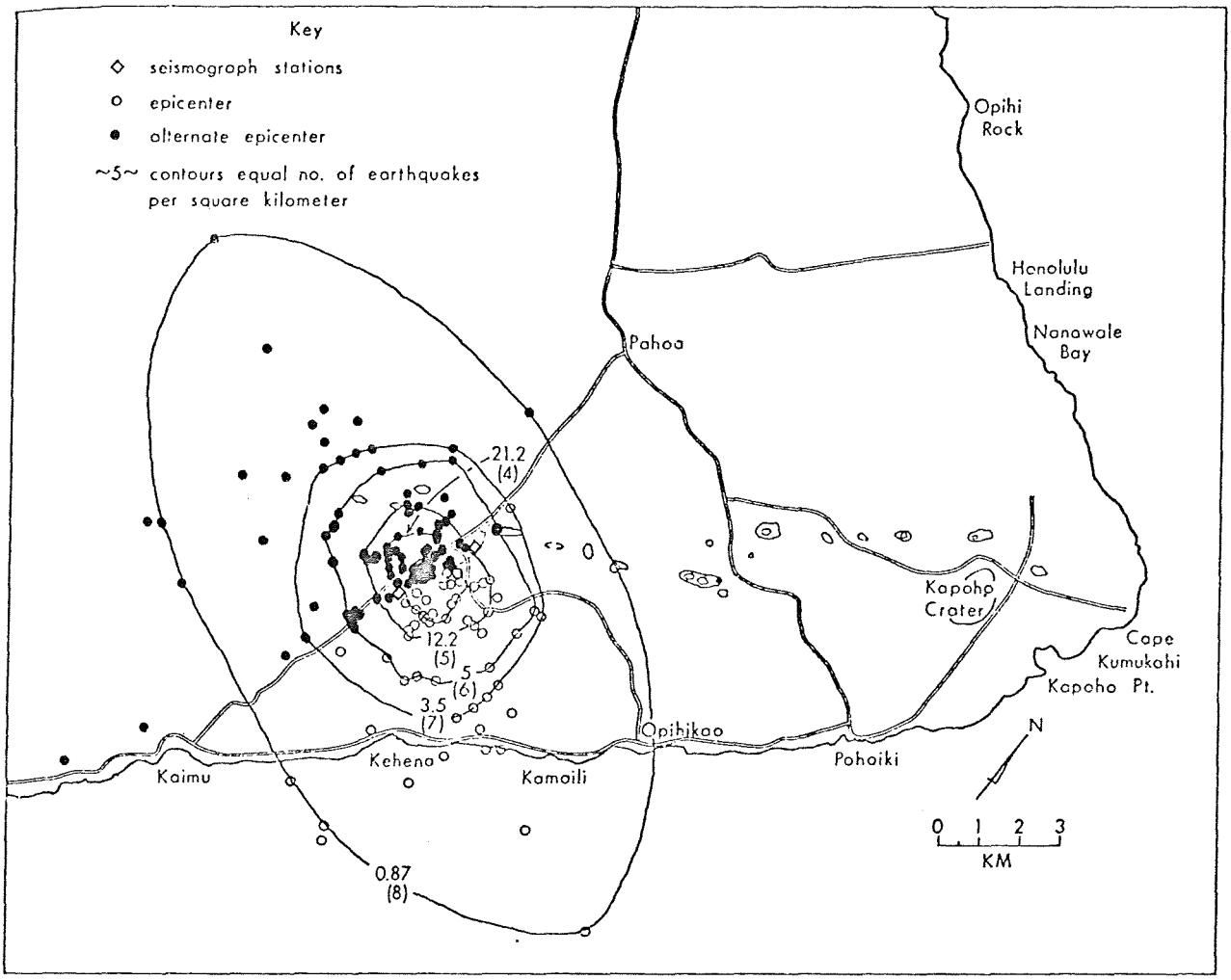

Figure 3. Earthquake density contours determined from epicenter locations.

square kilometer over a 15-day period. The number in parentheses in Fig. 3 represents the number of earthquakes per day in the area enclosed by its associated contour. For example, the contour labeled 0.87 enclosed the area in which eight earthquakes per day occurred. The contours show increasing seismic activity toward the Opihikao anomaly.

A microearthquake survey by Suyenaga and Furumoto in 1973 in the same area recorded only one event in 40 hours of recording.

A volcanic eruption approximately 7 km west of the station locations had ceased almost six months prior to this survey. Seismic activity associated with cooling appears to have decayed by mid-November 1977 (R. Koyanagi, pers. comm.), four months prior to this survey.

DISCUSSION

In the summer of 1974, Suyenaga and Furumoto (1978) carried out a microearthquake survey over the Pahoa anomaly, 7 km east of the Opihikao anomaly. In 1976 a geothermal reservoir was found in the Pahoa anomaly when the exploratory well, HPG-A, was drilled to a depth of 1960 m. The Pahoa anomaly recorded only 1.89 earthquakes per day, whereas the Opihikao anomaly recorded more than 8.5 per day. Clearly the Opihikao anomaly is seismically more active than the Pahoa anomaly. (Suyenaga, pers comm.).

A question may be raised whether the present study was carried out during a period of earthquake swarm, a phenomenon that occurs every so often. Such swarms are, however, readily detected by the seismograph network of the Hawaiian Volcano Observatory. When questioned, observatory personnel responded that "no unusual seismic activity occurred on the lower east rift during the period of this survey" (R. Koyanagi, pers. comm.). We conclude that the seismic level detected is normal for the Opihikao anomaly.

Figures 4 through 7 compare this study with the electrical surveys defining the Opihikao anomaly. Coincidence of the electrical anomaly with the seismic activity is striking. Even then we cannot conclude firmly that these geophysical parameters, especially the seismic activity, is hydrothermal in origin. The source can be magmatic. Nevertheless, the seismic data presented here do not detract from Keller's (1975) proposition that the Opihikao anomaly represents a viable geothermal source.

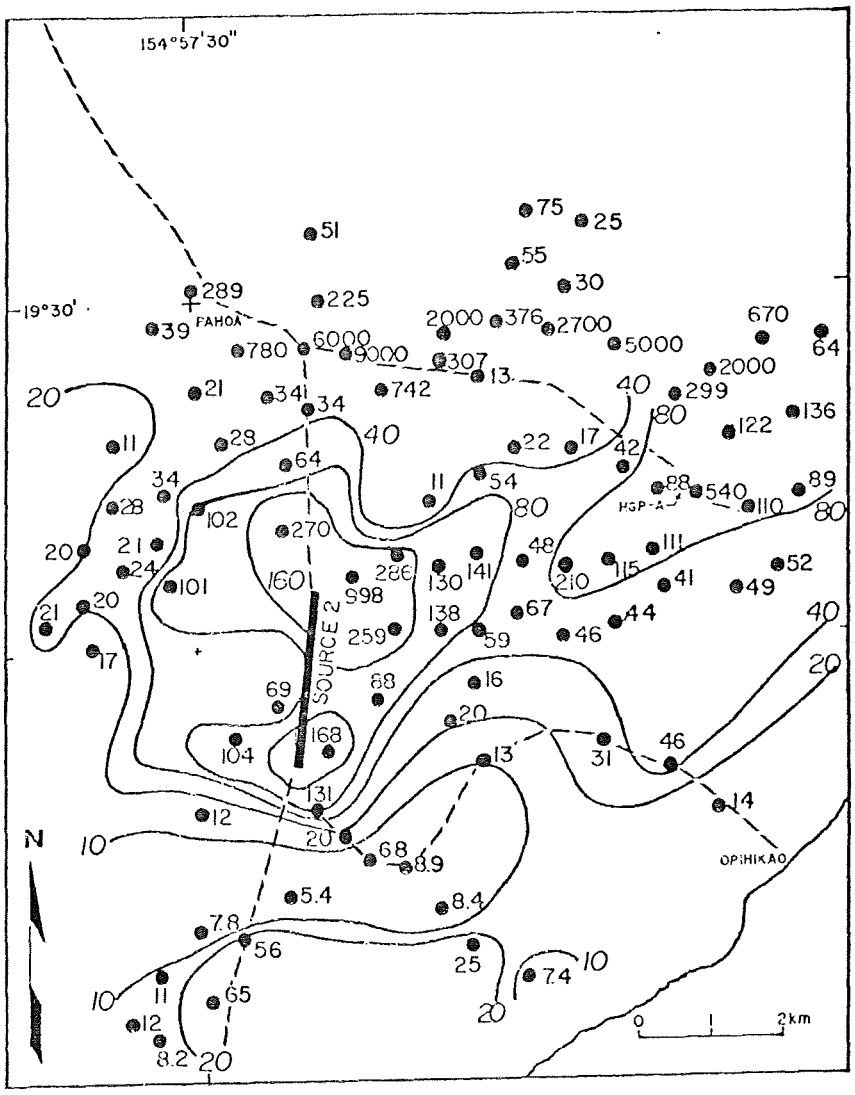

Figure 4. Apparent resistivity map of the Opihikao area (Keller et al., 1977).

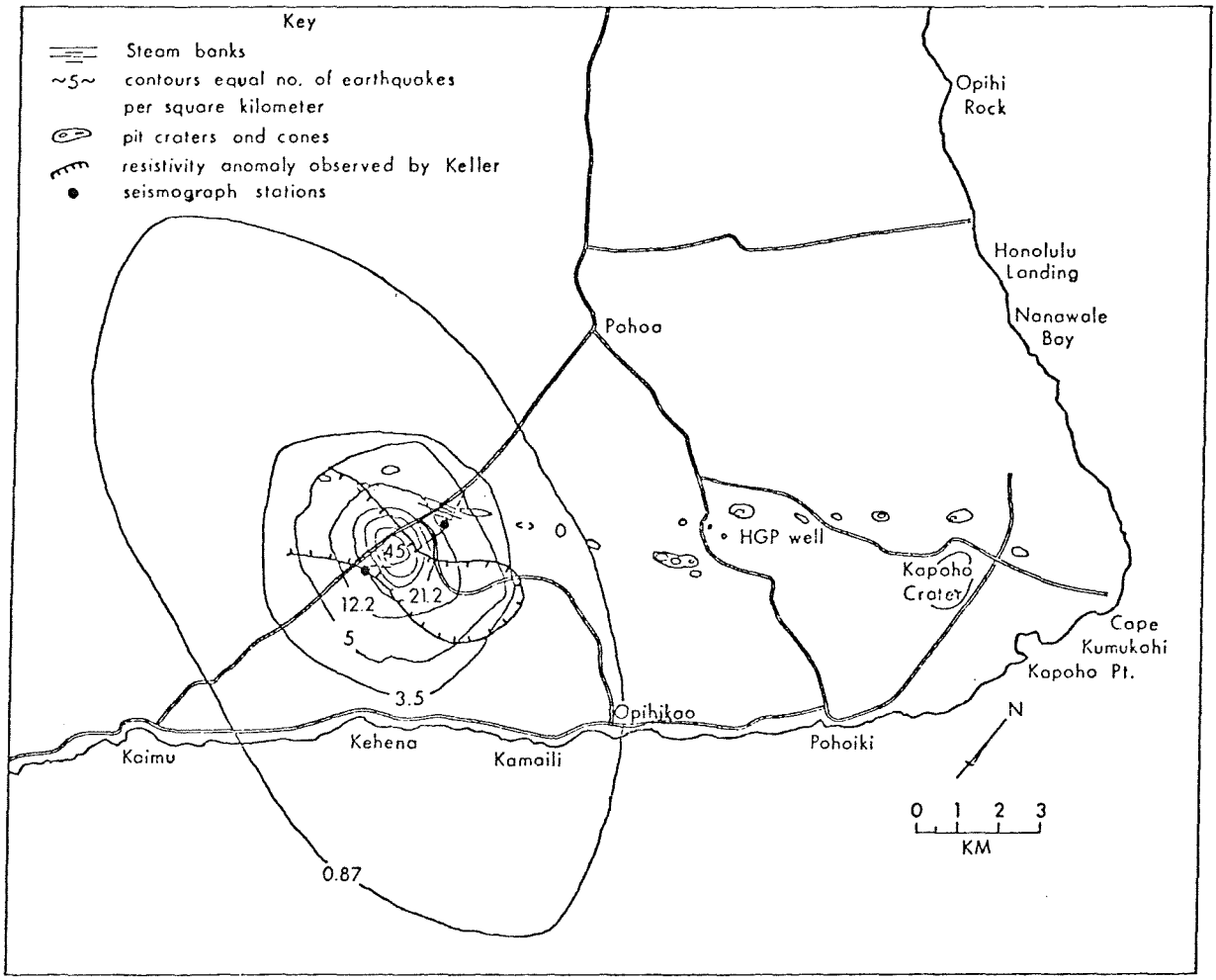

Figure 5. Comparision of microearthquake survey with resistivity survey done by Keller et al. (1977).

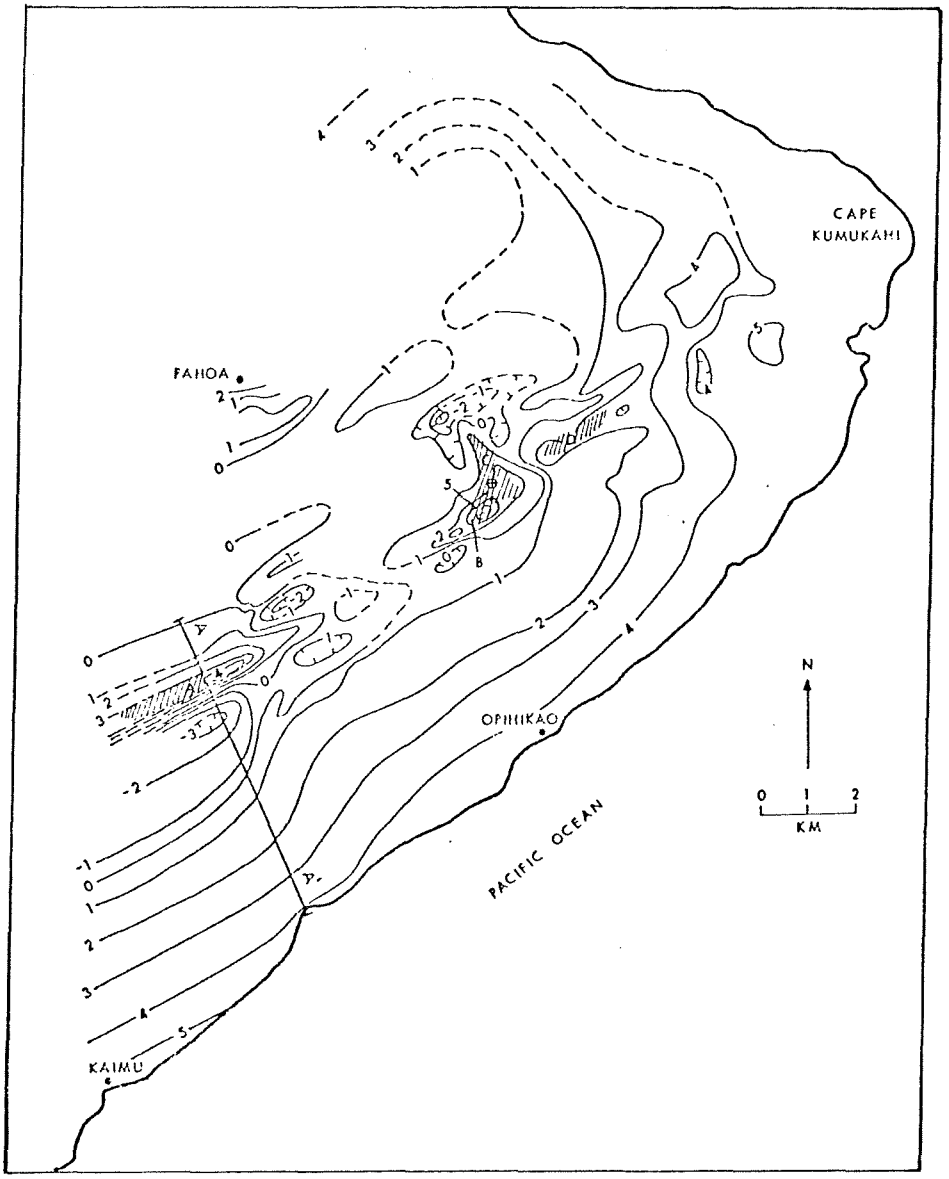

Figure 6. Contour map of the self-potential distribution in the area of Kilauea's east rift zone (dashed where inferred). Each unit contour interval represents 0.1 volt. (Reproduced with permission of C. Zablocki, 1977.)

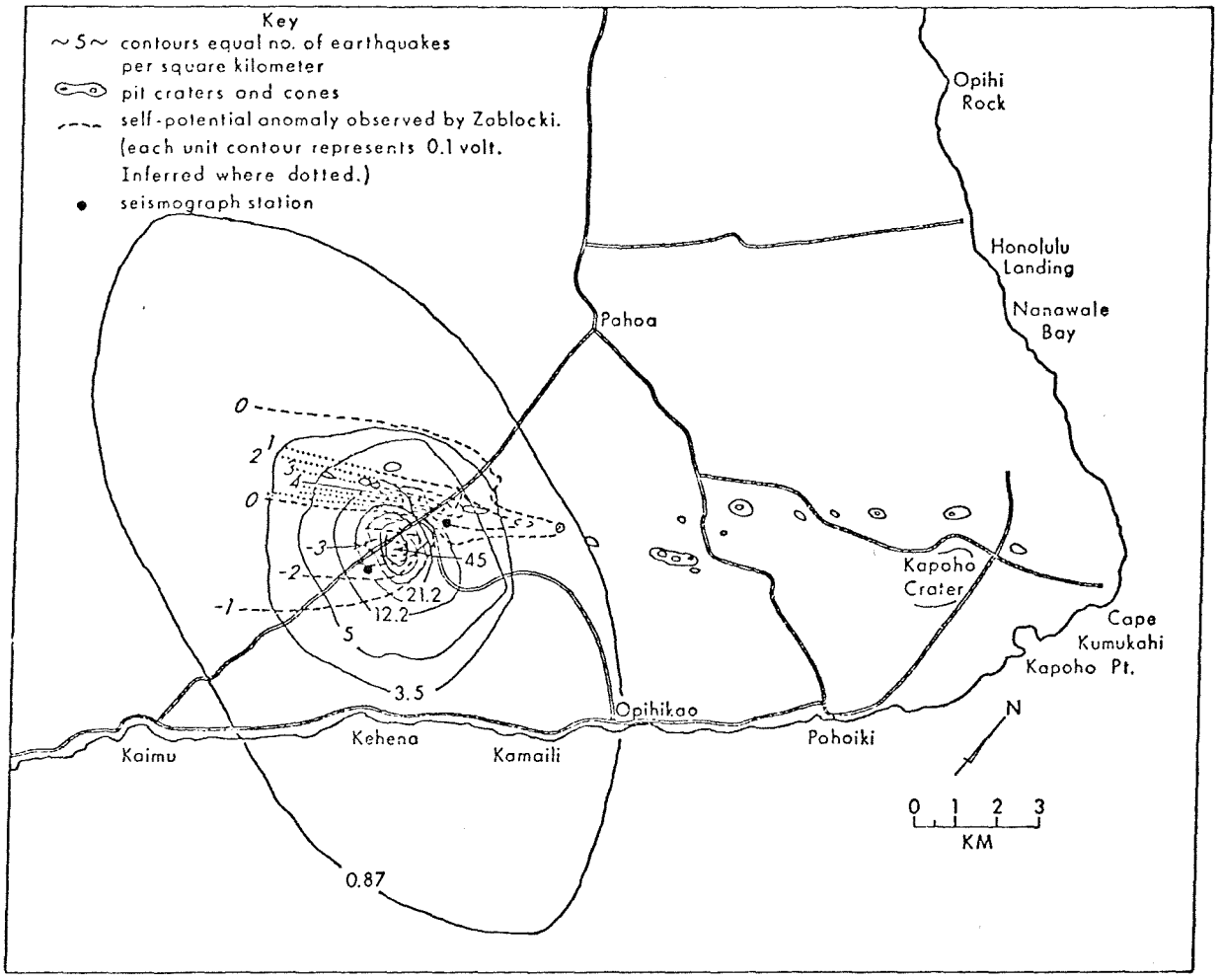

Figure 7. Comparision of microearthquake survey with self-potential survey done by Zablocki.

CONCLUSIONS AND RECOMMENDATIONS

Eight and one-half earthquakes per day occurred in the Opihikao anomaly, a suspected geothermal region. The steam banks in the anomalous area are geological evidence suggesting geothermal sources. The self potential anomaly in the area has been conceived as being derived from a geothermal reservoir (Zablocki, 1977), and the low electrical resistivity anomaly has been suggested as hydrothermal in origin (Keller, 1975). The microearthquake data corroborate the electrical data and geological evidence.

In 1961 a geothermal exploration well was drilled just outside the boundaries of the Opihikao anomaly. A bottom temperature of 102°C was encountered at 556 feet (TTW2 of Fig. 1) and the water table was not reached.

The Opihikao anomaly has more intense geophysical signatures than the Pahoa anomaly, which was proven to have a geothermal resource. We recommend that a well be drilled within the Opihikao anomaly as soon as possible to a depth of at least 2 km.

A more detailed microearthquake survey utilizing five or more stations would yield hypocenter locations that could outline the geothermal reservoir that may underlie the Opihikao anomaly.

REFERENCES

Broyles, M.L., 1978, Crustal Structure of the Lower East Rift Zone of Kilauea, Hawaii from Seismic Refraction, 2. Complete Structure, this volume.

Broyles, M., W. Suyenaga and A. S. Furumoto, 1978. Structure of the Lower East Rift Zone of Kilauea Volcano, Hawaii, from seismic and gravity data, submitted to J. Volcanol. and Geothermal Res.

Keller, G. V. 1975. The Opihikao Prospect, Puna District, Microgeophysics Corp, Golden. Colorado. A report submitted to Geothermal Energy Development Co., Honolulu.

Keller, G. V., C. K. Skokan, J.J. Skokan and J. Daniels, 1977. Electrical Resistivity and Time-Domain Electromagnetic Surveys of the Puna and Ka'u Districts, Hawaii County, Hawaii. Geoelectric Studies on the East Rift, Kilauea Volcano, Hawaii Island. Hawaii Inst. Geophys. Report HIG-77-15, p. 3-89.

Klein, D. P., J. Kauahikaua, J. Skokan, G. Keller, A. Furumoto, J. Daniels and C. Zablocki, 1975. Geoelectric Surveys on Hawaii: 1973-1975. The Hawaii Geothermal Project, Summary Report for Phase I. Geophysical program, Task 2.2. University of Hawaii, p. 32-47.

Koyanagi, R. Y., 1978. Preliminary compilation of Hawaiian Volcano Observatory seismic data for the first quarter of 1978. Unpublished report.

Suyenaga, W. and A. S. Furumoto, 1978. Microearthquake Study of the East Rift Zone of Kilauea, Puna, Hawaii. This vol.

Zablocki, C. J. 1977. Self-Potential Studies in east Puna, Hawaii. Geoelectric Studies on the East Rift, Kilauea Volcano, Hawaii Island. Hawaii Inst. Geophys. Report HIG-77-15, p. 175-195.

SEISMIC GROUND-NOISE SURVEY, PUNA, HAWAII

Roger Norris and Augustine S. Furumoto

Hawaii Institute of Geophysics
University of Hawaii
Honolulu, Hawaii 96822

ABSTRACT

A survey of seismic ground noise was made in summer 1974 to complement other geophysical surveys aimed at locating a geothermal power source in the Puna district of the island of Hawaii. The measure of ground noise was taken to be the mean-square vertical velocity, in a frequency band of 1 to 30 Hz, expressed in decibels (db) relative to a convenient reference. Contour maps of 5-db intervals were produced for narrow bands centered at 16, 8, 4 and 2 Hz. The contour maps indicate a local high of intensity in the vicinity of Puulena crater. As local highs were not found at the drill site of well HGP-A, which eventually penetrated a geothermal reservoir, it is concluded that ground noise is not spatially correlated with hydrothermal activity on the east rift of Kilauea. Ground noise can be correlated with magmatic activity.

INTRODUCTION

In this paper, we report the techniques and results of a seismic ground-noise survey made in conjunction with the Hawaii Geothermal Project. The survey covered the triangular area with vertices at the villages of Pahoa, Kapoho and Kalapana in the Puna district of the island of Hawaii.

Known geothermal areas seem to have a characteristic noise pattern. It is not surprising that near geothermal reservoirs high levels of noise are recorded relative to the surrounding areas, as has been reported by Clacy (1968), Whiteford (1970), Goforth et al. (1972) and others. It has also been noted that the noise seems to be concentrated in a limited frequency range. For instance, Clacy (1968) found high amplitude noise in the range 1 to 10 Hz in New Zealand. Douze and Sorrells (1972) found that measurements over geothermal reservoirs in the Imperial Valley, California, were enriched in frequencies between 1 and 3 Hz when compared with measurements two miles away. They also present a theoretical model of the noise source. Luongo and Rapolla (1973) studied ground noise on Lipari and Vulcano islands near the toe of Italy and concluded that frequencies higher than 10 Hz were due to fumaroles and hot springs and that the lower frequencies suggested a large geothermal system beneath both islands. They cautioned that the amplitude and frequency distribution were mainly controlled by the mechanical properties of the outcropping rocks. Iyer and Hitchcock (1974) made elaborate noise measurements of thermal areas in Yellowstone Park and they infer that the deeper geothermal noise was predominantly in the band of 2 to 8 Hz and postulate that higher frequency noise was generated by the surface activity of geysers and hot springs.

The Puna district is built up of layer upon layer of thin lava flows from the Kilauea east rift zone. In areas not covered by recent lava flows the ground is largely a porous aggregate of hard cinders with little soil. The rift zone is presumed to be penetrated by a multitude of dikes - denser and hotter and less permeable to ground water than the surrounding material. The combination of abundant rainfall, highly permeable ground, probable water traps among dikes and faults, the presence of an active volcano and warm springs makes the site a good prospect for hydrothermal activity which might generate ground noise. A reconnaissance survey of the southeast side of Hawaii Island in June 1974 resulted in a general pattern of high noise level near the sea shore with a fall-off inland. A slight exception to the pattern occurred in the vicinity of Puulena Crater where the noise seemed abnormally high for its 4-km distance from shore. Also, geological considerations, surveys of electrical self-potential

and resistivity, and of well temperature all indicated that this area was a good choice for a more detailed ground-noise survey. With these factors in mind, we carried out a detailed survey in August 1974.

A year and a half after our ground-noise survey was completed and the data were processed, an exploratory well, HGP-A, was drilled to a depth of 1900 m. In June 1976 the well flashed into steam. In this paper we were able to evaluate ground-noise data obtained before drilling disturbed anything in the light of the newly found hydrothermal activity. The conclusions we have reached, we must make clear, are relevant to the east rift zone of Kilauea volcano and may not be germaine to other geothermal areas.

Field Methods and Data Analysis

In the survey 59 stations were distributed about the 30 to 40 square mile Pahoa-Kapoho-Kalapana triangle (Fig. 1). The station density is roughly 1 to 2 per square mile, biased toward the network of roads in the area.

The recording system was a 1-Hz low-cutoff Mark geophone with a sensitivity of 273 microvolts/micron/second, a Mandrel seismic amplifier set at 84-db amplification and 30-Hz low pars filter, and a TEAC FM low-frequency cassette tape recorder (Fig. 2). One channel of the recorder was used for voice annotation and WWVH time broadcast. The system operated out of the trunk of a compact automobile, which was adequate for the unimproved roads in the area.

At each recording site, the geophone was buried in the cinders or dirt about 60 feet from the road. While a calibration signal was recorded on the geophone channel, a description of the site and other information was placed on the voice channel. Seismic ground noise with WWVH completed the recording. The calibration signal was a 36 microvolt-peak sinusoid at frequencies of 1.5 and 10 Hz. The amplitude is equivalent to 132 millimicrons/sec peak vertical ground velocity.

Each measurement was a ten minute sample. The recording period was extended if fluctuation was apparent (e.g. when there were moving vehicles in the vicinity). One station was measured at least once a day as a check on reproducibility or time variation.

The cassette-recorded geophone signal was processed for each station to yield an average sound intensity in decibels relative to an arbitrary reference. The resulting values were then plotted and contoured. Two processing methods and five frequency bands were used (Figs. 2 and 3). In the first method, the geophone signal was put through a band-pass

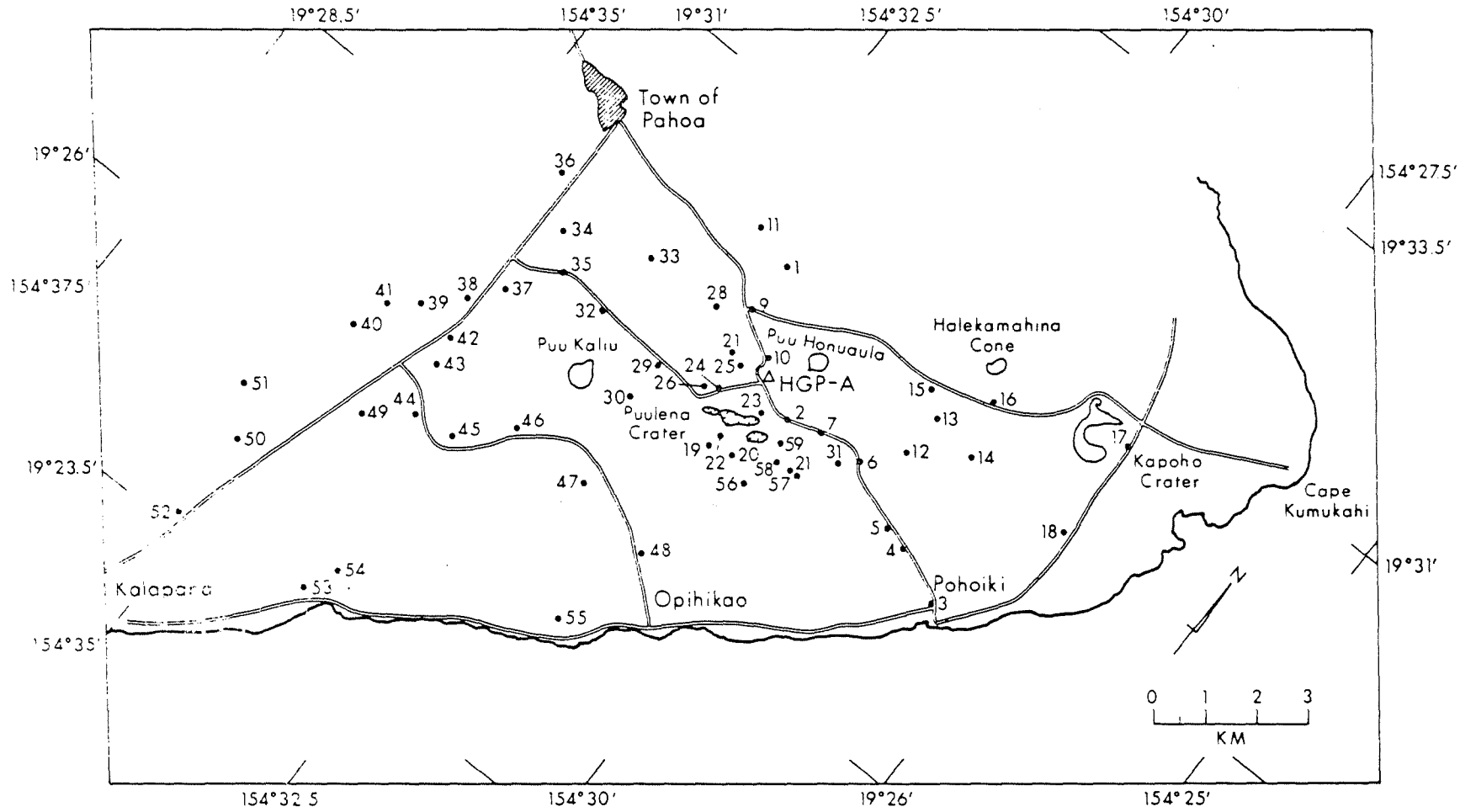

Figure 1. Map of Puna, Hawaii showing Pahoa-Kapoho-Kalapana triangle, geological features, HGP well site and noise station locations. Stations 30 and 46 were used for special comparison.

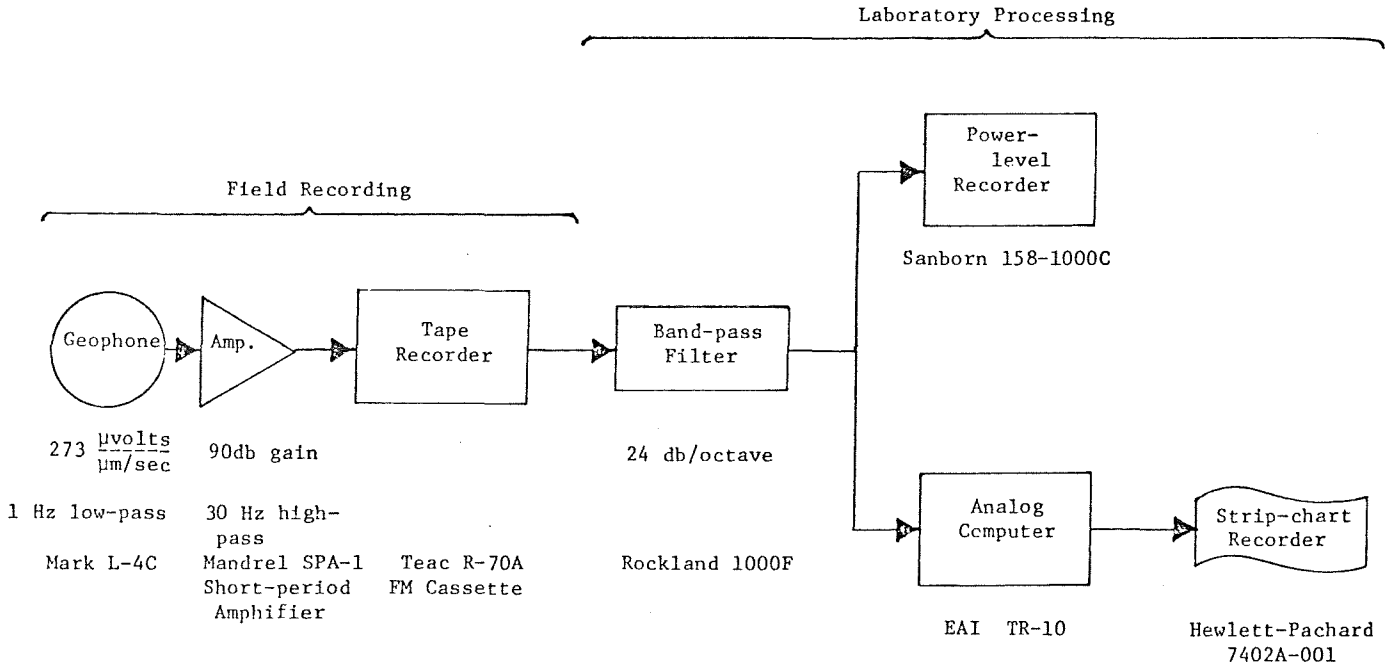

Figure 2. Ground-noise measurement apparatus.

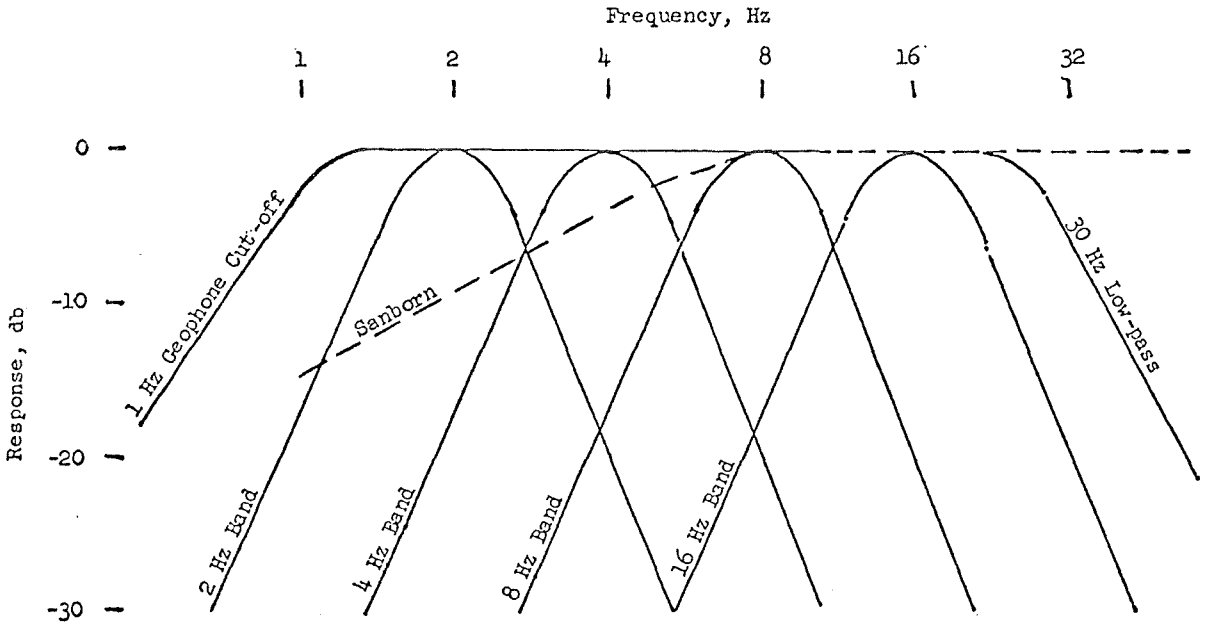

Figure 3. System response is flat between the 1-Hz geophone cut-off and the 30-Hz low-pass filter of the seismic amplifier. The narrow-band filters centered at 2, 4, 8, 16 Hz were used for making the contour maps of those frequencies.

filter (Fig. 2) into a Sanborn log-audio recorder which gives a strip-chart record of power level in decibels. The lowest one-minute level of the 10-minute sample was taken as the measure of ground noise. Since the response of the Sanborn recorder drops off below 8 Hz (Fig. 3), a second method was used for lower frequencies. In this method, the filtered signal was squared and integrated by an EAI TR-10 analog computer and then put on a strip-chart record. The record appeared as a line whose slope is the measure of average power. The slope was measured by superimposing a template over the record and interpolating by eye between the calibrated slopes on the template. Calibration was one with a signal generator and oscilloscope. During data processing, the geophone signal was observed on an oscilloscope to check for fading or clipping and to identify spurious departures from normal ground noise.

RESULTS AND DISCUSSION

Ground noise is composed of all the noises in the neighborhood, including the surface contributions of wind, rain, surf and traffic plus the subsurface sources: occasional earthquakes, possibly groundwater flow, and whatever contribution there might be from hydrothermal effects. Vehicle noises are distinguishable by their transiency and, beyond a distance of a mile or so, their level is below the background level. In our survey no recording was made during rainfall. Surf noise in the 1- to 30-Hz band seems to be below background at a distance of one mile from shore. It was difficult to judge the effect of wind; geophone was buried when possible and kept as distant as feasible from trees and tall grasses which might transmit wind forces to the geophone.

Three tests were made to determine whether or not there was long-term variation over the hours and days of the survey. First, during the survey, recordings were made at a single station every day at least once. The standard deviation of the measurements was 3 db. The final two tests used a seismic array deployed in the area for a microearthquake survey during the latter part of the ground-noise survey. Diurnal variation was examined by choosing a typical recording day and taking two-minute samples from three seismometers at every 100 counts of the tape recorder meter (which yielded between two and five samples per hour). The power levels of the three stations, which were roughly at a kilometer radius from a central recording trailer, showed a maximum peak-to-peak variation of 10 db with no evident diurnal components (Fig. 4). Longer term variation was examined using the same seismometers by taking ten-minute samples at 3 a.m., when wind and cultural noise is low (Fig. 4). Over a two-week

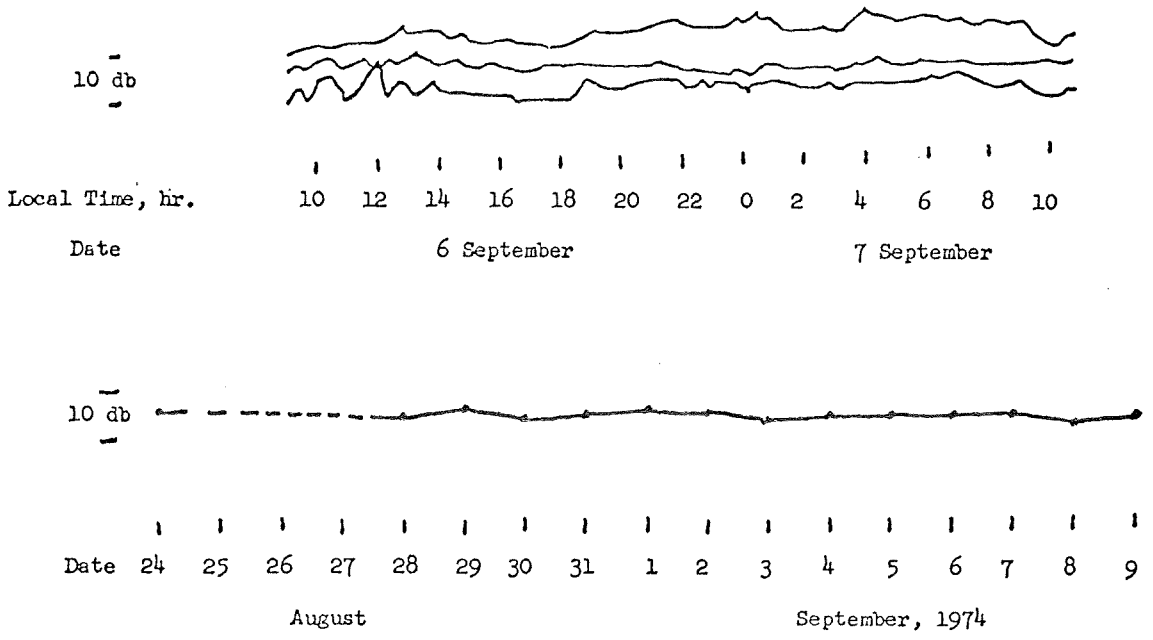

Figure 4. Time variation check. The top three traces are a plot of noise level at three widely spaced seismometers over a 24-hour period. Bottom trace is the 3 a.m. noise level over a 17-day period (dashed line indicates three days unrecorded).

period, one seismometer had a maximum peak-to-peak variation of two db and neither of the other two stations (which at times generated spurious noise by exceeding the FM frequency band limits) varied more than 10 db. Considering these tests, no time-corrections were applied to the ground-noise results.

Contour maps were made using SYMAP5, a mapping program developed at the Harvard Laboratory for Computer Graphics and Spatial Analysis. Figures 5 through 9 show the results of unfiltered signal (1 to 30 Hz) and of the noise filtered through bands centered at 2, 4, 8 and 16 Hz. Contours are at 5-db intervals, with darker shading indicating higher noise levels. The contour interval is equal to 1.4 standard deviations of the daily measurements at the reference site.

The low frequency narrow band maps have a simpler pattern. On all maps surf noise near the coast is apparent.

Also featured on all of the maps is a low noise band across the southern half of the survey area and a relative high in the vicinity of Puulena Crater. Since geothermal areas are characterized by a high noise level in a restricted frequency band, the spectrum of station 30 near the Puulena high was compared with that of station 46 with an overall lower noise level, a mile to the southwest (Fig. 10). The spectra are practically indistinguishable in shape; both show a steady decrease of about 2db/Hz between 1 and 10 Hz. However, in a narrow window surrounding 4 Hz, station 30 has a 7-db anomalous peak. Correspondingly, around station 30 is an area of high in the 4-Hz band (Fig. 7). The high in 4 Hz does not correspond to the geothermal reservoir found by HGP-A. In fact, pockets of high in the 4-Hz band ring the well HGP-A at a distance of 1 km, but near the well itself is an area of relative low.

Ground noise, no matter what frequency band was selected, did not show a spatial correlation with the geothermal reservoir at HGP-A. In fact, right at the well site there is a relative low on all frequency bands that were examined. It is concluded that at least for Kilauea east rift, ground noise does not have spatial correlation with known hydrothermal activity and associated processes.

On the other hand, there is a tendency of highs in all frequencies to be located in the northern part of the surveyed area. This is the area of the active rift zone, which on the surface is marked by alignment of craters, cracks and vents. Perhaps, ground noise correlates well with magmatic activity and associated processes.

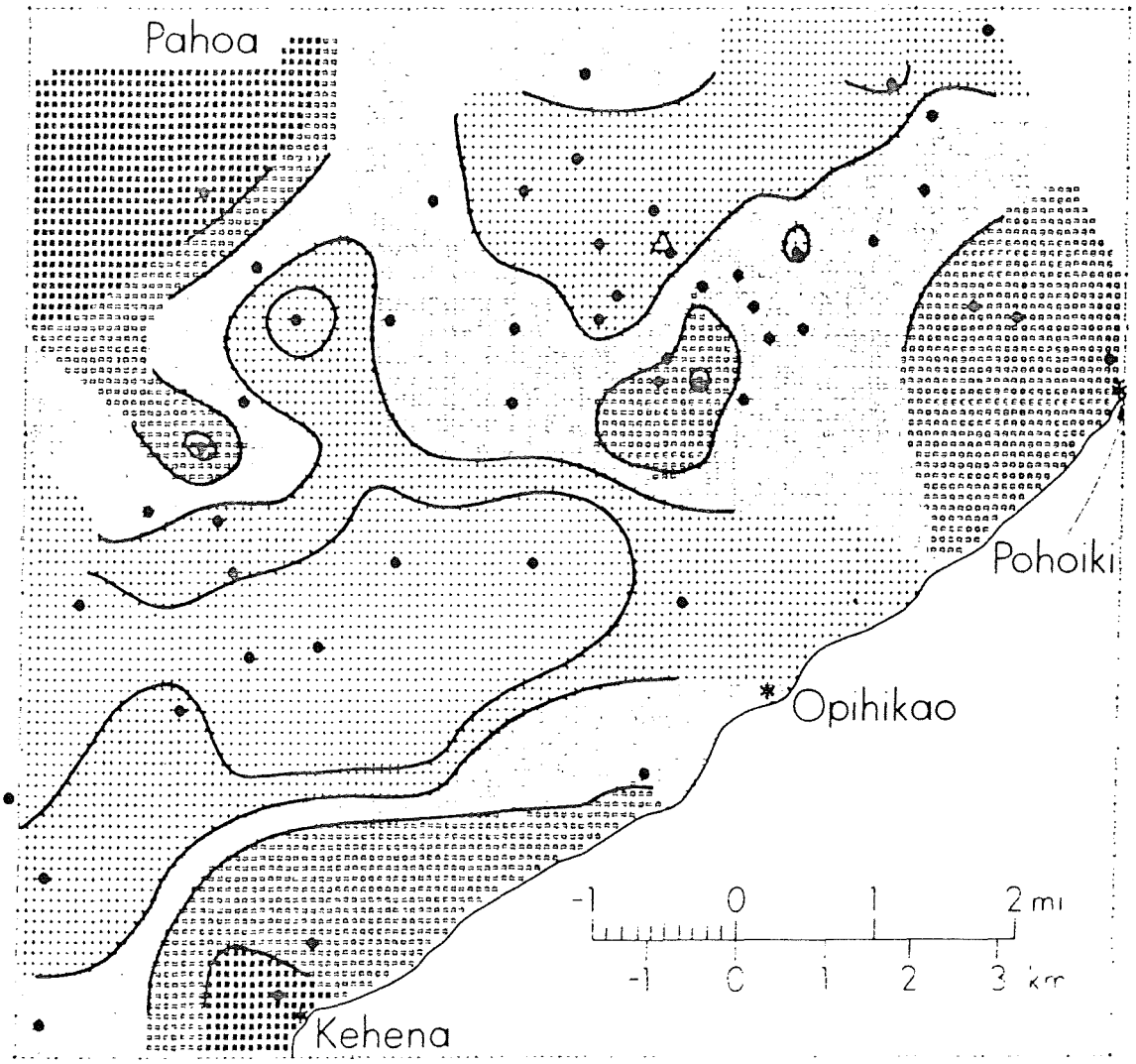

Figure 5. Seismic ground-noise intensity at 1-30 Hz. For Figures 4 to 8, contour interval in 5-db triangle denotes well site HGP-A. Circles show recording stations. Note differences in vertical and horizontal scales.

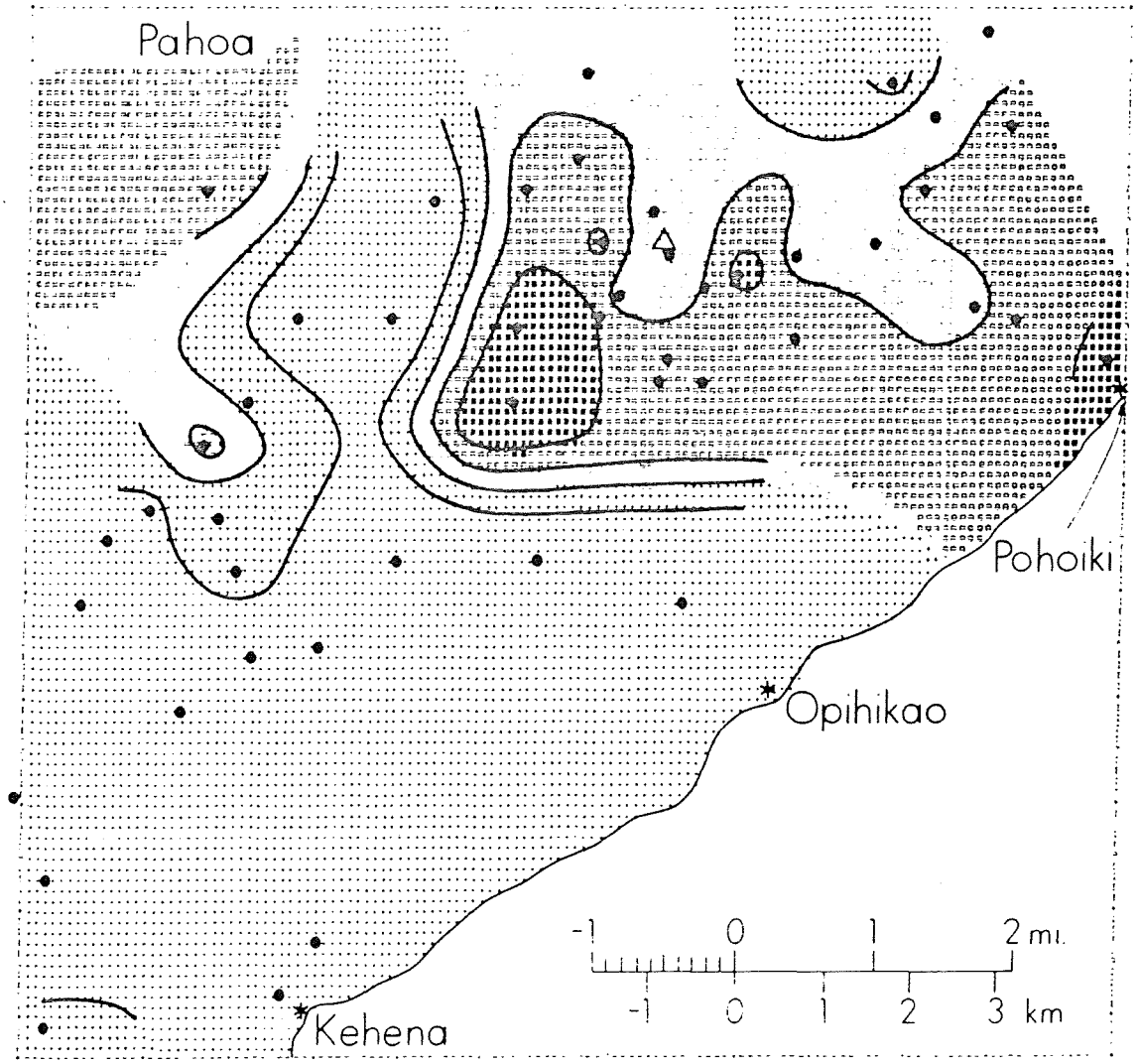

Figure 6. Seismic ground-noise intensity filtered at 2 Hz.

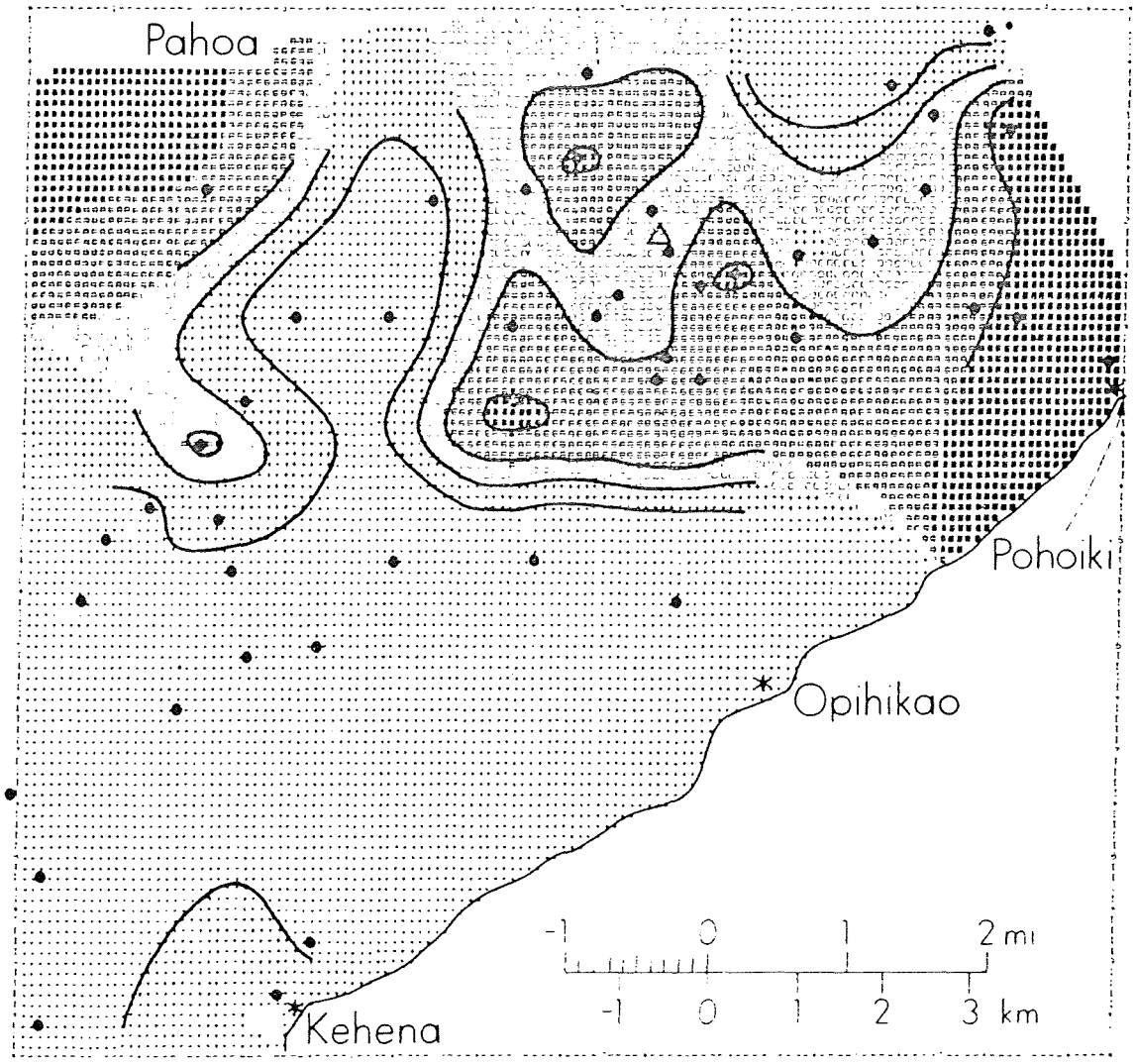

Figure 7. Seismic ground-noise intensity filtered at 4 Hz.

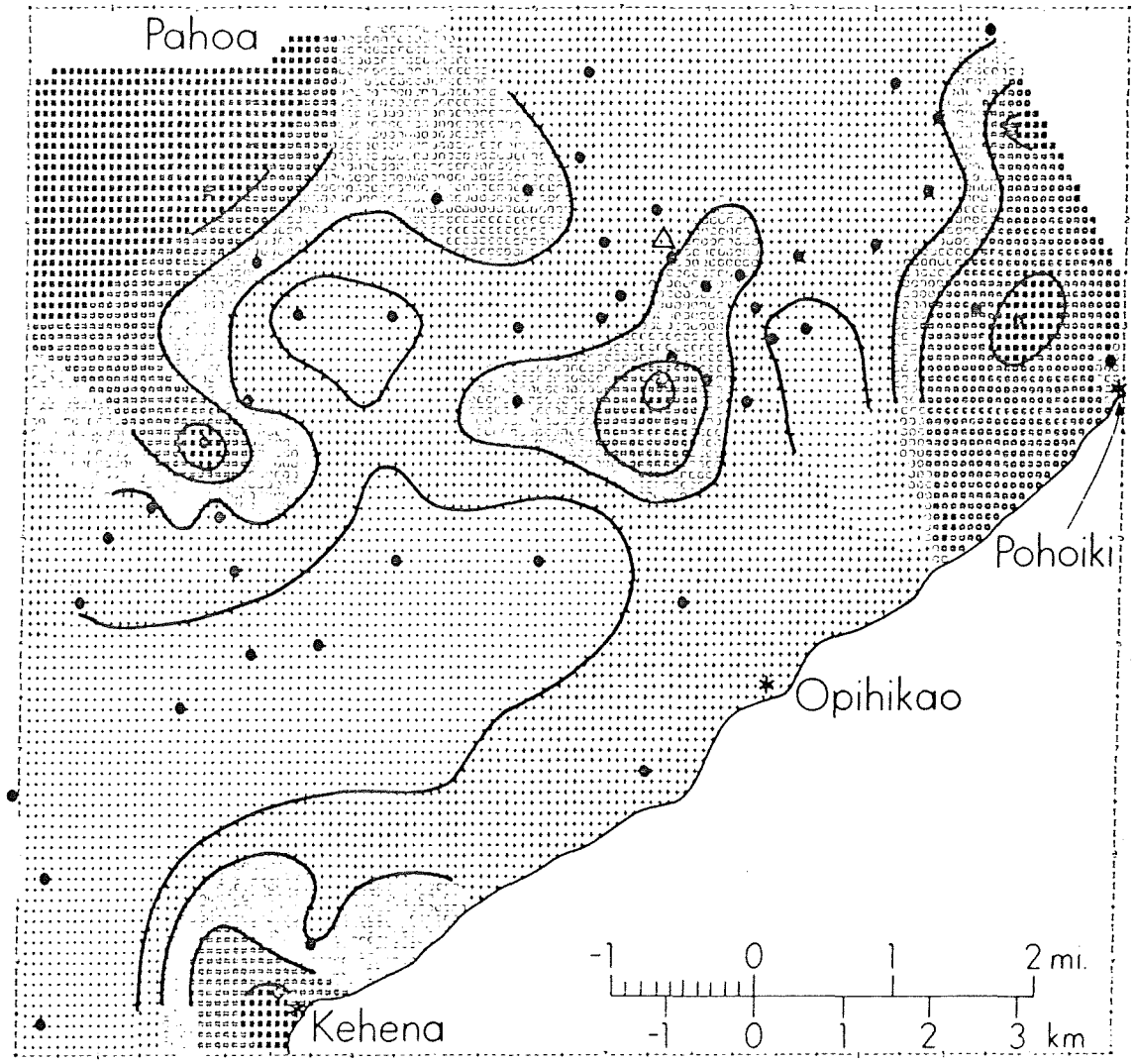

Figure 8. Seismic ground-noise intensity filtered at 8 Hz.

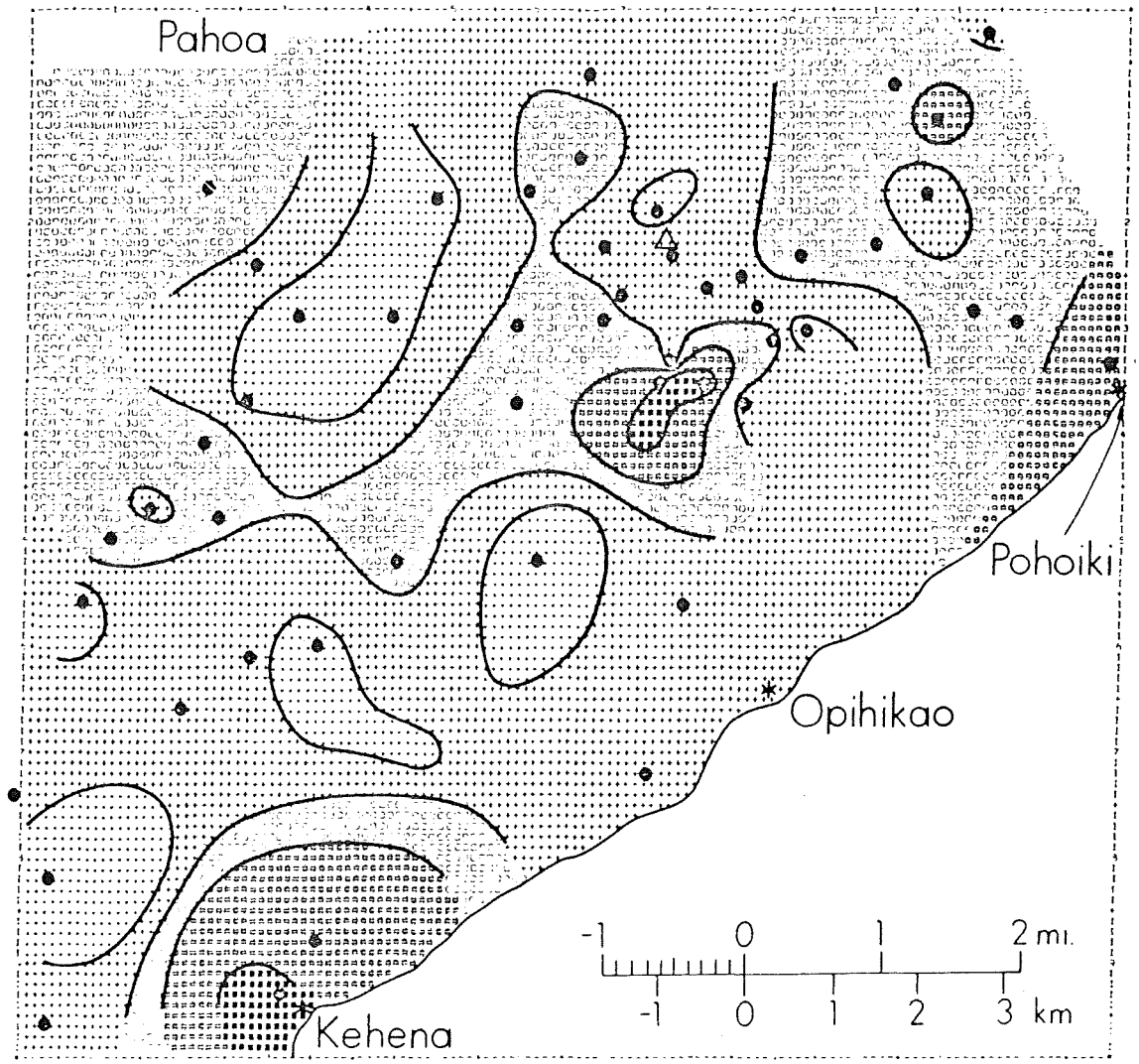

Figure 9. Seismic ground-noise intensity filtered at 16 Hz.

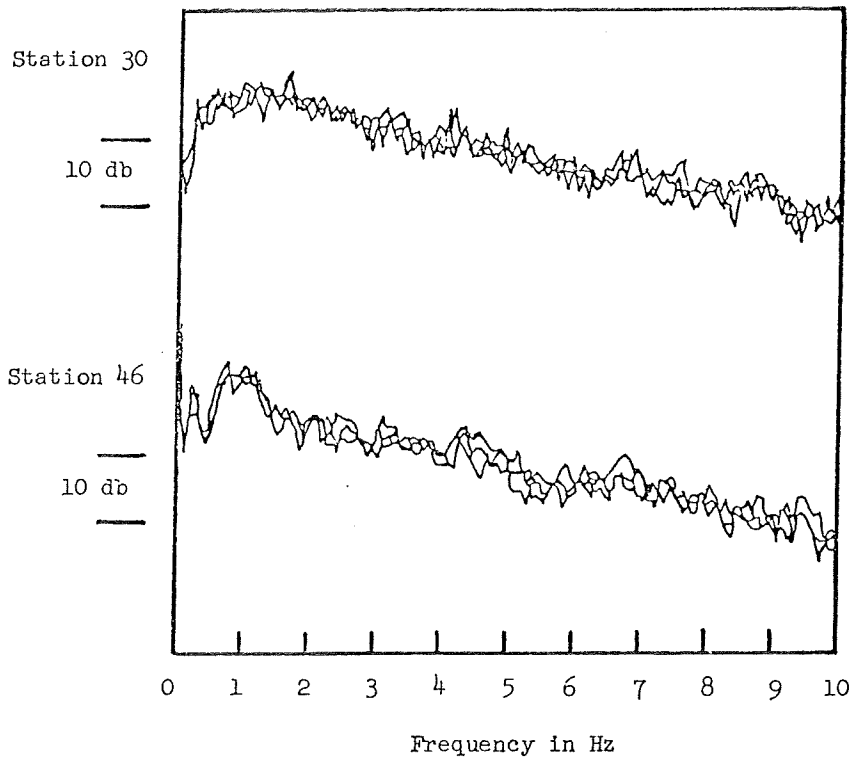

Figure 10. Comparison of ground-noise spectra at high noise station (30) near Puulena Crater (top graph) and a station in a low-noise region about a mile southwest of Puulena (46) (bottom).

ACKNOWLEDGMENTS

Seth Thompson helped with the fieldwork and did most of the data reduction. Siegfried Ching helped in the earlier reconnaissance survey. Candace Fenander produced the computer contour maps. Marlene Kam put together the figures for publication. Wayne Suyenaga helped us in the organization of the paper. This study was supported by grant E(04-3)-1093 from Energy Research and Development Agency.

REFERENCES

Clacy, G.R.J., 1968. Geothermal ground noise amplitude and frequency spectra in the New Zealand volcanic region. J. Geophys. Res., v. 73, p. 5377-5384.

Douze, E.J. and G.G. Sorrells, 1972. Geothermal ground noise surveys. Geophysics, v. 37, p. 813-824.

Goforth, T.T., E.J. Douze and G.G. Sorrells, 1972. Seismic noise measurements in a geothermal area. Geophys. Prosp., v. 20, p. 76-82.

Iyer, H.M. and Tim Hitchcock, 1974. Seismic noise measurements in Yellowstone National Park. Geophysics, v. 39, p. 389-400.

Luongo, G. and A. Rapolla, 1973. Seismic noise in Lipari and Vulcano Islands, Southern Thyrrenian Sea, Italy. Geothermics, v. 2, p. 29-31.

Whiteford, P.C., 1970. Ground movement in the Waiotapu geothermal region New Zealand. Geothermics (special issue on U.N. Symp. Dev. Util. of Geoth. Res.), part 2, p. 478-486.

CRUSTAL STRUCTURE OF THE EAST RIFT ZONE OF KILAUEA, HAWAII FROM SEISMIC REFRACTION. 1. NEAR-SURFACE STRUCTURE

Wayne Suyenaga

Hawaii Institute of Geophysics
University of Hawaii
Honolulu, Hawaii 96822

ABSTRACT

A seismic refraction survey designed to provide the near-surface seismic structure of the axis and flank of the east rift zone of Kilauea volcano was carried out in January 1976. Results reveal a surface layer of very low velocity (0.7 to 1.6 km/sec), which is probably interlayered lava flows with very large voids. Beneath the surface layer, velocities of 2.5 km/sec on the flank and 3.1 km/sec on the rift are observed. The change in velocity between the surface and second layer probably reflects the saturation of water at the water table. This structure differs from previous models based on studies which, because of the shot receiver distances, could not distinguish the surface layer.

INTRODUCTION

Seismic refraction studies of the island of Hawaii have generally involved shot-receiver distances greater than several kilometers (Ryall and Bennett, 1968; Hill, 1969). Thus knowledge of the shallow seismic structure less than one-kilometer depth is limited. Hill (1969) circled Hawaii with shots at sea and recording stations on land. Surface velocities were derived by connecting the nearest first arrival with the origin. For example, data recorded at Kamoamoa (Fig. 1) from shots at distances of 3 to 6 km toward the northeast delineate a layer with velocity of 3.1 km/sec. By connecting the nearest first arrival with the origin, a 780-m-thick surface layer of 1.8 km/sec was derived. The shortest shot-receiver distance occurred in an experiment by Ryall and Bennett (1968), who recorded a shot near the Kilauea summit (Fig. 1) at distances of 0.73 km to more than 6 km. A surface layer of 1.66 km/sec was inferred from second arrivals at distances between 1.3 and 6.5 km; its thickness was established as 0.2 km.

This report describes a seismic refraction survey designed to provide near-surface seismic structure of the axis and flanks of the east rift zone of Kilauea volcano in Puna, Hawaii.

SETTING

The east rift zone of Kilauea extends southeast from the summit caldera for about 8 km, where it bends east-northeastward, extends for another 50 km on land, and continues out to sea (Fig. 1). The easternmost end of the rift zone is known as Puna (Fig. 2). The rift zone is characterized by pit craters, cinder cones, and cracks in the ground. Eruptions in Puna last occurred in 1955 and 1960 (Macdonald and Abbott, 1970, p. 85-96).

The east rift zone has built up a flank that consists entirely of lava flows; it is possible that these flows overlie a flank of Mauna Loa.

A Bouguer gravity anomaly of about 10 to 20 mgal associated with the east rift has been interpreted as indicating a high density area on the axis of the rift zone.

Field Methods and Data Reduction

Two short reversed refraction lines were completed in January 1976. The Leilani line, with shotpoints W and E, was located approximately over the crest of the rift zone and the Kalapana line, with shotpoints N and S, was on the southern flank of the rift zone (Fig. 2).

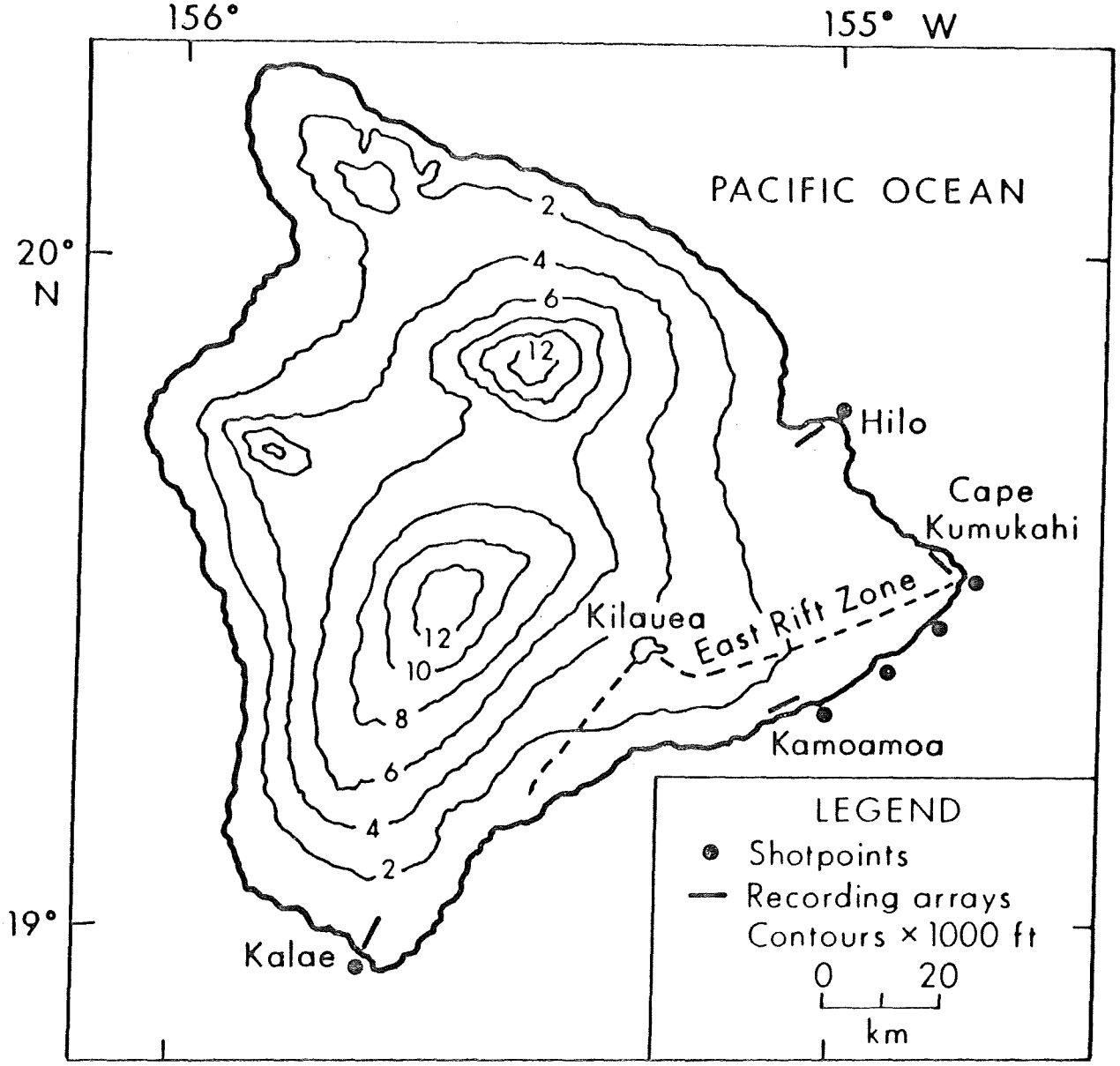

Figure 1. Map of island of Hawaii showing Kilauea caldera and its rift zones, shotpoints and near recordings of refraction line from Hilo to Kalae (Ryall and Bennett, 1968), and seismic receivers at Cape Kumukahi and Kamoamoa with intervening shotpoints (Hill, 1969).

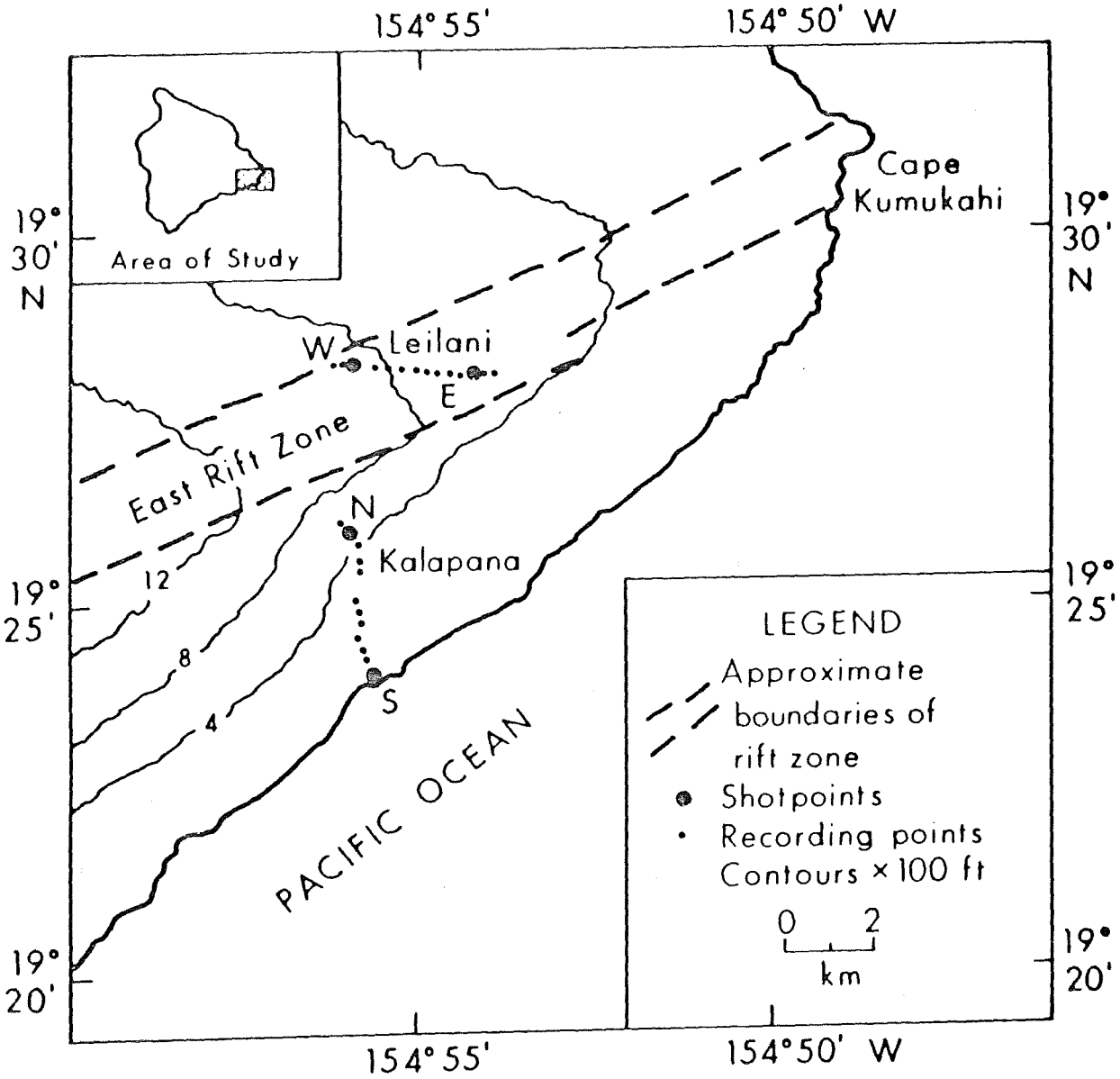

Figure 2. Map of Puna, Hawaii showing the approximate boundaries of the surface expression of the east rift zone of Kilauea and the refraction lines discussed in this paper. W, E, N, and S are shotpoints and dots are recording points.

Two recording systems were deployed. One system consisted of twelve Mark Products L-25 4.5-Hz geophones amplified by two six-channel multiplexed components and recorded on a TEAC R70A cassette data tape recorder. Geophone spacing was in-line at 50-foot intervals. The other system consisted of two L-25 geophones each amplified by a Sprengnether AS110 amplifier and recorded on a similar TEAC tape recorder. The geophones were placed along the shot-receiver line at an approximate 500-foot spacing. Each tape recorder recorded time marks and voice commentary with shot tone.

At each end of the two refraction lines six shots were fired. Size of the shots ranged from four to sixteen pounds of Aquagel. At shot point N, shots were limited to four pounds due to the proximity of a house. The depth of most of the shots was fifteen feet. Distances were measured by tape to the nearest intersection of the main roads in the area. From that point shot-receiver distances were calculated directly from subdivision maps.

The data were bandpass filtered at 5-30 Hz and recorded on paper. The quality of first arrivals was good out to 2-km distance but very poor beyond about 3 km. Arrival times were corrected for elevation but not for weathering because the thickness of the soil layer in all cases was negligible.

Results

The results of the survey are summarized in Figure 3. Figure 3a is the travel time plot for the Leilani line. From shotpoint W, a low-velocity surface layer of approximately 0.7 to 0.8 km/sec is defined by two points on both sides of the shot. A second layer is defined by first arrivals at 1.0 and 2.0 km/sec and a second arrival at 2.4 km. This layer has an apparent velocity of 2.5 km/sec. At about 2.4 km, the slope of the travel time plot first decreases then increases gradually to a distance of about 3 km, beyond which first arrivals were not recorded.

From shotpoint E, the surface layer is recorded by one point on each side of the shot (one geophone was inoperative). Velocity to the east was 1.1 km/sec and to the west it was 1.6 km/sec. Large amplitude secondary arrivals at 1.0 to 1.2 km were interpreted as direct arrivals and had a velocity of 0.9 km/sec. Thus, the surface layer has a low but highly variable velocity. A shot recorded between 1.0 to 1.2 km showed a very poor pattern of arrivals. This plus the change in slope at 2.3 km from W suggests that the structure is very complex in that vicinity. At distances between 1.8 and 2.5 km from E, first arrivals indicate a high apparent velocity of 3.9 km/sec. The extension of this velocity indicates a travel time of 1.2 sec at W, which is within 5 per cent of

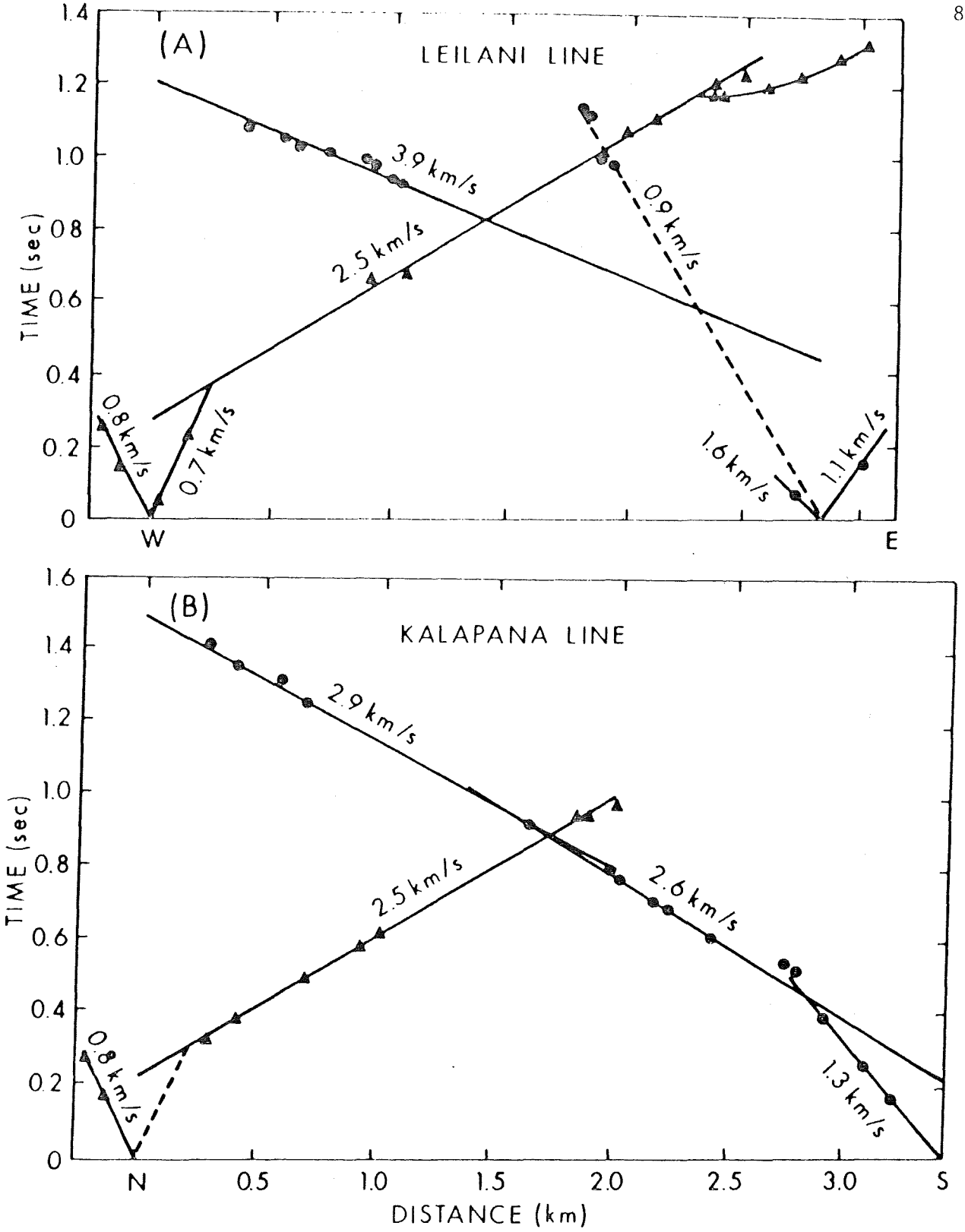

Figure 3. Travel times of first arrivals for the Leilani (A) and Kalapana (B) lines. Times were fitted by eye and resulting velocities calculated (km/sec). Dots denote arrivals from E and S. Triangles denote arrivals from Ward N. Travel times of only end members of twelve geophone array have been plotted. Distance between shotpoints W and E is 2.83 km. Distance between shotpoints N and S is 3.44 km.

the travel time in the other direction, indicating that the high apparent velocity probably continues out that far.

The Leilani travel times were fitted by eye to the standard form $t = t_i + \Delta/V$, where t is travel time, t_i is the intercept time, Δ is distance, and V is velocity (Table 1). Neglecting the already noted complexity near 1 km from E, a simple model was constructed by assuming a surface velocity of 0.8 km/sec with a dipping second layer (Fig. 4). The interface between the two layers dips 3° toward the east and the velocity of the second layer is 3.1 km/sec.

Figure 3b is the Kalapana travel time plot. From N, a surface velocity of 0.8 km/sec was measured toward the north. This velocity was assumed to apply southward and is indicated by the dashed line. An apparent velocity of 2.5 km/sec was measured for a second layer by first arrivals from 0.3 to 2.1 km. Since shot size was limited at N, the latter arrivals are weak and one recording at a greater distance was not used. From S, a surface velocity of 1.3 km/sec was measured using three first arrivals and a well-defined second layer of 2.6 km/sec was recorded out to 1.7 km. Velocity increased at that point to 2.9 km/sec.

The Kalapana travel times were analyzed in a manner similar to the Leilani data (Table 1). The data indicate a surface layer of variable velocity (0.8 to 1.3 km/sec) overlying a layer of 2.5 km/sec. The interface between the two layers was assumed to have no dip since the apparent velocities in either direction are comparable and the travel time plots intersect at the midpoint of the line. A third layer of velocity 2.9 km/sec is indicated from one end of the line. Data were not available from the other end. A three-layer model was derived (Fig. 1) using an average surface velocity of 1.0 km/sec. The depth to the 2.5- and 2.9- km/sec layers were 110 m and 320m, respectively.

DISCUSSION and CONCLUSIONS

The low velocity layer is comprised of interlayered aa and pahoehoe lava flows (D. Palmiter, unpub. rept., Hawaii Inst. Geophys. 1976). Rinehart and Greeley (1971) reported near-surface velocities of 1.2 to 2.4 km/sec on a pahoehoe flow. The lower velocities reported here are attributed to the large voids between flows and within the aa flows, which decrease the bulk density of the entire structure.

Beneath the surface layer, velocities of 2.5 km/sec are observed on the flank and 3.1 km/sec over the rift zone. Such high velocities are not thought to be associated with any drastic change in lithology (D. Palmiter, unpub. rept., Hawaii Inst. Geophys. 1976). The change in velocity between the surface and second layer probably reflects the saturation with

Travel times for east rift refraction

Table 1.

Refraction Line	Shot-point	Travel time curves*
Leilani	W	$T_0 = 0.00 + \Delta/0.66$
		$T_1 = 0.27 + \Delta/2.51$
	E	$T_0 = 0.00 + \Delta/1.61$ (0.93)
		$T_1 = 0.44 + \Delta/3.86$
Kalapana	N	$T_0 = 0.00 + \Delta/0.82$
		$T_1 = 0.202 + \Delta/2.51$
	S	$T_0 = 0.00 + \Delta/1.35$
		$T_1 = 0.215 + \Delta/2.56$
		$T_2 = 0.30 + \Delta/2.92$

* Travel time curves in seconds. Δ is distance in km.

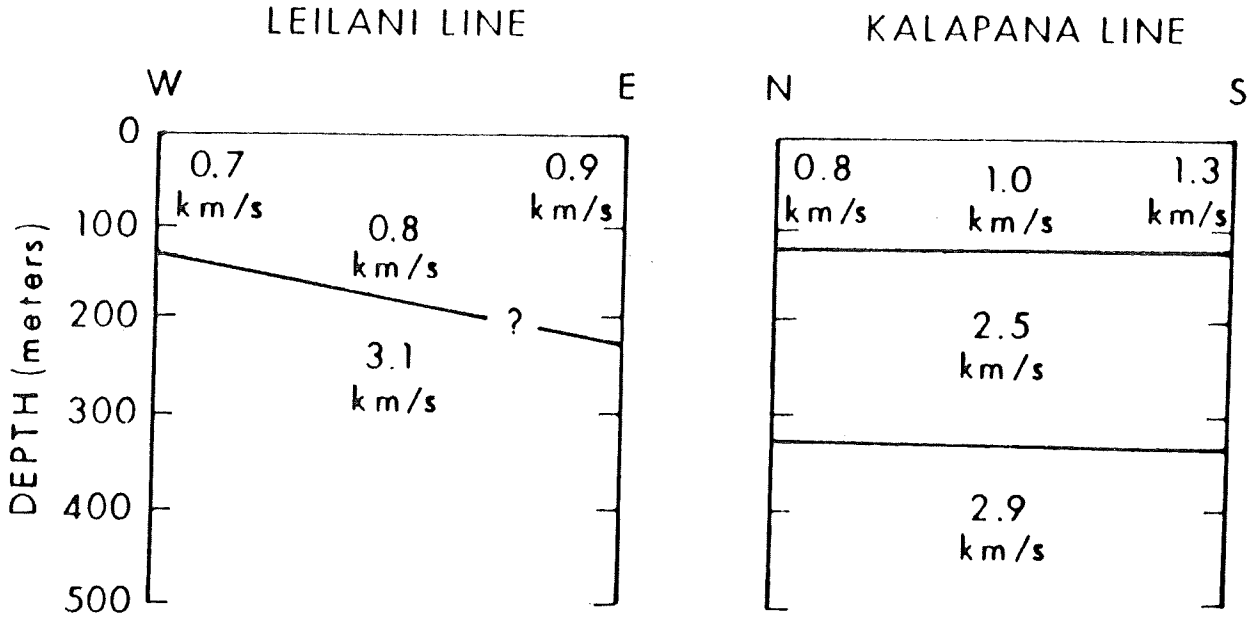

Figure 4. Shallow crustal models derived for crest of rift zone (Leilani) and flank (Kalapana). Vertical exaggeration is approximately 6:1.

water at the water table. At low pressures, the compressional velocity in rocks is strongly affected by saturation. Christensen and Salisbury (1975) show that in basalts from the East Pacific Rise, velocity increased from 4.1 km/sec (dry) to 6.0 km/sec (saturated) at atmospheric pressure.

Seismic data and models presented here suggest why the shallow structure of Hill (1969) is not applicable to the Puna region. If Hill (1969) had closer shot positions at Kamoamoa, they probably would have plotted on the extension of the 3.1-km/sec line or slightly lower (Fig. 5). In analysis, the effect of this would be to decrease both velocity and thickness of the surface layer. We conclude that the presently accepted shallow seismic structure does not properly describe the Puna area. However, the change in the near-surface seismic structure does not affect the applicability of present models to earthquake studies (e.g. Ward and Gregerson, 1973) since travel times vertically (or nearly vertical) through them and the models presented here are almost identical.

Two seismic studies have indicated that beneath the East Rift zone near the summit there exists a high velocity layer (Ward and Gregerson,1973; Ellsworth and Koyanagi, 1977). Based on the mislocation of earthquakes at the summit by a seismic array in Puna, it has been suggested by Suyenaga and Furumoto, 1978) that this high velocity layer extends along the rift zone to Puna and that it probably coincides with a high density formation associated with a gravity maximum over the rift zone (Kinoshita, 1965; Furumoto et al., 1976).

This refraction survey was not successful in determining the depth to the high velocity-high density material. Gravity (Furumoto et al., 1976) studies indicate that the zone is expected at about depths of one kilometer or slightly deeper. Second layer velocities of 3.1 km/sec at 100-200 m depths were measured under the rift zone. This is higher than the 2.5-km/sec measure under the flanks, but is not indicative of a high density zone which would probably have a velocity near 6 km/sec (Manghnani and Woollard, 1965). If a refractor of 6 km/sec did underlie the 3.1-km/sec layer at about one kilometer, first arrivals would be received at distances greater than four kilometers. Shot sizes used in this work were the largest that safety permitted, and arrivals were very poor to useless at distances greater than three kilometers. A suggested experiment would involve shots over the extension of the rift zone at sea east-northeast of Cape Kumukahi with recording on the rift zone on land.

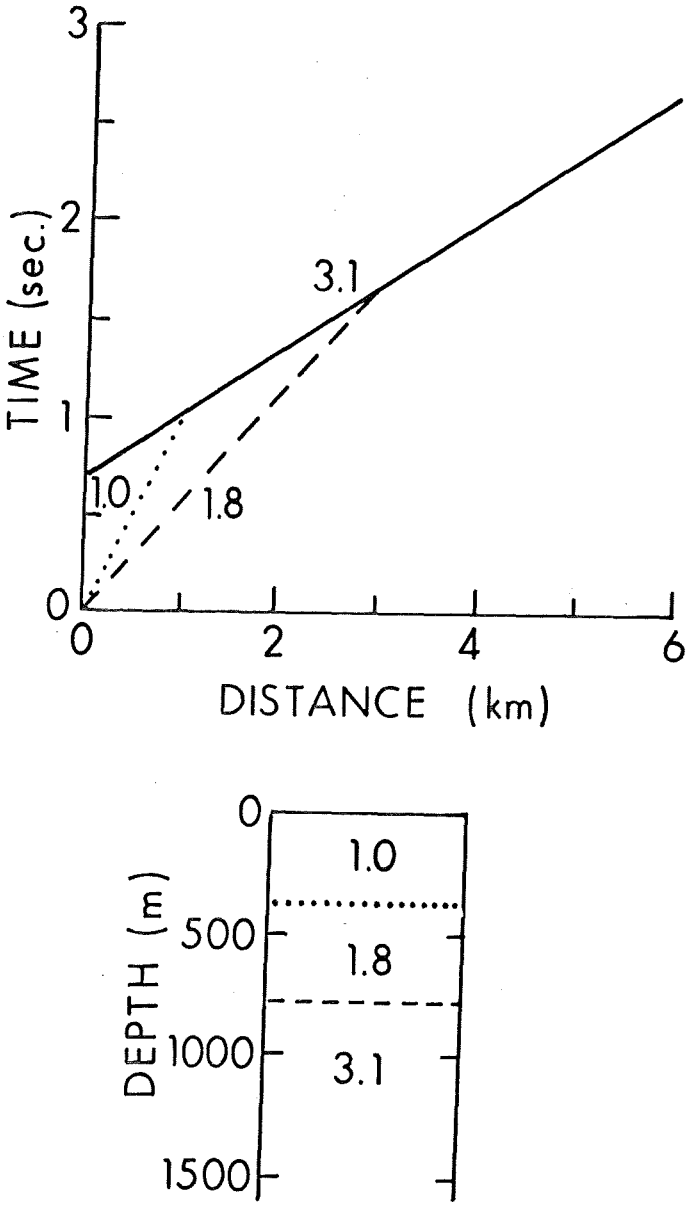

Figure 5. Travel time plot of data recorded at Kamoamoa from shots to the northeast at distances of 3 to 6 km and derived shallow seismic structure (after Hill, 1969). Dashed lines on travel time plot and model denote Hill's assumed surface layer velocity and thickness. If recordings to 1 km revealed extension of the 3.1-km/sec line then assumed surface layer velocity and thickness would be reduced as shown by dotted lines on travel time plot and model.

ACKNOWLEDGMENTS

A. S. Furumoto initiated this project and was involved in all of its phases. Carrol Dodd designed and constructed one of the seismic amplifier systems. Mike Broyles and Pat Lineberger helped in organizing and carrying out the instrument testing and fieldwork. Candy Fenander, Marlene Kam and Roger Norris assisted in the field work and the data processing; and Carol Yasui helped coordinate the entire effort. The author would especially like to thank Steve Hammond and Don Hussong for handling the explosives and aiding in repairs in the field. Samuel Kamau, Peter Shayne and Art Isemoto (for the County of Hawaii) permitted use of their land. Al Rudman greatly improved an early manuscript.

REFERENCES

Christensen, N. I. and M. H. Salisbury, 1975. Structure and constitution of the lower oceanic crust. Rev. Geophys. Space Phys., v. 13, p. 57-86.

Ellsworth, W. L. and R. Y. Koyanagi, 1977. Three-dimensional crust and mantle structure of Kilauea Volcano Hawaii. J. Geophys. Res., v. 82, p. 5379-5394.

Furumoto, A. S., R. Norris, M. Kam and C. Fenander, 1976. Gravity profile and the intrusive zone. Hawaii Geothermal Project Initial Phase II Progress Report, Univ. of Hawaii, Honolulu, p. 26-31.

Hill, D. P., 1969. Crustal structure of the island of Hawaii from seismic-refraction measurements. Bull. Seism. Soc. Am., v. 59, p. 101-130.

Kinoshita, W. T., 1965. A gravity survey of the island of Hawaii. Pac. Sci., v. 19, p. 339-340.

Macdonald, G. A. and A. T. Abbott, 1970. Volcanoes in the sea: The geology of Hawaii. 441 pp., Univ. of Hawaii Press, Honolulu.

Manghnani, M. H. and G. P. Woollard, 1965. Ultrasonic velocities and related elastic properties of Hawaiian basaltic rocks. Pac. Sci., v. 19, p. 291-295.

Palmiter, D., 1976. Lithology of HGP-A, unpublished report of Hawaii Inst. of Geophysics.

Rinehart, J. S.and R. Greeley, 1971. Seismic-wave velocity patterns in some pahoehoe basalt flows. J. Geophys. Res., v. 76, p. 5765-5769.

Ryall, A. and D. L. Bennett, 1968. Crustal structure of southern Hawaii related to volcanic processes in the upper mantle, J. Geophys. Res., v. 73, p. 4561-4582.

Suyenaga, W. and A. S. Furumoto, 1978. Microearthquake study of the East Rift Zone of Kilauea, Puna, Hawaii, this volume.

Ward, P. L. and S. Gregersen, 1973. Comparison of Earthquake locations determined with data from a network of stations and small tripartite arrays on Kilauea volcano, Hawaii, Bull. Seism. Soc. Am., v. 63, p. 679-711.

CRUSTAL STRUCTURE OF THE LOWER EAST RIFT ZONE OF KILAUEA, HAWAII FROM SEISMIC REFRACTION.

2. COMPLETE STRUCTURE

Michael L. Broyles
Augustine S. Furumoto

Hawaii Institute of Geophysics
University of Hawaii
Honolulu, Hawaii 96822

ABSTRACT

The 1977 seismic refraction survey of the Puna region of the East Rift Zone of Kilauea was an attempt to interpret the structure within the east rift outlining the arrangement of the dike intrusions and their relationship to the regional crustal structure. Previous studies of the crustal structure of Hawaii have either used long refraction lines that could not delineate the fine structure in the rift zones or short refraction lines unable to penetrate of the depth of the high velocity material comprising the intrusive dike complex.

From this study, it is concluded that the depth to the top of the intrusive complex averages 2-2.5 km. Other studies indicate that the lower limit of the intrusion is at 4-5 km. This analysis also suggests that the subsurface lateral extent of the rift complex is much wider, 12-19 km, than the surface expression would indicate.

A northward dip of 6-9° on the upper surface of the main complex is compatible with the seismic refraction and gravity data and suggests lateral development of the rift to the south.

INTRODUCTION

The purpose of this paper is to report the methods and results of the 1977 Puna seismic refraction experiment. The refraction project recorded two lines in an attempt to outline the lateral extent of the east rift as well as to determine the depth of the intrusive anomaly or main dike complex.

The landward expression of the east rift extends for more than 60 km from the summit of Kilauea volcano to Cape Kumukahi (Fig. 1), while the seaward expression of the east rift extends for another 60-80 km from Cape Kumukahi northeastward. Studies by Malahoff and McCoy (1967) indicate that the seaward expression of the rift is characterized by high gravity and magnetic values.

Within the landward expression of the rift zone, four distinct surface features occur in this order from north to south (Moore and Krivoy, 1964): (1) eruptive fissures, (2) eruptive cones, (3) pit craters, (4) fault scarps. These features are aligned in northeasterly direction forming the dominant trend of the rift zone (Fig. 1). At the surface, steam seeps from these features in areas of recent lava flows.

The eruptive fissures, according to Moore and Krivoy (1964), mark the intersection of the surface with a fault plane. Furthermore, Moore and Richter (1962) and Moore and Krivoy (1964) suggest that the regularity in placement of the vents, craters and scarps delineate not only the surface expression of the rift but possibly a subsurface southward dip as well. The example of these relationships discussed by Moore and Krivoy (1964) is the Hilina fault system, which they believe is a gravity fault intersecting the main rift system. Swanson et al. (1976) agree that gravity faults characterize the Hilina fault system but hypothesize that these features are secondary and point out a region south of the rift and north of the Hilina fault system that is unfaulted (Fig. 1).

Below the surface, the rift is believed to be an arrangement of dense, nearly vertical dikes, each dike about 2 meters wide (Macdonald, 1956). The vertical extent of the dikes in the rift system is unknown, as pointed out by Fiske and Jackson (1972), but Macdonald (1956) suggested that the dikes reached the level of the magma reservoir of the summit region, about 2-4 km below the surface.

The nature of the gravity anomaly over the east rift may provide some clues as to the shape of the intrusive complex. The asymmetric shape of the gravity anomaly on

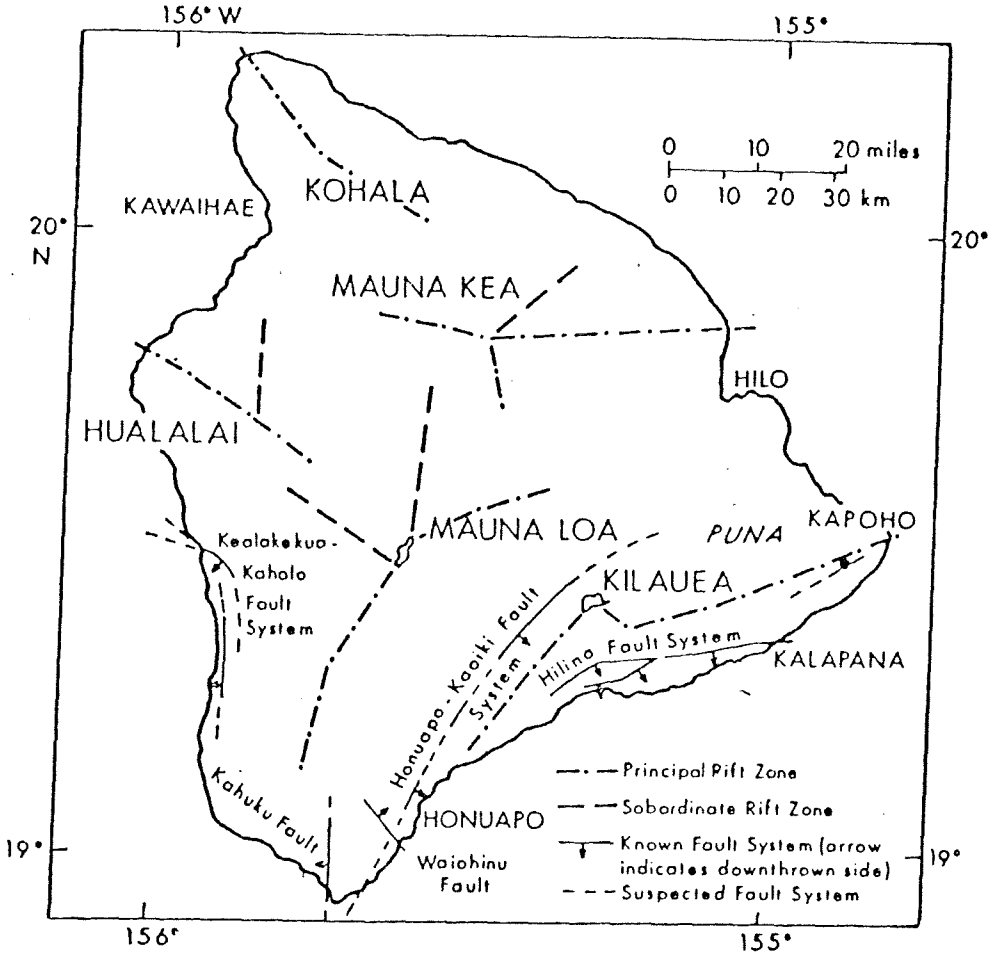

Figure 1. The island of Hawaii and the east rift zone of Kilauea (From Macdonald, 1956).

the east rift with steeper gradients on the south side is the result of a wedge-shaped prism with a gentle sloping north face and a steep sloping south face, according to Swanson et al. (1976). The prism would be the expected result of southward growth of the rift as the younger dikes intrude on top of the older dikes to the north. As the younger dikes intrude at higher elevations, the rift would grow southward and upward.

One of the questions that the 1977 refraction survey expected to answer was the orientation of the intrusive structure at depth. Does the intrusive body dip? And, if so, in what directions? The orientation of the intrusive complex might shed some light on the present development of the rift.

In addition to investigating the nature of the intrusive body, other aspects of the crustal structure that we expected to study included:

(1) The lateral extent of the rift and its subsurface conformity to the regional crustal structure.

(2) The velocity structure of the crust from seismic refraction analysis as compared to the velocity structure of the core samples from the geothermal well site (Fig. 2, pt. A).

PREVIOUS SEISMIC REFRACTION STUDIES

Previous seismic refraction studies of the island of Hawaii involved either long refraction lines with shot-receiver separations of two kilometers or more (Ryall and Bennett, 1968; Hill, 1969) or short refraction lines with shot-receiver separations of generally less than 3 km (Suyenaga, 1978).

Based on a partly reversed seismic refraction profile conducted from Hilo to Kalae (Fig. 1), Ryall and Bennett (1968) indicated that the crust on the northeast coast of Hawaii in the vicinity of Kilauea could be separated into three layers:

(1) A basal layer from 6-7 km thick with P-wave velocities of 7.0 km/sec;

(2) A second layer with a velocity of 5.3 km/sec and less of regular thickness;

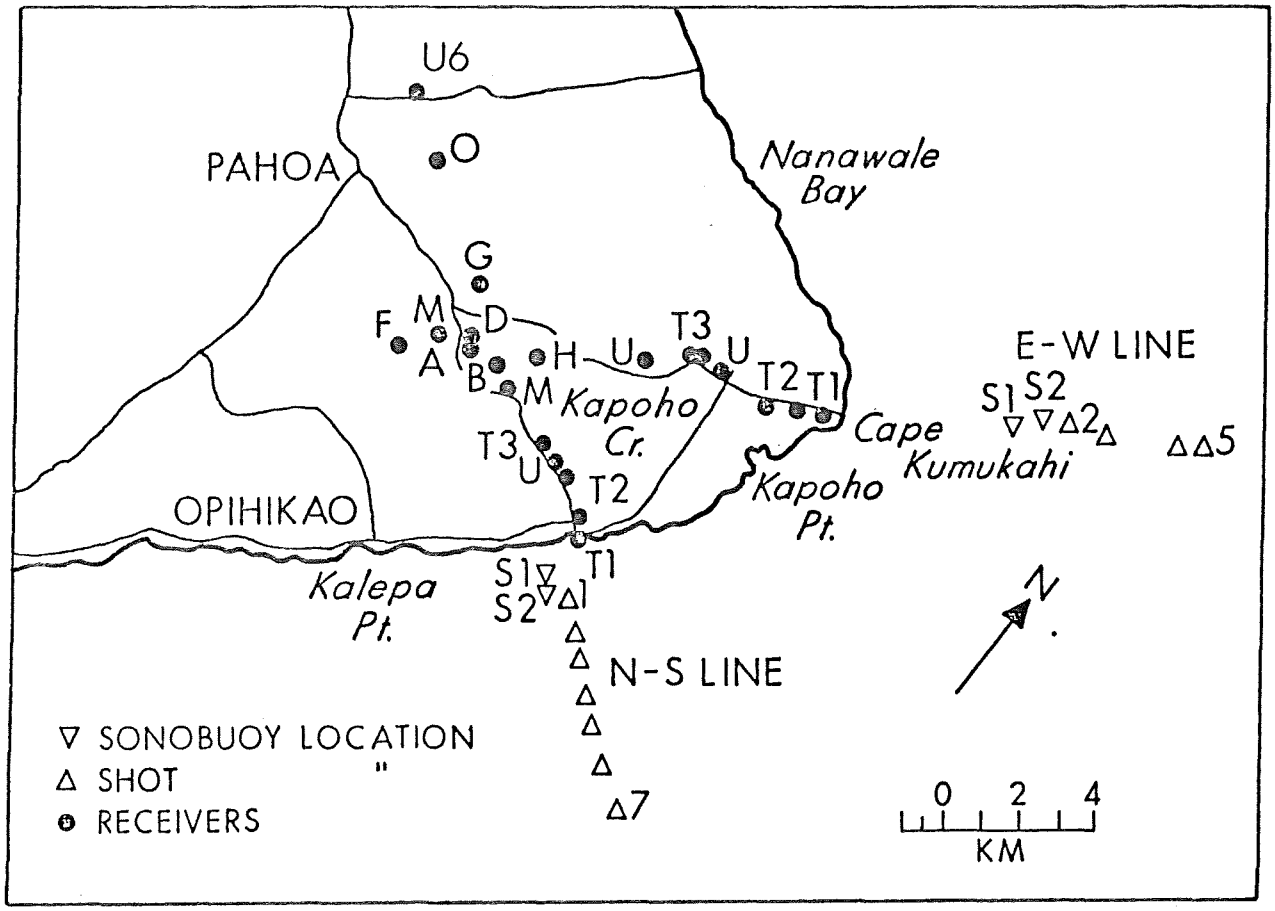

Figure 2. Locations of shots and recorders used in the refraction survey. S1 and S2 are positions of recording of sonobuoys before and after each recording session.

(3) An upper layer varying in thickness from 1.2-2.5 km and represented by P-wave velocities of 3.0 km/sec. This layer is believed to be a series of fractured vesicular flows.

The results of Hill's study suggested that the crust under Hawaii can be separated into two principal layers:

(1) A basal layer from 4-8 km thick with P-wave velocities of 7.0-7.2 km/sec.

(2) An upper layer from 4-8 km thick with P-wave velocities of 1.8-3.3 km/sec at the surface to 5.1-6.0 km/sec at depth.

Hill (1969) speculated that the basal layer was probably the old oceanic crust under Hawaii and that the upper layer probably consisted of lava flows. He also noted that the early P-wave arrivals from the summits and major rift zones of the volcanoes are indicative of material of velocities up to 7.0 km/sec approaching the surface to within 2 or 3 km.

Suyenaga (1978) recorded two refraction lines, about 3 km long, one across the rift and the other just off the rift. Beneath a low velocity surface layer, velocities of 2.5 km/sec and 2.9 km/sec were observed on the flank and 3.1 km/sec over the rift. The experiment did not succeed in determining the depth to which velocities higher than 3.1 km/sec were observed.

FIELD DATA

Two refraction lines were completed in Puna, Hawaii in January 1977. One line, the EW line, spanned some 22 km along the strike of the east rift from south of Pahoa through the geothermal well site (Fig. 2, pt. A) to cape Kumukahi. The other line, the NS line, stretched 12 km from north of Pahoa to the coast (Fig. 2).

Various types of seismometers were deployed along these lines. The manned stations (Fig. 2, pts. T) consisted of 4 channel TEAC R-70 cassette recorders connected to an amplifier on two to three seismic channels. The fourth channel was used to monitor WWVH radio time signals with on-station voice announcements. The tape cassettes were turned on a few minutes before each shot and off when there was a delay in the shooting schedule.

The unmanned systems (Fig. 2, pts. U) used a magnetic tape recorder set on a 10-day cycle. The system contained both a WWVH receiver and an auxiliary time code generator synchronized with a traveling clock. The geophone was connected to the recording unit with a 20-foot cable.

At one location on both the NS and EW lines, a Sprengnether microearthquake system (Fig. 2, pts. M) was used with smoked paper.

Around the well sites at locations A, B, C, D, F, G, and H were located the array network. The transducers used in the array were Mark Products L-25, 4.5-Hz geophones. Three of the elements A, F and G were telemetered on frequencies of 162-166 MHz from the positions indicated (Fig. 2). The other elements of the array were hardwired with disposable type torpedo wire placed on the surface with distances of up to 1 km.

The signals from the telemetered and hardwired geophones were amplified by twelve channel system that multiplexed the signals into two channels of a tape recorder. The tape recorder used was a Hewlett-Packard reel-reel type unit located at a temporary field communications center.

Three ocean bottom seismometers (OBS) were borrowed from the marine geology group at H.I.G., but as none of the units functioned properly, data from these instruments were not used in the analysis.

The 60-foot vessel Noi'i fired shots outward from the coast along both the EW and NS lines (Fig. 2). The charges were alternately detonated in 60- and 120-lb sizes. All shooting was performed at night on January 13 and 14, 1977.

To improve the positioning of each shot, a sonobuoy, deployed about 1 km offshore on both lines, relayed the water wave arrival time to the nearest onshore stations (T1 and T2, Fig. 2). Surveyor's transits were positioned at two points on either side of stations T1 and T2 for locating both the sonobuoy and shots. Upon completion of the shooting each night, the sonobuoys were picked up and fixes were taken again to determine the drift.

The time signal that was recorded on all of the instruments was the radio-transmitted WWVH. To prevent interference at critical moments during the recording, auxiliary timers such as traveling clocks or other standby radios tuned to other frequencies of WWV helped to remedy this hazard.

DATA REDUCTION AND ANALYSIS

Refraction data from the TEAC cassette recorder and Hewlett-Packard recorder were played back on a six-channel visicorder and on a two-channel pen-recorder.

Interference and poor reception over WWVH radio obscured some of the time marks on the tapes. For these records, the time signals were passed through a band filter centered at 900-1100 Hz to reduce the background noise as much as possible.

Determining shot points accurately on the EW line presented additional problems. A factor was that the surveyors' transits were close together compared with the shot positions offshore; this meant that a small difference in angular displacement would lead to significant errors in offshore positioning. All the transit data were therefore checked with respect to the recorded landmarks. The shot positions on the EW line appear to be more irregular and further apart than on the NS line with fog preventing the sighting of shots 1, 6, and 7.

As a check on the sonobuoy position, the T-phase was subtracted from the P-wave arrival for each shot at the TEAC 1 site and then multiplied by the velocity of water, 1.50 km/sec (Matthews, 1939). This procedure gave distances very close to those measured by the transits for the two sonobuoy positions and additional indication that the transit data were reasonable (Fig. 3).

It was discovered that the sonobuoy drifted during the course of the experiment. The apparent drift was from S1 to S2 on the map, Figure 2 (note the apparent larger drift on the EW line). The assumption was made that the sonobuoy drift was linear as transit sightings were taken only just before and just after sonobuoy deployment and recovery.

To check the validity of the assumption of linear drift for the sonobuoy, the T-phase arrival times were compared to the sonobuoy arrival times for the NS and EW lines (Figs. 4 and 5). The results for the NS and EW lines seem to indicate that there was greater drift of the sonobuoy positioned on the EW line as compared to the sonobuoy on the NS line. This increase of distance appears to be explained by the sonobuoy's drift away from its initial deployment position. Thus the sonobuoy's position at any given shot may be determined by subtracting the P-wave arrival from the T-wave arrival and multiplying by the velocity of water.

In order to obtain a shot instance or origin time for each shot on the EW line the approximate distances from the

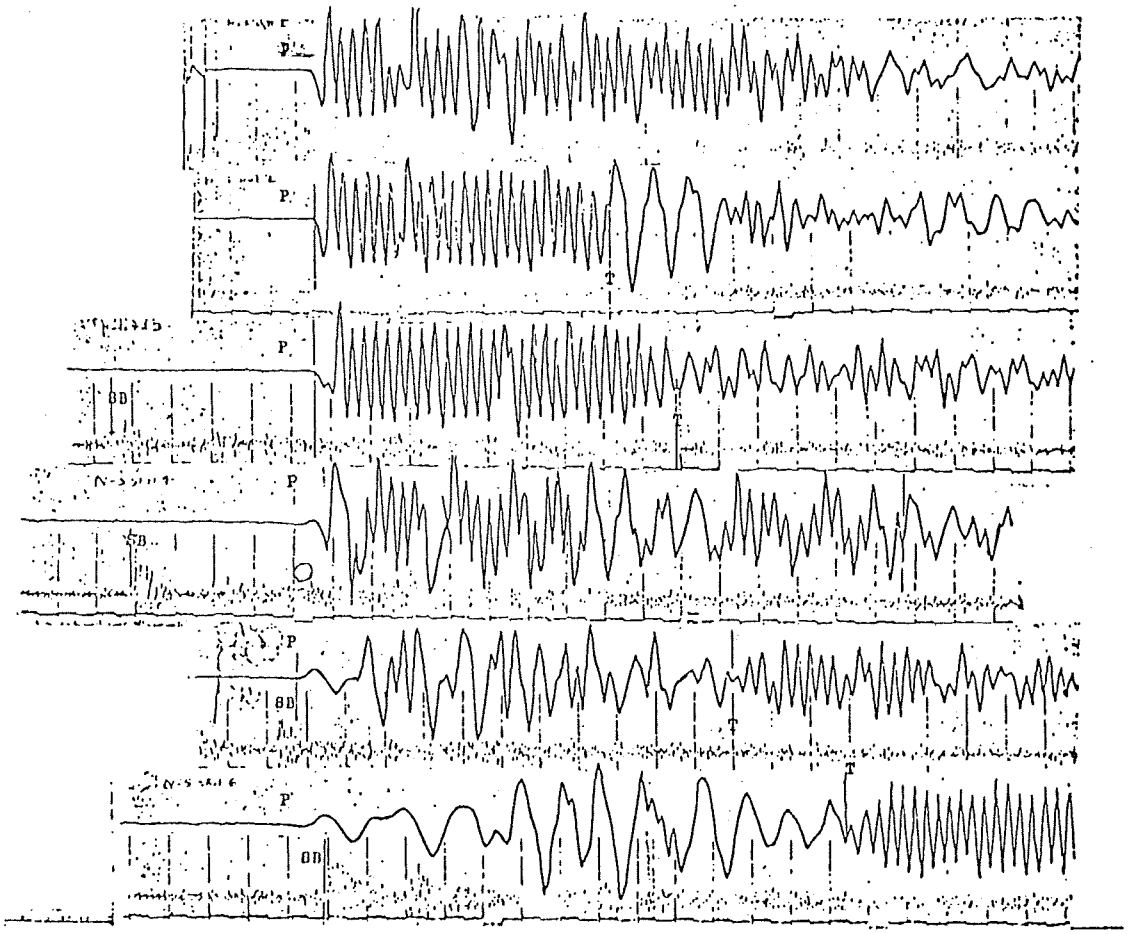

Figure 3. Seismograms centered on the P-arrival. The T-phase and sonobuoy arrivals are also visible.

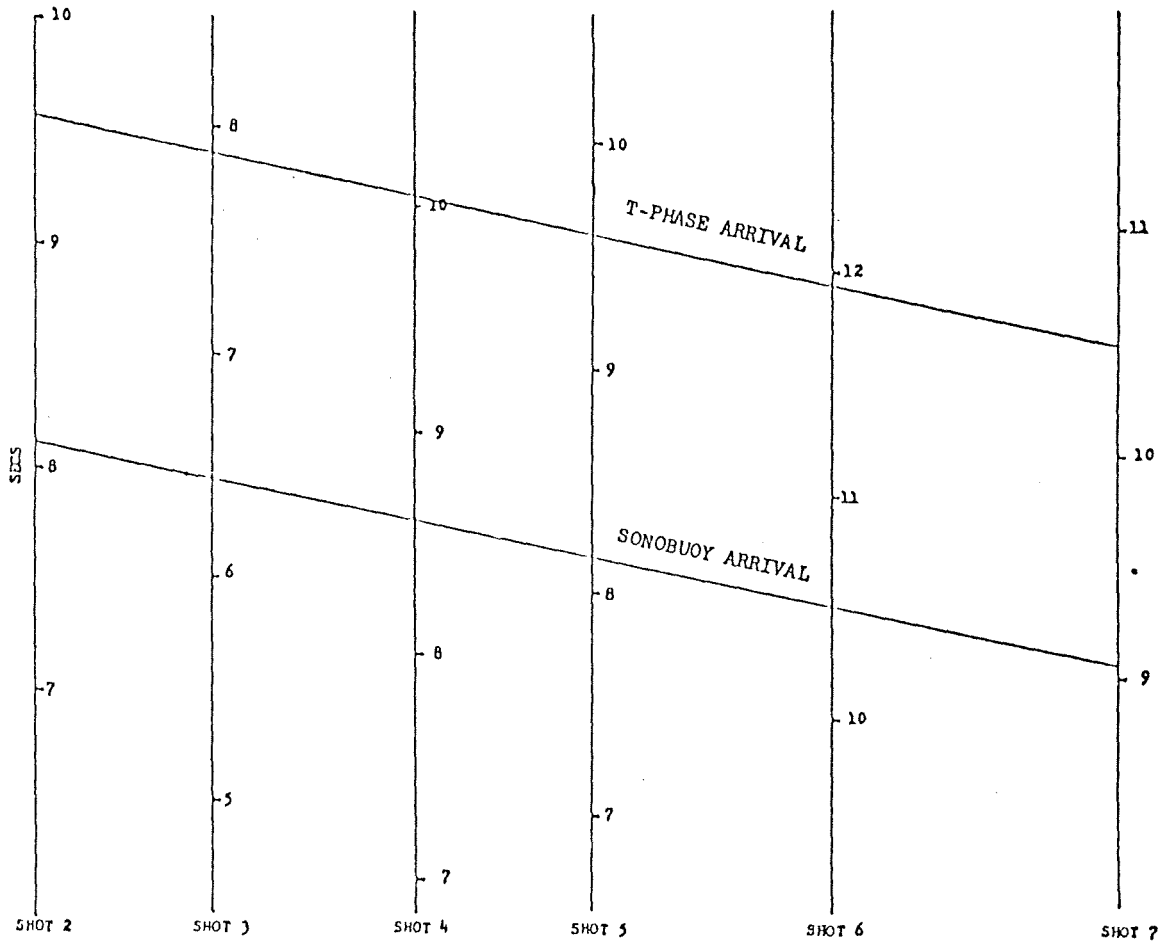

Figure 4. The NS TEAC 1 (T1) seismogram arrival times of the sonobuoy and T-phase for shots 2-7.

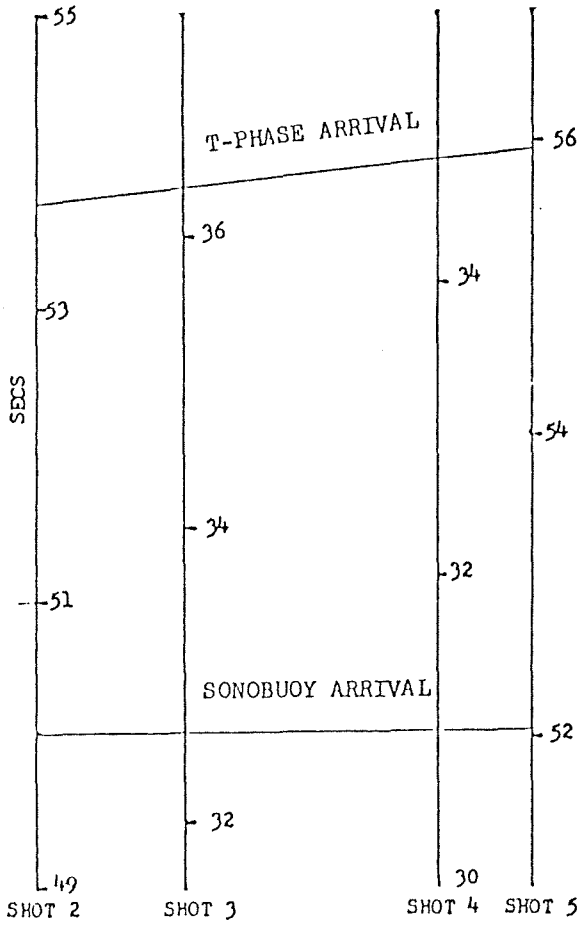

Figure 5. The EW TEAC 1 (T1) seismogram arrival times of the sonobuoy and T-phase for shots 2-5.

sonobuoy to each shot were used as discussed above. The shot instance was obtained by subtracting the correction time, (sonobuoy distance to each)/(velocity in water), from the sonobuoy arrival time broadcast to the TEAC 1 site.

The next correction was for water depth or bathymetry. To measure the approximate depths along each shot line, the boat's course was plotted on a bathymetric chart of Hawaii (C.G.S. 4115) as well as a chart based on a study by Malahoff and McCoy (1967). Approximate depths were measured for each shot for both lines with bottom contours indicating a steep offshore slope, varying from 15-21° along the NS shot line.

Using a water velocity of 1.5 km/sec for this area (Matthews, 1939) and an upper layer velocity of 1.0 km/sec (this average velocity was assumed from Suyenaga's (1978) refraction study), delay times were calculated for the shots and refracting horizons using the principles as outlined by Nettleton (1940) and Dobrin (1960). These delay times were subtracted from the elevation corrected shot times to arrive at the travel times through the datum plane at sea level. The intercept times differences varied from 0.10-0.20 sec for the travel-time plots of the same refractor velocities (Figs. 7 and 8). Those were, however, larger differences in intercept times for some of the shots; this will be discussed in the next section.

Travel time plots were constructed after subtracting the elevation corrections of a given receiver assuming a sea level datum plane. The elevation corrections ranged from 0.0-0.3 sec using the upper layer velocities as discussed above. Two types of travel time plots were used:

(1) a given shot vs the station position or "array plots".

(2) a given station vs shots 1-7 or 2-5 or "station-shot plots".

In calculating the crustal structure, flat-lying layers of homogeneous composition were assumed (Nettleton, 1940 ; Dobrin, 1960) along with the velocities and structures of prior surveys in the region (Ryall and Bennett, 1968; Hill, 1969; Suyenaga, 1978).

On the NS line, depths were calculated using the critical distance technique as well as the time intercept method (as an upper layer of 3.0 km/sec was observed on three of those plots). Both of these techniques yielded similar results.

On the EW line, the first branch in the travel time plot was the 6.8-7.0 km/sec slope. But the intercept time of 1.4

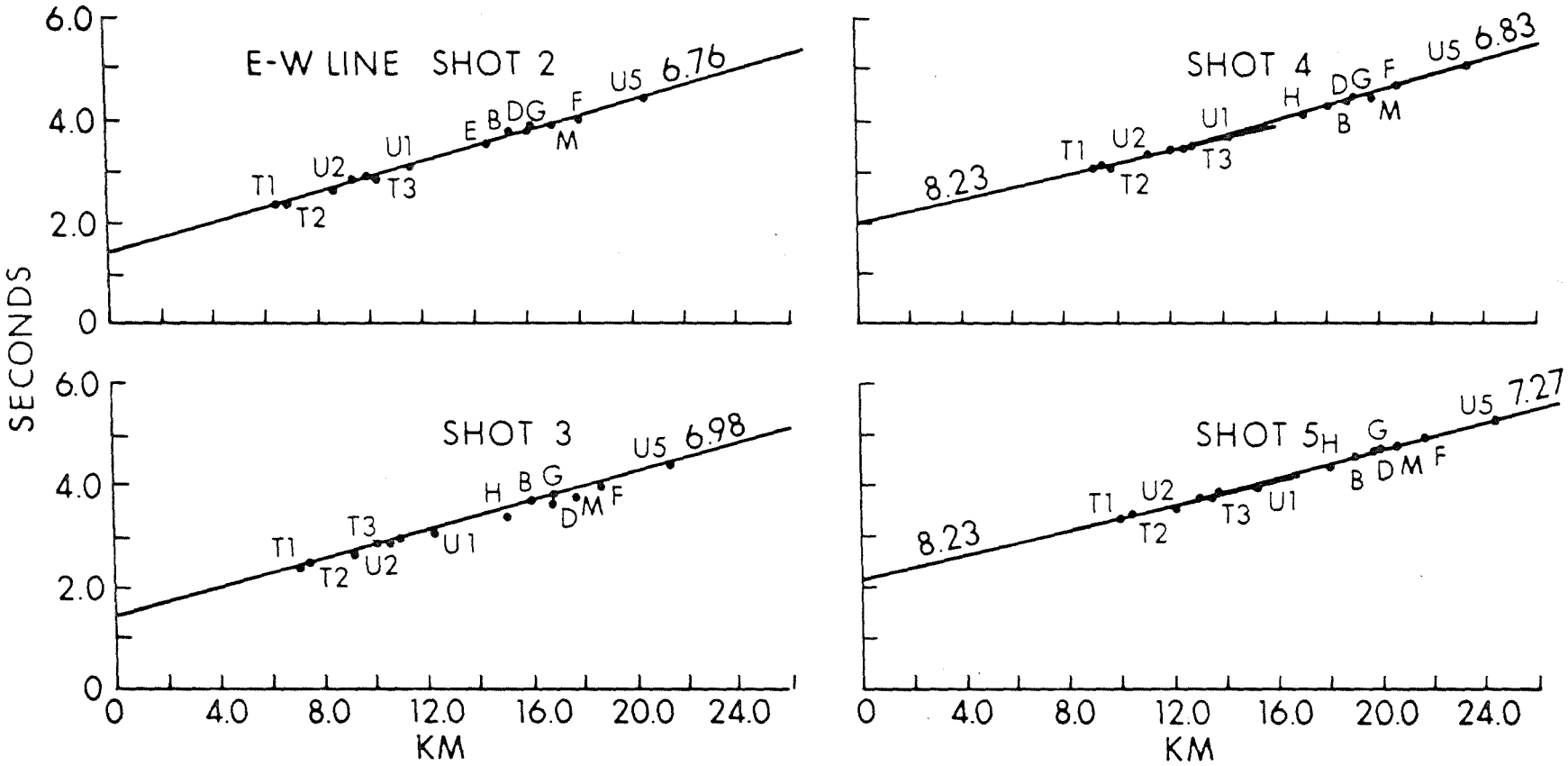

Figure 6. Travel time plots of the EW line for shots 2-5 with recorders as stepout variable. The surface layer was not detected.

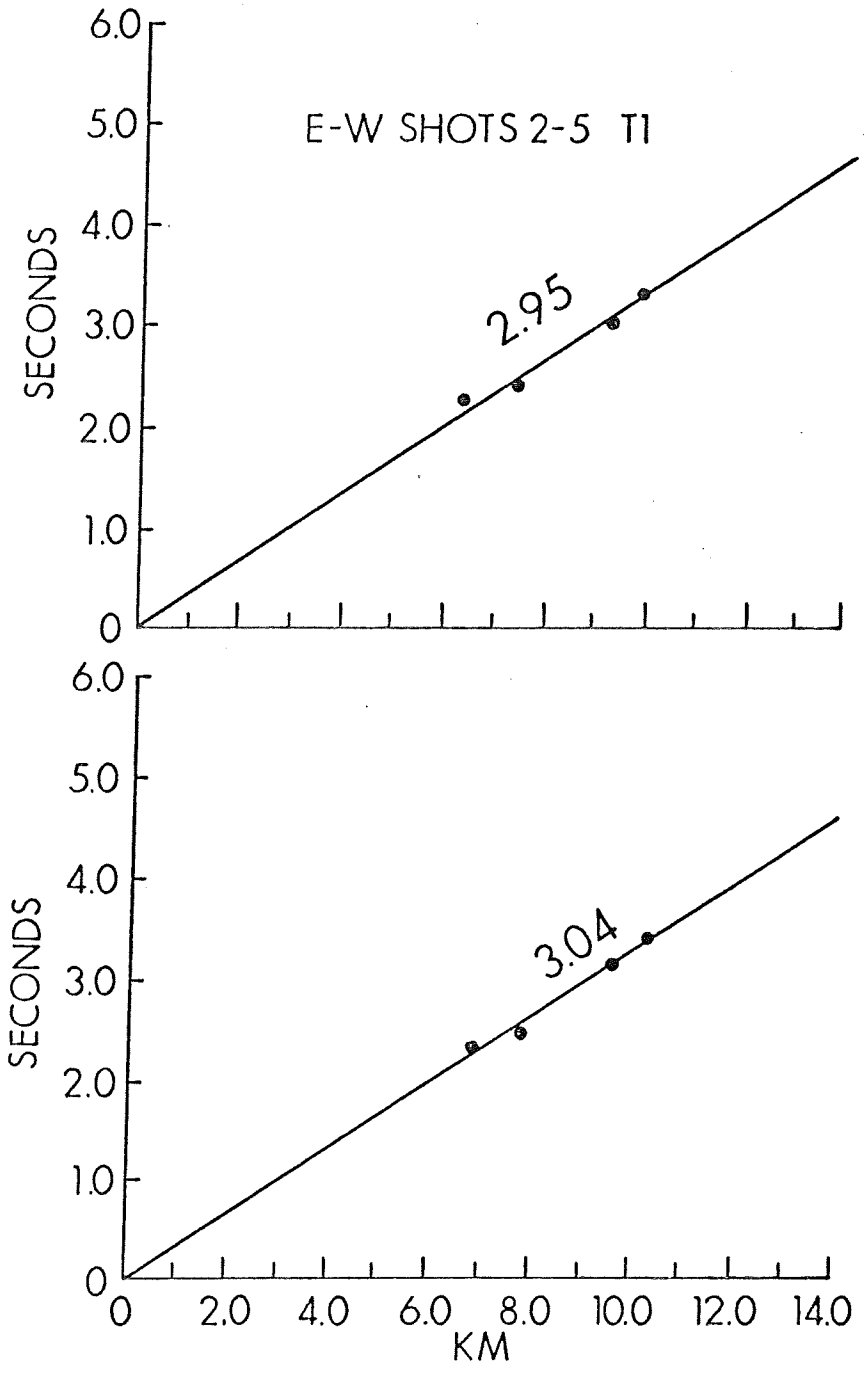

Figure 7. Travel time plots of EW line for stations T1 and T2 with shots as stepout variable.

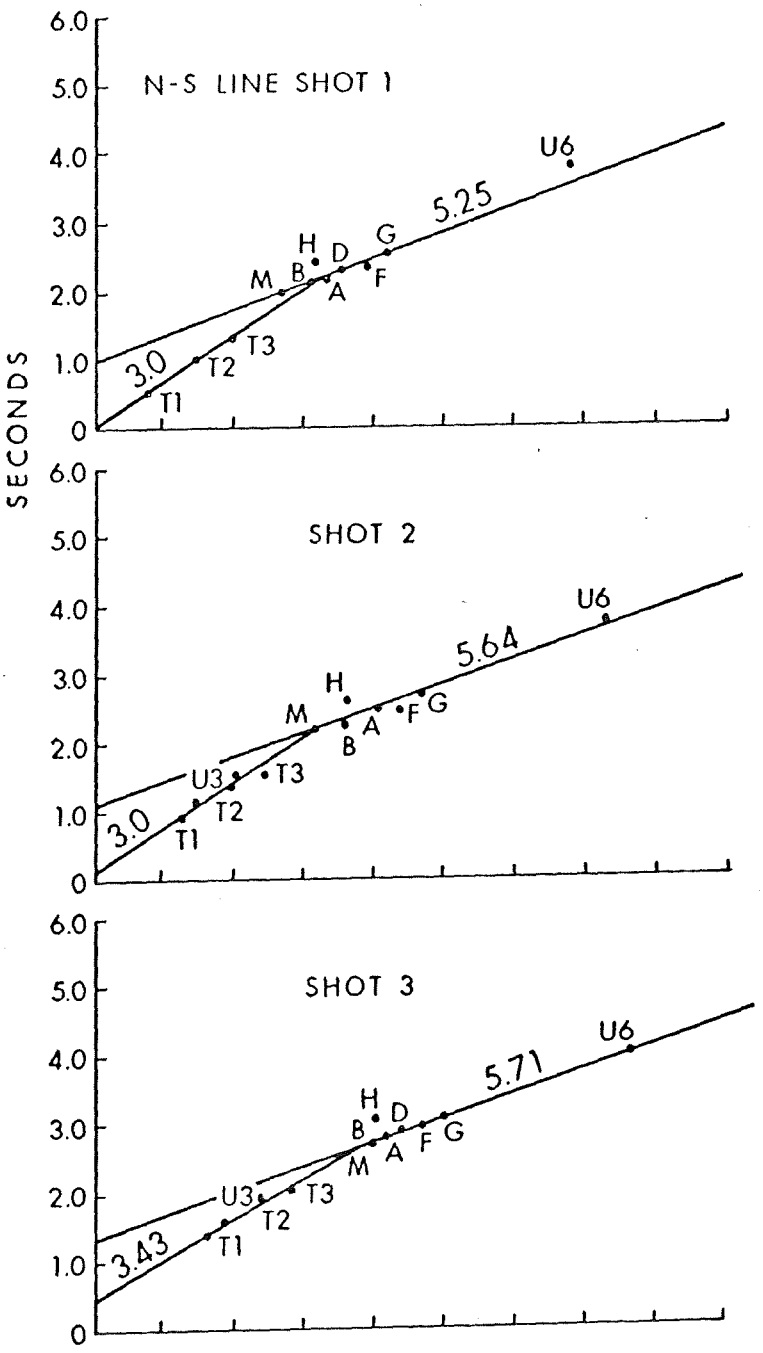

Figure 8. Travel time plots of NS line for shots 1-3.

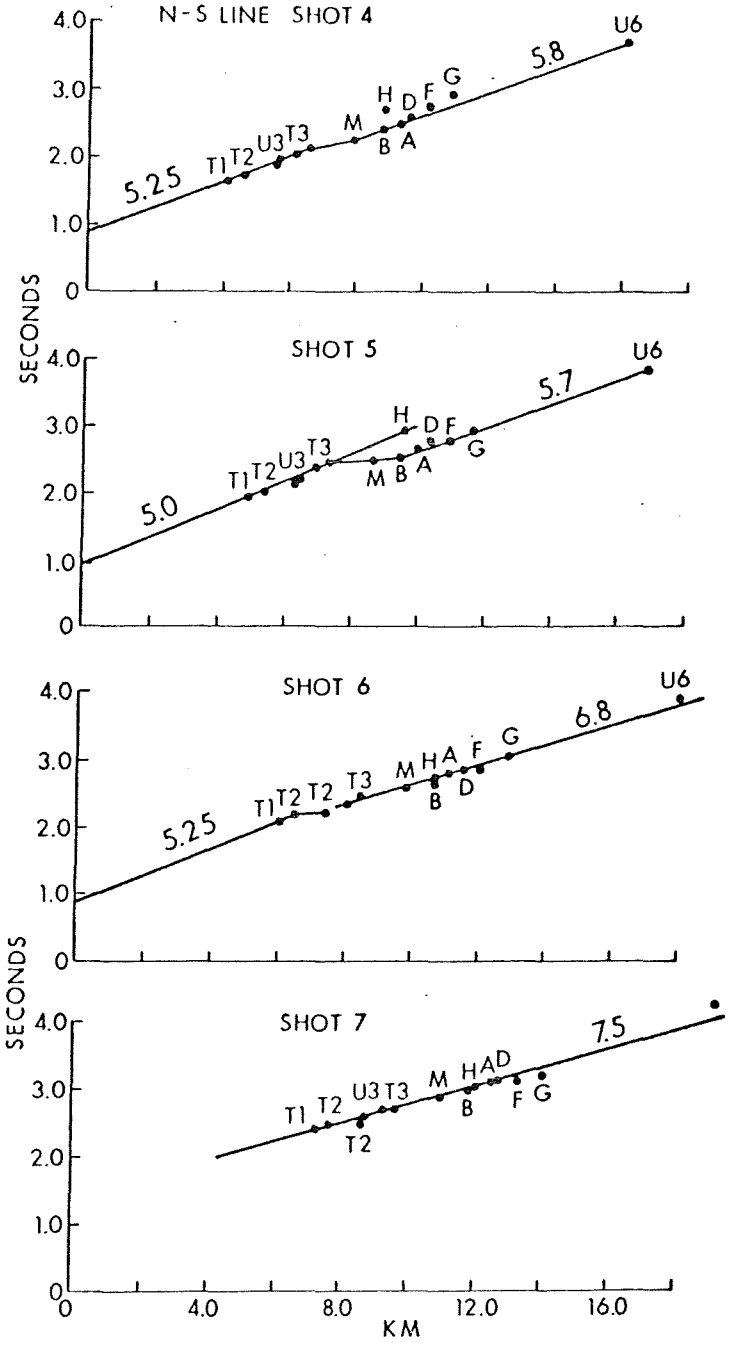

Figure 9. Travel time plots of NS line for shots 4-7. Note the "kinks" in the lines.

sec for this branch suggests that at least one shallow layer with lower velocity exists. If, on the other hand, the time-distance plots of shots 2 to 5 with respect to stations T1 and T2 were constructed (Fig. 7) we notice that a 3.0- to 3.1-km/sec branch with near zero intercept times appears. The simple case is now taken whereby along the EW line, a 3.0-km/sec layer is underlain by a 7.0 km/sec layer.

DISCUSSION OF TRAVEL TIME PLOTS

The seismic refraction data corrected for both elevation and water depths were next subjected to analysis using standard travel-time plots. The first type of plot, the array plot (Figs. 6, 8 and 9), shows a given shot vs the various receiving stations. This type of plot was constructed by scaling the distances from the various receiving stations to the shot point against the corresponding travel time. The advantages of using this type of travel time plot are:

(1) Variations in time from one shot to the next are eliminated as just one shot is plotted at a time.

(2) The structure deduced from this type of plot is indicative of the structure directly beneath the station.

For the second type of plot, data were plotted in the form of station-shot configurations. In this case a station, for example T1 (Fig. 7), is scaled against the corresponding positions and times of the shots on the line. If the origin time of the shots was not precisely determined, as was the case for some shots in this survey, one might expect to see large variations in the data on this type of graph.

A description of the various travel-time plots included in this section will now follow and refer to Figures 6-9. First the travel-time data for the EW line (Fig. 6) will be discussed.

The travel-time data for EW shot 2 show a velocity of 6.76 km/sec across the entire array with all time variations less than 1/10 sec. There were no other velocities observed on this plot.

The travel-time data for EW shot 3 indicates a velocity of 6.98 km/sec for all receiving stations across the array with most time variations less than 1/10 sec. Notice that the travel time intercepts are about the same for both EW

shots 2 and 3 at 1.4 seconds and this indicates that we are seeing the same layer.

Shots 4 and 5 have an anomalously high velocity of 8.23 km/sec through the first five stations followed by a return to velocities of 6.83 km/sec and 7.27 km/sec, respectively. All but a few data points fall within 1/10 of a second of the estimated velocity. The high velocity of 8.23 km/sec indicates that we are encountering some sort of structural anomaly in the Kapoho region (Fig. 2). However, the EW line is not reversed and it is not certain whether this anomaly is due to high velocity rock near the surface or anomalously dipping rock horizons.

Next, a brief description will be made of the travel-time plots for the NS line (Figs. 5, 8 and 9). The NS line travel-time data for shots 1-3 are very similar in that they show two refractors, an upper velocity of 3.0 km/sec and a second layer velocity of 5.25 km/sec with a "kink" in data of apparent high velocity between the two refractors. The travel time intercepts are also very close.

In summary, on the NS line travel-time plots, the following velocities are observed: 3.0 km/sec, 5.25-5.83 km/sec and 7.0-7.1 km/sec. Upon examination of these plots, one can observe that there are no shooting configurations or travel-time data that show all three apparent velocities (3.0, 5.25 and 7.0 km/sec) occurring together on the same travel-time plot. It should also be apparent from these travel-time graphs that we are handicapped by a lack of data points between the array stations and remote recording station U6 (Figs. 2 and 8). One cannot be certain, therefore, of the relationship of the 5.25-km/sec (apparent average velocity of the 2nd layer) refractor to the 7.0-km/sec refractor across the rift.

The apparent average velocity of 5.25 km/sec from the NS line is not observed on the EW travel-time plots and some possible reasons for this are:

(1) The 5.25-km/sec layer may lie principally within the hydrothermal zone surrounding the geothermal well site. This layer would be highly fractured and probably permeable causing a low velocity zone within the intrusive anomaly which is not observed in certain recording configurations.

(2) The 5.25-km/sec velocity may be the result of the intrusive body dipping northward at a 6-9° angle. From flat layer refraction analysis, we know that the velocity structure observed near a receiver will be true only if the effect of the dip or inclination of the rock layer is determined

(Nettleton, 1940 ; Dobrin, 1960). If a refractor is dipping it will give an apparent velocity higher than the actual velocity if the structure dips upward from the shot path origin toward the receiver and lower than the actual velocity if the structure dips away from the receiver and upward toward the shot point. To be sure of the actual dip, one would have to account for the ray paths on both sides or ends of the shooting-receiving profile, and this cannot be verified as the NS line is only a single ended profile.

Velocities less than 3.0 km/sec were not observed in the 1977 refraction survey. Other studies have resolved this upper structure somewhat. Suyenaga (1978) indicates that a surface layer of 0.7-1.6 km/sec extends from 100-300 meters deep and overlies layers of 2.5 and 2.9 km/sec. Hill (1969) found a 3.1-km/sec layer extending regionally 2-3 km deep with a surface layer of 1.8 km/sec.

From the EW line using the data from shots 2 and 3, the average of the depth determinations to the 7.0-km/sec horizon using both critical distances and intercept times and on an overlying layer of 3.0 km/sec was found to be 2.5 km after 0.2 km were added to reduce the well site of sea level. Calculations were performed using the data from the NS line as well. Assuming that the 5.25-km/sec layer is real, the depth to 7.0-km/sec layer would be from 1.6-1.8 km using the velocity-time relationships observed from shots 1-3 (Fig. 8).

The travel-time intercepts for shots 5, 6 and 7 on the NS line are at variance from the intercepts of the refractors of about the same velocity on the EW line (Figs. 6 and 9). The travel-time plots for the NS line shots 6 and 7 indicate velocities of 7.0 and 7.1 km/sec, respectively. These velocities are closely matched to the corresponding velocities observed on the EW lines shot 2-5 and are presumably the same refracting horizon. The timing error as discussed earlier enters the picture here, and is responsible for delays of 0.5 sec for shot 5 and 1.0 sec for shot 7 on this line. As the timing error is responsible for this difference in the intercept time, we cannot be certain of the exact magnitude and cause of this error other than it appears to increase with distance. Because of this error all structural calculations were determined from the shots closer to the shoreline on both the NS and EW lines (shots 2 and 3 on the EW line and shots 1-4 on the NS line).

From the array plots for shots 2-5 on the EW line and for the station-shot plots on the NS line, travel-time equations were derived (Table 1). These travel-time equations were used to derive the velocity-depth structure to be discussed.

TABLE 1

Travel times for the 1977 east rift refraction

Refraction line	Shot point	Travel time (seconds)
EW	2	$T = 1.40 + \Delta/6.76$
	3	$T = 1.40 + \Delta/6.98$
	4	$T = 2.00 + \Delta/8.23$
		$T = 1.70 + \Delta/6.83$
	5	$T = 2.20 + \Delta/8.23$
		$T = 2.00 + \Delta/7.27$
NS	1	$T = 0.00 + \Delta/3.00$
		$T = 1.00 + \Delta/5.25$
	2	$T = 0.15 + \Delta/3.00$
		$T = 1.10 + \Delta/5.64$
	3	$T = 0.45 + \Delta/3.43$
		$T = 1.35 + \Delta/5.71$
	4	$T = 0.9 + \Delta/5.25$
		$T = 0.9 + \Delta/5.80$
	5	$T = 1.0 + \Delta/5.0$
		$T = 0.9 + \Delta/5.7$
	6	$T = 0.9 + \Delta/5.25$
		$T = 1.2 + \Delta/6.8$
	7	$T = 1.45 + \Delta/7.5$

A model (Fig. 10) conbines the results of this study with those of shallow seismic refraction (Suyenaga, 1978) and gravity (Furumoto et al., 1976) and interpreted elsewhere (Broyles, 1977; Furumoto and Broyles, 1977; Broyles et al., 1978).

Figure 10 indicates that a velocity of 3.0 km/sec extends down to 1.6-1.8 km. An intermediate layer of 5.25-km/sec average is found between the 3.0-km/sec layer and the high velocity 7.0 km/sec anomalous dike complex at depths of 2.0-2.5 km. The intermediate layer is the 2nd layer as discovered by Hill (1969).

The depth to the anomalous dike complex was determined from refraction data, the width constrained by gravity. The intrusive complex was also assumed to dip 6-9° toward the northwest as an explanation for the anomalous travel-time data as observed on the NS travel-time plots.

Travel times were computed graphically for the model using Snell's Law for both the NS and EW directions. Satisfactory agreement with the observed travel times were obtained by adding the travel times for the ray paths shown in the model.

CONCLUSIONS REGARDING THE STRUCTURE OF THE EAST RIFT

In summary, the following are conclusions regarding the structure of the anomalous area of the east rift as delineated by the various geophysical methods as described in this paper:

(1) The zone of dense material is located at depths of 2-3 km reaching depths of only 1 km in some regions (Fig. 10). The bottom of the complex is probably at 4-5 km.

(2) The upper surface of the main dense zone appears to have a gentle 6-9° northward slope. This northward slope could produce the anomalous velocity of 5.25 km/sec as observed only on the NS line. This northward-sloping structure was modeled to fit the observed Bouguer gravity field (Furumoto, 1978). Swanson et al.(1976) believe that such a wedge-shaped structure would be the product of southward and upward migration of progressively younger dikes. In this model there

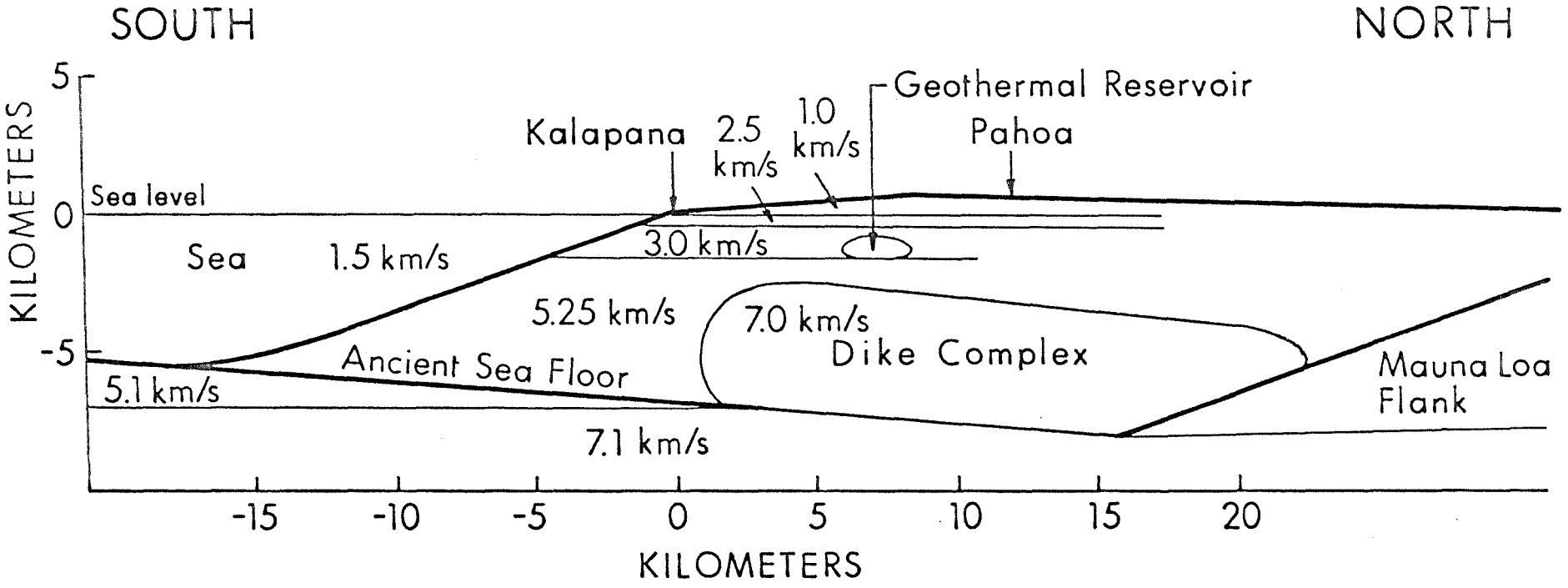

Figure 10. Model of the east rift of Kilauea from seismic and gravity data.

would be lateral growth of the rift to the south, as gravity would favor south-southeastward displacement. Younger dikes would be preferentially formed southward, as the lava flows for these dikes that intrude at progressively shallower depts cover up the older flows.

Seismic and gravity data (Furumoto and Broyles, 1977; Broyles et al., 1978) indicate that the depth to the main intrusive dike complex is about 2 km and probably reaches depths of 4-5 km. The bottom of the complex would agree with the ideas of the growth Hawaiian volcanoes that form by extruding onto the ancient ocean floor, the average depth being 5 km (Macdonald, 1965).

Such high velocity material close to the surface in volcanic or rift regions has been detected in other refraction studies as well. In the analysis of the structure of the Koolau volcano from seismic refraction studies, there are indications of material with velocities as high as 7.7 km/sec reaching depths less than 2 km (Furumoto et al., 1965).

The results of the present studies are summarized in a model (Fig. 10) that shows the structure of the dike complex beneath the east rift zone. The following features are indicated on the model:

(1) The main intrusive complex is located on the slopes of Mauna Loa with a thickening of the complex southeastward.

(2) The geothermal reservoir is a region of fractured and permeable rocks within the dike complex.

(3) The ancient seafloor forms the lower limit of the dike intrusions.

(4) The surface of the dike structure dips at a shallow angle to the north and abruptly to the south.

ACKNOWLEDGMENTS

The 1977 Puna Refraction survey could not have been successfully completed without the help of the following people: Dr. Charles Helsley for his role in directing the field operations and helpful advice in reducing the data, Carroll Dodd for assembling and operating the array network and communications center, Edward Sakoda, Roger Norris and Patrick Lineberger for assisting with the field work and Pete Pozzi and Lee Smith for handling the scientific operations on board the Noi'i. A special thanks to Candy Fenander, Douglas Klein and Wayne Suyenaga for their helpful comments in drafting this report.

REFERENCES

Broyles, M.L., 1977. The Structure of the East Rift Zone of Kilauea, Hawaii from Seismic Refraction, Gravity and Magnetic Surveys. MS thesis, University of Hawaii.

Broyles, M.L., W. Suyenaga and A.S. Furumoto, 1978. Structure of the Lower East Rift Zone of Kilauea Volcano, Hawaii, from Seismic and Gravity Data. Journal Volcanol. Geothermal Res., in press.

Dobrin, M.B., 1960. Introduction to Geophysical Prospecting. McGraw Hill Book Co., New York, 446 pp.

Fiske, R.S. and E.D. Jackson, 1972. Orientation and Growth of Hawaiian volcanic rifts; the effect of regional structure and gravitational stresses. Proc. Roy. Soc. Lond. p. 299-326.

Furumoto, A.S., 1978. Nature of Magma Conduit under East Rift Zone of Kilauea Volcano, Hawaii. Bull. Volcanol., in press.

Furumoto, A.S. and M.L. Broyles, 1977. Dimensions and thermal processes of the magma conduits underlying the east rift zone of Kilauea volcano. Inter. Assoc. of Seis. Ear. Int., Volcan. and Chem. Ear. Int., Joint General Assemblies, Durham, England.

Furumoto, A.S., R. Norris, M. Kam and C. Fenander, 1976. Progress report, Gravity profile and the Intrusive zone, in The Hawaii Geothermal Project, Initial Phase II progress report, February.

Furumoto, A.S., N.J. Thompson and G.P. Woollard, 1965. The structure of the Koolau volcano from seismic refraction studies. Pac. Sci., v. XIX, p. 306-314.

Hill, D.P., 1969. Crustal structure of the Island of Hawaii from seismic-refraction measurements, Bull. Seism. Soc. Am., v. 59, p. 101-130.

Macdonald, G.A., 1956. The structure of Hawaiian volcanoes. Verh. K. Ned. Geol. Mijnbouwkd. Genoot. v. 16, p. 274-295.

Macdonald, G.A., 1965. Hawaiian calderas. Pac. Sci., v. 19, p. 320-334.

Malahoff, A. and F. McCoy, 1967. The geologic structure of the Puna submarine ridge, Hawaii. J. Geophys. Res., v. 72, p. 541-548.

Matthews, F.I.C., 1939. Tables of the velocity of sound in pure water and sea water for use in echo-sounding and sound ranging, publ. by the Hydrographic Depart. Admiralty.

Moore, J.C. and H.L. Krivoy, 1964. The 1962 flank eruption of Kilauea and structure of the east rift zone. J. Geophys. Res., v. 69, p. 2033-3245

Moore, J.C. and D.H. Richter, 1962. The 1961 flnak eruption of Kilauea volcano, Hawaii. Trans. Am. Geophys. Union, v. 43, p. 446

Nettleton, L.L., 1940. Geophysical Prospecting for Oil. McGraw-Hill Book Co., New York, 444 pp.

Ryall, A. and D.L. Bennett, 1968. Crustal structure of Southern Hawaii related to volcanic processes in the upper mantle. J. Geophys. Res., v. 73, p. 4561-4582.

Swanson, D.A., W.A. Duffield and R.S. Fiske, 1976. Displacement of the south flank of Kilauea volcano; the result of forceful intrusion of magma into the rift zones. Geol. Surv. Prof. Pap. 963,

Suyenaga, W., 1978. Crustal structure of the east rift zone of Kilauea, Hawaii from seismic refraction, 1., Near-surface structure, this volume.

THERMAL PROCESSES OF KILAUEA EAST RIFT INFERRED FROM SEISMIC DATA

Augustine S. Furumoto

Hawaii Institute of Geophysics
University of Hawaii
Honolulu, Hawaii 96822

ABSTRACT

Seismic data provided insight into the tectonic and thermal processes of Kilauea east rift. Microearthquakes outlined a region with a volume of 6 km^3 around the exploratory well HGP-A. The region probably represents a geothermal reservoir. The earthquakes also outlined a discontinuity at 5-km depth, which is thought to be the unconformity between the volcanic edifice and oceanic crust.

Source mechanism data showed that tensional forces are in operation over the east rift. These tensional forces are produced by an expanding rift zone due to forceful intrusion of magma from the summit holding reservoir. The result is formation of fractures in the layers above a hot dike complex. Groundwater seeping into the fractures is eventually trapped by a self-sealing process to form geothermal reservoirs.

INTRODUCTION

The foregoing articles in this volume presented varied seismic data collected over the lower east rift of Kilauea volcano during the course of geothermal exploration. The data included seismic refraction surveys, ground noise survey and microearthquake surveillance. Those reports gave a rather restricted interpretation of the data. This article attempts to draw more inference by considering data from surveys and published results of other investigators.

MICROEARTHQUAKE DATA

Suyenaga and Furumoto (see this volume), from their earthquake surveillance project produced a map of epicenters and a plot of foci upon a vertical plane drawn perpendicular to the trend of the east rift (Figs. 7 and 8 of Suyenaga and Furumoto). The foci plot consists of three groups of earthquakes which can be classified in the following way (Fig. 1): the first group is clustered around the well HGP-A (shaded region); the second group is aligned along a plane 5 km deep; the third group is clustered around a plane dipping 60° to the southeast. The three groups will be discussed separately.

The First Group: The Cluster Around HGP-A

The earthquakes that are clustered around HGP-A outline an ellipsoid 3 km x 2 km x 1.5 km. Since the depth determination of earthquakes is notoriously inaccurate, the vertical dimensions of the ellipsoid is questionable.

The ellipsoid can be identified as the geothermal reservoir which HGP-A well ound by drilling. The microearthquakes are considered to be the result of minor fracturing due to contact of groundwater with hot rock. If we proceed with the assumption that the ellipsoid is the reservoir, then we can fix the vertical dimension by consulting the temperature profile of HGP-A. The temperature profile from engineering reports shows an isothermal region 1 km thick. From this, we estimate that the geothermal reservoir is about 1 km thick.

From these considerations we can estimate that the volume of the geothermal reservoir is approximately 6 km^3. If we take the ellipsoid as determined by earthquake data only, the volume is then about 9 km^3. Earthquake data provided us with a ball park figure of the volume of the reservoir.

Next, we speculate on the available energy in the reservoir. To estimate the energy capacity of the reservoir, the

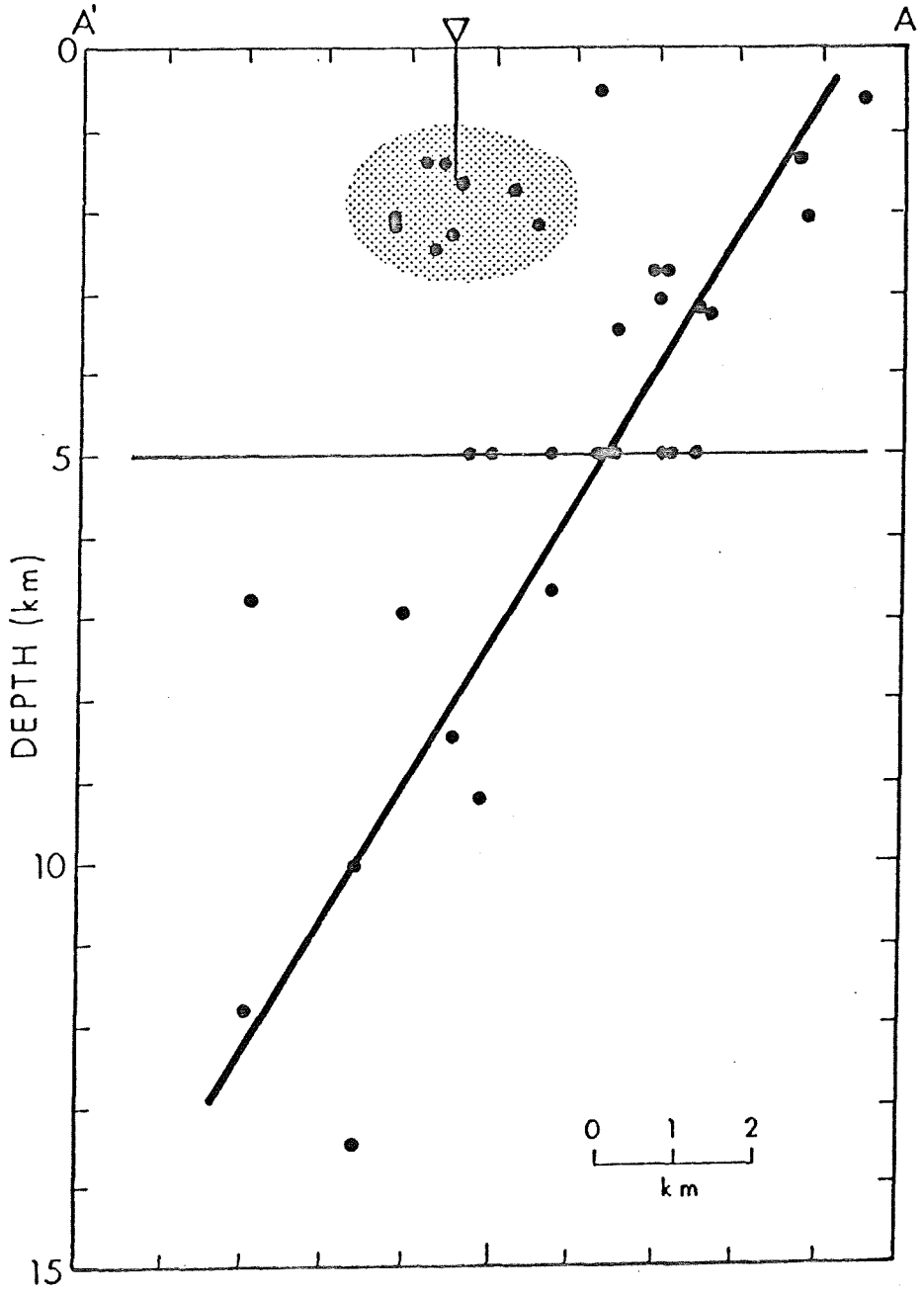

Figure 1. Depth distribution of earthquakes along a vertical plane transverse to east rift trend. The shaded area encloses well HGP-A. The lines represent planes referred to in the text.

heat content of the rocks is calculated. Since water amounts to only a few percent by mass, the heat content of water can be neglected. Available energy is a function of the final temperature of the reservoir after extraction of heat. A practicable level to which the temperature of the reservoir can be lowered is 200°C, as the reservoir is very deep. For the sake of speculation, we shall also consider the level of 150°C.

To estimate the heat content or enthalpy, the following factors are multiplied together: volume, density (2.5 g/cm^3), specific heat (0.33 cal/g), and temperature difference. Then the enthalpy is converted to electrical energy by transfer factor of 0.15, as the best geothermal power plants are about 15% efficient. The calculations show following results:

Volume km^3	Temperature Difference °C	Enthalpy calories	Electrical Energy megawatt-years
6	100	5×10^{17}	9,500
6	150	7.4×10^{17}	14,300
9	100	7.4×10^{17}	14,300
9	150	11×10^{17}	21,400

If we are talking in terms of a hundred year supply, the reservoir can generate 100 to 200 megawatts.

These estimates are based on the assumption that the microearthquake data outlined the volume of the geothermal reservoir.

Second Group: Along a Plane 5 km Deep

The second group of earthquakes are neatly aligned along a horizontal plane 5 km deep. This alignment is so uniform that suspicion arises whether it was an artifact of the epicenter determination program, since epicenter programs start off with an assumed depth. The earthquake data were actually processed twice, the first time with an initial assumed depth of 5 km and then a second time with an initial depth at 10 km. Figure 1 represents the results of the first run. In the second run, most of the earthquakes in question had depths ranging from 4 to 6 km. Hence these earthquakes are clustered around a plane with a median depth of 5 km.

This manner of clustering leads to the inference that there is some sort of discontinuity at 5-km depth. The most likely discontinuity is the ancient sea floor, which pre-existed the birth of Hawaiian volcanoes. The volcanoes at their births broke through the oceanic crust and began pouring out lava onto the then-existing sea floor. Hence there is unconformity

between the oceanic crust and island mass. As the ocean basin north and south of the Hawaiian Islands is roughly 5 km deep, the expected depth of the ancient sea floor is also about 5 km. The sea floor may have been depressed 1 km or so because of the load of the island mass. However, we can equate the 5-km plane, which the earthquakes outlined, with the transition from the volcanic pile or edifice to the oceanic crust.

Further information on the bottom of the dike complex was made available by the Kalapana earthquake of November 29, 1975. The parameters of the earthquake were: epicenter of 19°21'16"N, 155°01'45"W; depth 7 km; origin time November 29, 1975, 14 h 47 m 42 s (GMT); magnitude 7.2. The analysis of its source mechanism by use of teleseismic and local P-wave arrivals and Love wave distribution pattern showed that the slip motion was a low-angle overthrust of the southern flank of the east rift across a fault plane with a 4° slope to the south, Furumoto and Kovach, (1978). The interpretation of the source mechanism in terms of geological structure is shown in Figure 2. The fault plane with the 4° slope to the south was equated to the unconformity between the island mass and the oceanic crust.

The foregoing analysis results in a model where the ancient seafloor is dipping under the island at 4°, a downwarping of the oceanic crust caused by the load of the island mass. The depth of the earthquake was given as 7 km, a value 2 km deeper than the bottom of the dike complex determined by microearthquake data. As discrepancies of 2 km can be expected in depth determinations of earthquakes, there is no inconsistency in affirming that the Kalapana earthquake occurred at the ancient seafloor.

The Third Group: Along a 60° Dipping Plane

The third group of earthquakes, aligned roughly along a plane dipping 60° to the south-southeast, disclosed an active local tectonic process. Further data on this cluster were provided by Keller (1975), who encountered the same 60° dipping plane during a similar microearthquake survey in the area. From first motion data, he was able to obtain a composite source mechanism solution, which is shown as upper hemisphere projection in Figure 3 (Keller, 1975). Keller interpreted the mechanism in terms of a series of normal faults with 45° dip arranged en echelon along a plane dipping 60°. A tectonic process to account for such faulting was not proposed.

The source mechanism of Figure 3 can also be interpreted in terms of a system of tensional and compressional stresses, whereby the tensional stresses are horizontal in the north-south direction, the compressional stresses are vertical, and the neutral axis is horizontal in the east-west direction. Such a pattern of stresses can be produced by forceful intrusion of magma into fissures, which causes dilatation and

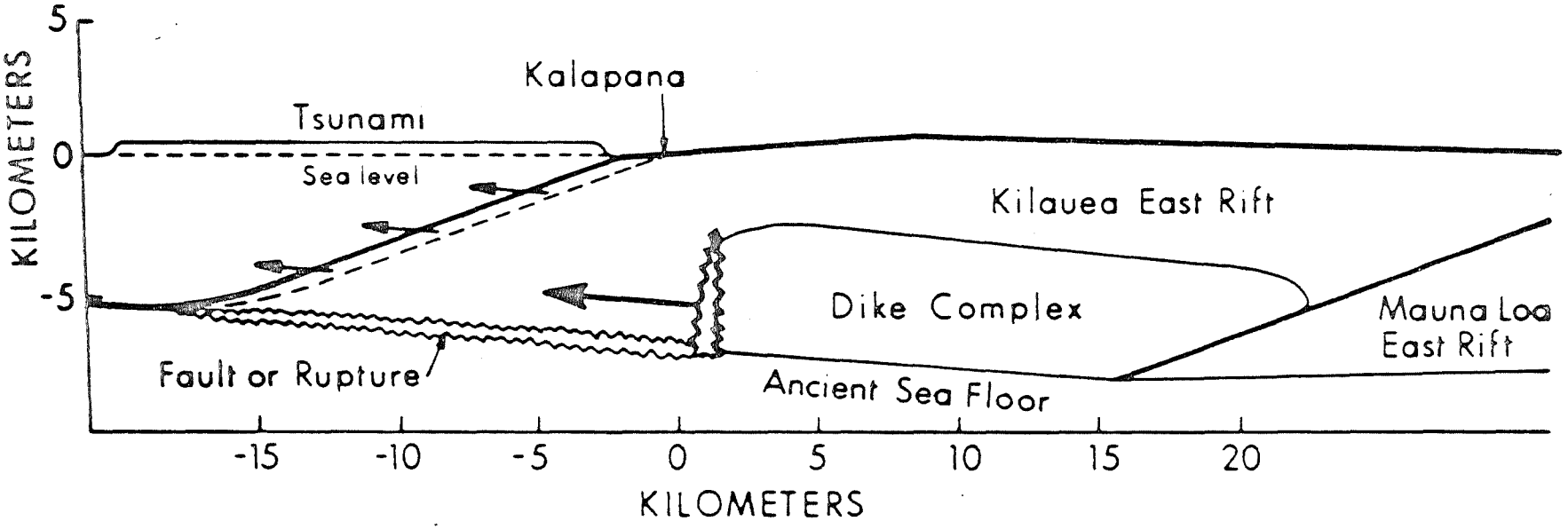

Figure 2. Slip vector of the 1975 Kalapana earthquake (Furumoto and Kovach, 1978).

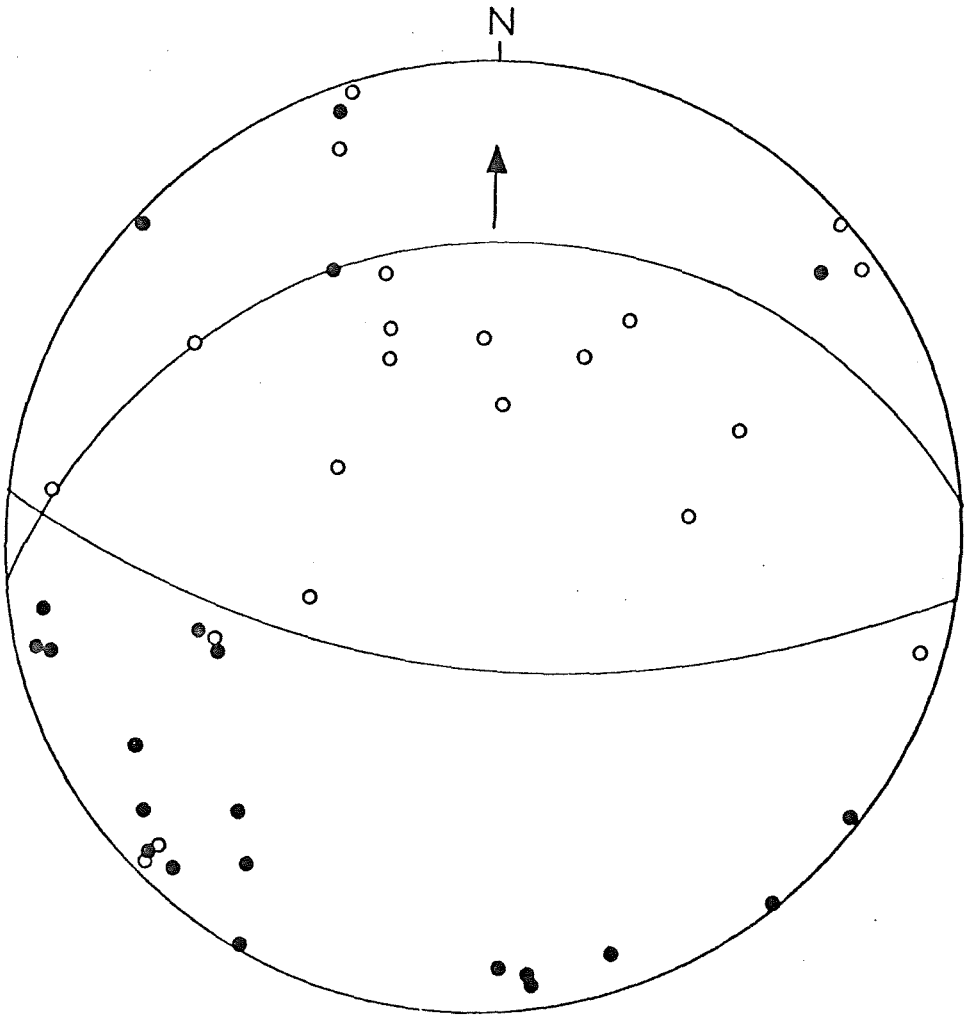

Figure 3. Composite source mechanism solution of microearthquakes on the east rift (Keller, 1975).

expansion of the dike complex. These stresses would induce earthquakes in the vicinity of the dike complex, but at distances away from the dike complex the diminishing effect of the stresses would not be able to induce earthquakes. This explains the shallow depths of the earthquakes. In a different study, Koyanagi et al. (1972) also proposed the expanding dike complex as the cause of earthquakes that they observed on the south flank of the east rift of Kilauea.

The Geothermal Reservoir in a Tectonic Setting

In Figure 4, where a map of the Puna District shows the Kilauea east rift running through it, the lateral extent of the dike complex underlying the east rift is outlined by dashed lines. The dike complex is the lower east rift which was delineated by seismic refraction methods and gravity analysis (Broyles et al., this volume). The upper part of the rift was determined by gravity and magnetic methods.

From about 155° W. the dike complex starts narrowing. To the west the complex is about 20 km wide while to the east it narrows down to 12 km. The narrowing down can be interpreted as an expression of the expanding front of a growing dike complex. The dike complex has many magma passageways; at about 155° W, the number of passageways decreases by about half. In future geological ages, the complex to the east will expand and probably be as broad as the western portions, as more passageways will work their way eastward.

The star in Figure 4 indicates the spot where the geothermal well HGP-A was drilled. Around the well, the geothermal reservoir covers an oval area roughly 3 km by 2 km. The reservoir is located where the dike complex begins to narrow. It can be looked upon as existing right where expansion is taking place.

Figure 5 shows the geological structure of a vertical section transverse to the trend of the east rift running through the geothermal reservoir. The village of Kalapana and the town of Pahoa have been projected onto the vertical plane to show their positions with respect to the dike complex. The reservoir is located in the 3.0 km/sec layer.

When forceful intrusion of magma occurs in the dike complex, the structure of the complex expands and causes cracks and fractures to appear in the overlying layers. Groundwater can then find its way into these fractures to be heated. If somehow the hot water can be trapped, a geothermal reservoir will be formed. However, there is a reservoir which was probably formed by a self-sealing process of secondary mineralization as proposed by Facca and Tonani (1967).

The occurrence of the reservoir in a particular place is not a chance phenomenon. The reservoir is located where the

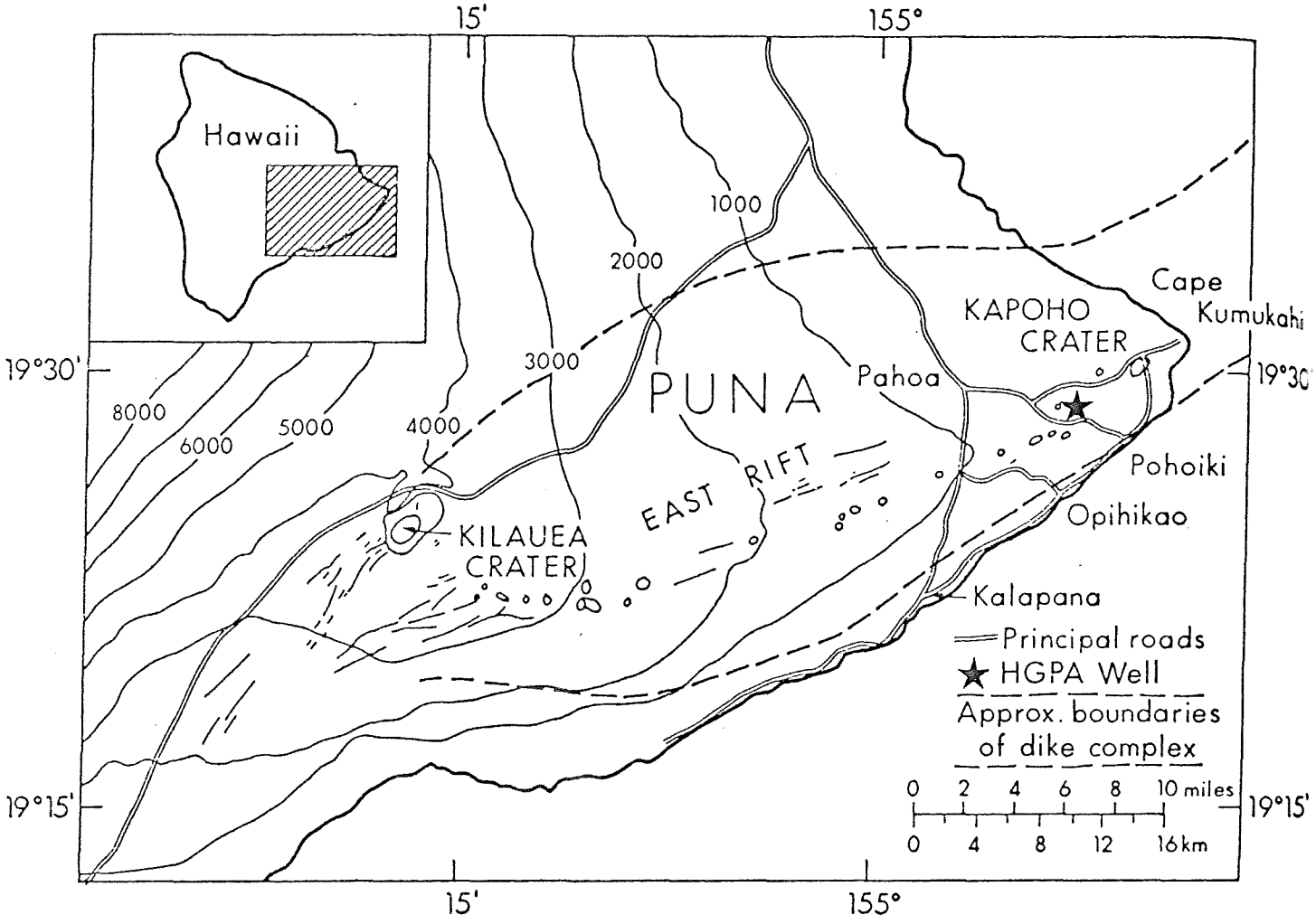

Figure 4. Map of Puna district with the outline of the subterranean dike complex (base map from Dept. of Geography).

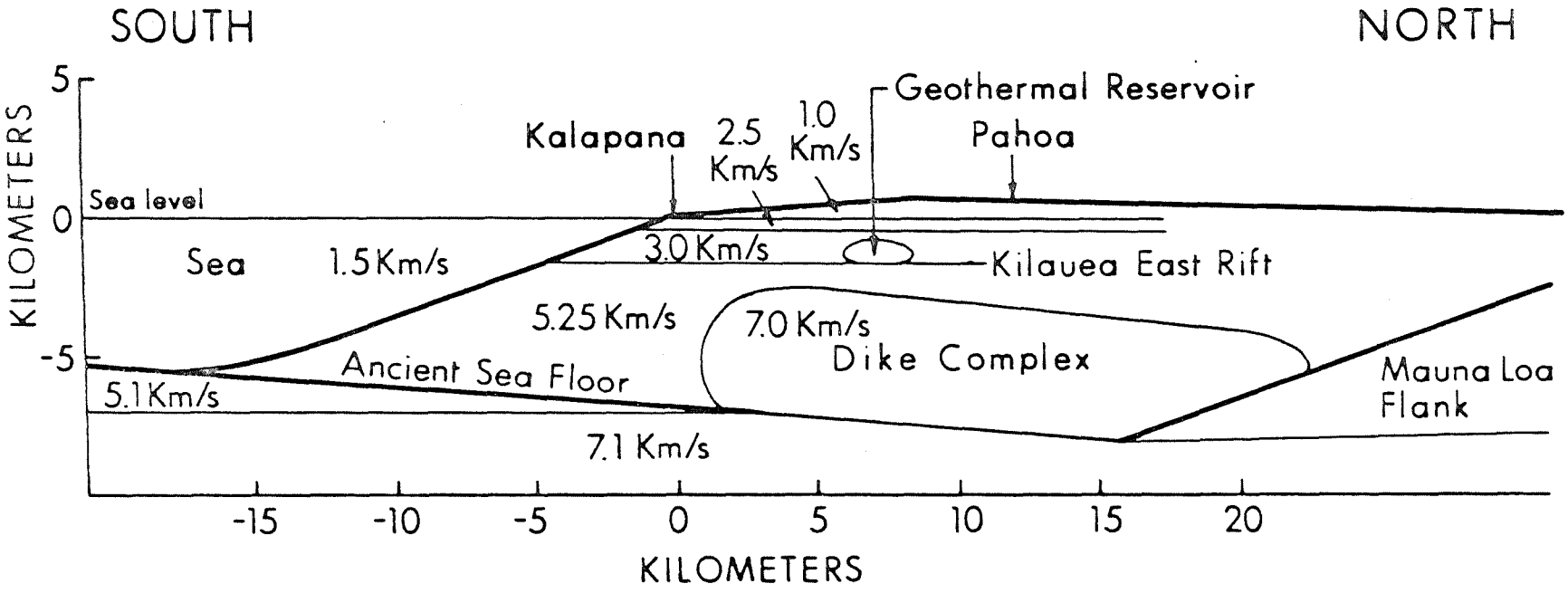

Figure 5. Structure of the Kilauea east rift along a vertical plane transverse to rift trend. Kalapana and Pahoa were projected on to the plane to show their relative positions with respect to the rift zone.

expansion of the east rift is most conspicuous, right where the expanding front of the dike complex is found.

Thermal Source

The temperature of the dike complex in some parts is probably as high at 1000°C. The latest eruption, October 1977, occurred where the east rift crosses the 155° W. meridian. The temperature gradient in the bottom of well HGP-A was 3.1×10^{-3} °C/cm and the conductive heat flux along part of the well was as high as 15 microcal/sec cm^2 (Furumoto, 1978). The dike complex is an abundant source of thermal energy for the hydrothermal reservoir.

The main mode of heat transport through the intervening layer of rock from the dike complex to the hydrothermal reservoir is a conductive process. It is doubtful that liquid phase convection is taking place in the 5.25-km/sec layer. The critical point of water, 374°C, where the density of the liquid phase is the same as the density of the vapor phase, is attained at only 158 m below the bottom of the well if the temperature gradient holds steady downward. Convective transport of heat is not much if the medium is gaseous.

SUMMARY

Seismic data provide an estimate of the size of the geothermal reservoir. With this information, the available energy of the reservoir has been calculated to be between 100 and 200 megawatts for a hundred years.

Seismic data also indicated that the volcanic edifice bottoms out somewhere around 5-km depth below sea level.

Another inference drawn from seismic and other data is that the dike complex under the east rift is growing and expanding. This expansion causes fractures to appear in the overlying rock layers. Groundwater trapped in these fractures by a self-sealing process due to secondary mineralization contributes to the formation of the geothermal reservoir. The thermal energy for the reservoir is transported from the hot dike complex by a conductive process.

REFERENCES

Broyles, M.L., 1978, Crustal Structure of the Lower East Rift Zone of Kilauea, Hawaii from Seismic Refraction, 2. Complete Structure, this volume.

Department of Geography, Univ. Hawaii, 1972. Atlas of Hawaii.

Facca, G., and R. Tonani, 1967. Self-Sealing Geothermal Field. Bulletin Volcanologique, v.30, 271-273.

Furumoto, A. S., 1978. Nature of the Magma Conduit under the East Rift Zone of Kilauea Volcano, Hawaii. Paper presented at International Geodynamics Symposium, Magma Genesis, Tokyo, Japan. Manuscript also submitted for publication.

Furumoto, A. S., and R. H. Kovach, 1978. The Kalapana Earthquake of 1975: An Intraplate Earthquake and Its Relation to Geothermal Processes. Abst. in Earthquake notes, 49, 1, 65. Also, Phys. Earth Planet. Int., v.18, 1979 (in press)

Keller, G. V., 1975. The Opihikao Prospect, Puna, Hawaii. Microgeophysics Corp., Golden, Colo.

Koyanagi, R. Y., D. A. Swanson, and E. T. Endo, 1972. Distribution of Earthquakes Related to Mobility of the South Flank of Kilauea Volcano, Hawaii. U. S. Geological Survey Professional Paper. 800-D, D 89-D 97.

Suyenaga, W. and A. S. Furumoto, 1978. Microearthquake Study of the East Rift Zone of Kilauea, Hawaii, this volume.